Waves in Partially Ionised Multi-Fluid Solar Atmospheric Plasmas

Abdulaziz Hamadi H Alharbi

Supervisors:

Dr Istvan Ballai

Dr Gary Verth

Dr Viktor Fedun

The University Of Sheffield.

University of Sheffield

School of Mathematics and Statistics

A thesis submitted in partial fulfilment of the requirements for the degree of

Doctor of Philosophy

January 2022

I would like to dedicate this thesis to my father, my mother, my wife (Mashael), and my kids (Omer, Motaz, Farah and Ameer).

Acknowledgements

First of all, I would like to thank God for completing my PhD study which is a great milestone in my academic life.

I would like to thank my supervisors, Drs. Istvan Ballai, Viktor Fedun, and Gary Verth, for their continuous support and helpful guidance, which helped me to clarify my thesis ideas and express them in the best academic form that I can provide. This thesis could not be done without them.

I would want to thank my academic advisor, Dr. Ashley Willis, for his support and the academic advice he has provided.

A great thanks from the depths of my heart to my father, Hamadi and my mother, Samirah, (the best parents anyone could ever wish for) for their love, support, and prayers that helped me stand up and stay up. Many thanks to them for believing in me.

My huge thanks and gratitude go to my lovely wife, Mashael Alhomrani, who dropped out of her bachelor's studies in my country to come with me to the UK and share the stresses of this journey with me. I thank her for her love, support, patience, encouragement, and everything else she has given to me. I want to thank my sweet children (Omar, Motaz, Farah and Ameer), for their love and support. I do apologise to them for not spending enough time with them playing and enjoying togetherness during this period.

I want to thanks my brothers and sisters for their love and support. I would like to thank all my friends in Sheffield, School of Mathematics and Statistics and back home, in Saudi Arabia.

Last but not least, I would like to thank the Saudi government, Umm Al-Qura University, and the Ministry of Education for their financial support. Thanks to the Royal Embassy and the Saudi Cultural Bureau in London for the support while carrying out studies at the University of Sheffield.

Declaration of Authorship

I hereby declare that, except where clear reference is made to the work of others, the contents of this dissertation are original and have not, in whole or in part, been submitted to this or any other university for consideration for any other degree or qualification. This dissertation is my own work and contains nothing which is the outcome of work done in collaboration with others, except as specified in the text and Acknowledgements.

Abdulaziz Alharbi
January 2022

Abstract

Waves in solar and space plasma are one of the most natural manifestations of dynamics. Waves are driven by restoring forces that oppose changes in the equilibrium state.

The solar atmospheric plasma is a complex environment, where the plasma changes from being controlled by pressure forces to a regime where dynamics is driven by magnetic forces, but also where the plasma changes from being partially ionised to fully ionised.

The present Thesis deals with the study of waves in partially ionised plasma using a multi-fluid framework. In particular, we study the nature and characteristics of waves propagating in partially ionised plasmas in the strongly and weakly ionised limits.

By means of analytical and numerical investigations of small amplitude waves with frequencies comparable with the collisional frequency between particles are analysed by solving the governing equations. Our research focused on the limiting cases of weak and strong ionisation.

We have shown that in the strongly ionised limit only the slow waves associated to the charged species are affected by cut-off effects, and the dynamics of waves connected to neutrals is driven by the collision with charges.

In the weakly ionised limit the dynamics of the plasma depends on the strength of collisions and their relative magnitude compared to the gyro-frequencies of charged particles. In the photosphere the particles are not magnetised and acoustic modes undergo a very quick damping. The cut-off wavenumbers are determined only by collisional frequency. With the decrease of number density of particles, only electrons are magnetised, while ions are tightly coupled to neutrals. Due to the different motion of the charged particles, electric currents develop that could play an important role in the process of plasma heating.

The present Thesis constitutes a presentation of my results I obtained during my PhD studies at the University of Sheffield.

List of Publications

This Thesis is based on the following publications:

- Alharbi, A., Ballai, I., Fedun, V. and Verth, G. (2021), 'Slow magnetoacoustic waves in gravitationally stratified two-fluid plasmas in strongly ionized limit',Monthly Notices of the Royal Astronomical Society (MNRAS), 501(2), 1940–1950.
- Alharbi, A., Ballai, I., Fedun, V. and Verth, G. (2022), 'Waves in weakly ionised solar plasmas', Monthly Notices of the Royal Astronomical Society (MNRAS), (submitted).

Contents

List of Figures

List of Tables

CHAPTER 1
Introduction

1.1 The Sun

Our Sun is a huge plasma ball held together by its gravity. It is the only star that can be studied with high accuracy. The Sun is classified as a G2 V star, with a surface temperature about 5,800 K, and it is situated on the main sequence of the Hertzsprung–Russell (HR) diagram. Although it falls midway between the biggest and smallest stars of its type, there are so many dwarf stars that the Sun falls in the top 5 percent of stars in the neighbourhood that immediately surrounds it. The next nearest star to it is Proxima Centauri at 4.25 light years distance.

The importance of studying the Sun resides in its capacity of maintaining life on Earth. The Sun stays at the centre of the solar system and it is at 93 million miles away from the Earth (1 astronomical unit). It contains 99 % of the total solar system's mass. Given its proximity and importance, the Sun is probably the most studied celestial body since ancient times. In addition the Sun is the only place where plasma physics can be studied under extreme conditions. As a result, it is not surprising that the Sun has been, and continues to be a fertile field of research. The physical parameters of the Sun are in Table 1.1.

Since the ancient Chinese believed that the observed movements of stars were closely related to the destiny of the country and its rulers, the evolution of stars were recorded with great accuracy for thousands of years. From the 16th century BC to the end of the 19th century AD, almost every dynasty appointed officials whose sole task was observing and recording the changes of stars. Such observations and records have left a very rich astronomical legacy. Chinese astronomers were the first who documented for almost 300 years more than 35 solar eclipses.

The earliest records of sunspots were made in 28 BC by Chinese astronomers

The Sun's physical parameters	
Age	4.5×10^9 yr
Mass	1.99×10^{30} kg
Radius	696,000 km
Mean density	1.4×10^3 kg m^{-3}
Mean distance from Earth	1 AU$=1.5 \times 10^{11}$ m
Surface gravity	274 km s^{-2}
Escape velocity at surface	618 km s^{-1}
Radiation emitted	3.86×10^{26} W
Equatorial rotation period	26 d
Angular momentum	1.7×10^{41} kg m^2 s^{-1}
Mass loss rate	10^9 km s^{-1}
Effective temperature	5,785 K
1 arc sec $\equiv 1''$	726 km

Table 1.1: The fundamental physical parameters of the Sun. These values were adapted from Priest (2014).

during the reign of Emperor Cheng of the Western Han Dynasty. From then until the late Ming Dynasty in the mid-17th century, Chinese history books recorded more than 100 sunspots. Furthermore, they also took note of other phenomena concerning the Sun, such as solar prominences and the solar corona. The first record of a solar prominence has been found in a tortoise shell inscription, which describes "three suddenly bursting fires eating a chunk of the Sun" (Parenti, 2014).

Greek astronomers had remarkable contributions to the study of the Sun. Aristarchus of Samos accurately predicted that the Earth revolved around the Sun in 280 BC. He even calculated the distance between the Earth and the Sun to be 8 million km. Although this estimate was wrong by a factor of around 20, it is no little achievement, particularly when we consider that Euler's exact estimate of 149.6 million km in 1770 took more than two millennia to arrive at. Unfortunately, Ptolemy, who argued for an Earth-centric Universe, substituted Aristarchus' idea, a notion that was not disputed for 1400 years! Historical documents show that the Sun played an important role in every civilisation, throughout the evolution of the human kind. Accurate and scientifically valid

measurements were available only in the last few hundred years, however our knowledge about how the Sun works is far from being complete.

Nowadays a large number of space satellites (e.g. SoHO, TRACE, Hinode, IRIS, Solar Parker Probe, etc.) and high resolution ground-based telescopes (e.g. SST, DKIST, DSO, etc.) are providing unprecedentedly high-resolution observations that have helped obtaining a deeper and more complete knowledge of our star. After all, the Sun is a plasma laboratory in extreme conditions. So far we managed to gain valuable information about its structure of, how it works on a long time and spatial scales, however, we are still far away from being able to really understand the physics that stays behind many important phenomena, especially the ones that occur over smaller scales.

Primarily the Sun can be divided into its inner and the outer regions. It is customary to consider that the surface of the Sun, separating the interior and exterior, is the layer below which the Sun becomes opaque to visible light. The solar atmosphere is the only region in the Sun that can be observed in many wavelengths. A schematic diagram of the internal and external structure of the Sun is shown in Figure 1.1.

In what follows we will review a few key properties of these regions of the Sun.

1.1.1 Solar Interior

The solar interior can be separated into three sections, each with specific properties: the core, the radiative zone, and the convection zone. Information about solar interior can be gained only indirectly either via the study of trapped sound waves (helioseismology) that cause the surface of the Sun to oscillate with a period centered around 5 mins, or we can "look" into the solar interior by studying the solar neutrino problem, however, this gives information mainly about the inner core of the Sun (Priest, 2014).

The solar core contains approximately 50% of the Sun's mass. It has temperature of about 15 million K, density $1.6\times\ 10^5$ kg m^{-3} and radius about 150 Mm. It is the central region of the Sun where thermonuclear reactions take place and enourmous energy is releases in form of photons. As moving outwards of the core, the temperature and density are decreasing. The primary thermonuclear reaction in the core is the proton-proton (or p-p) cycle in which hydrogen is converted into helium, various nuclear particles and energy. The p-p fusion can occur only if the kinetic energy (i.e. temperature) of the protons is high enough to overcome their electrostatic repulsion. Comparing the mass

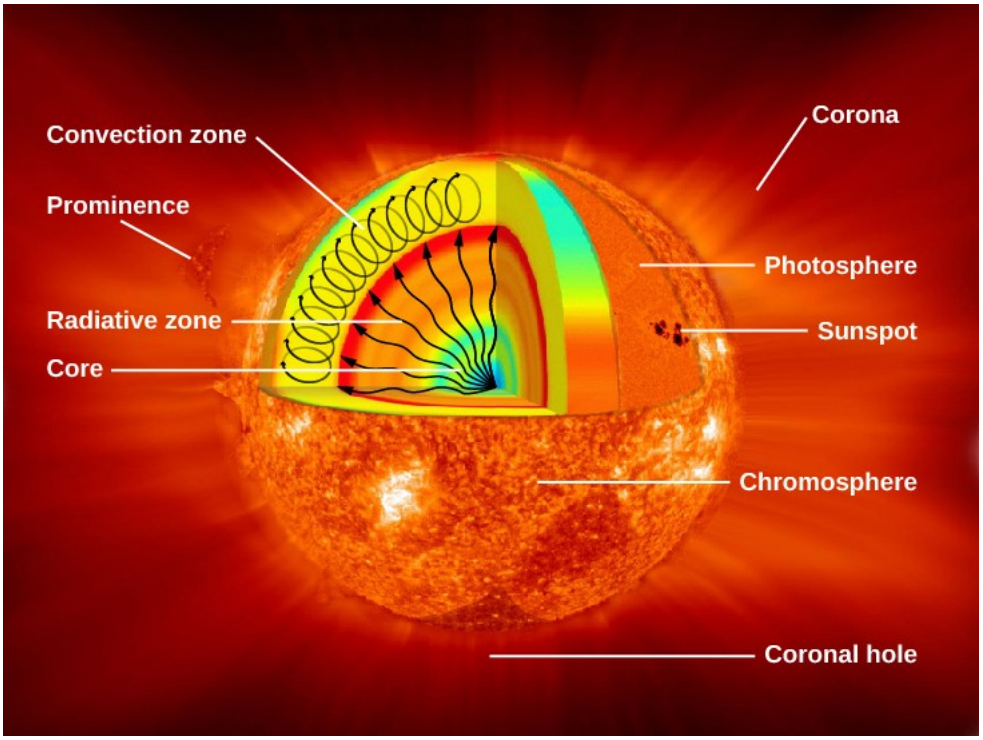

Figure 1.1: The structure of the Sun. The inner layers are the core, radiative zone, and convective zone, while the visible outer layers are the photosphere, chromosphere, and corona. The figure also shows some observable solar atmospheric phenomena, such as solar flares, prominences, sunspots and coronal loops, all studied in great details. Credit: NASA/Goddard Space Flight Centre.

of the final helium with the masses of the four protons reveals that 0.7% of the mass of the original protons has been lost. This mass has been converted into energy, in the form of kinetic energy of produced particles, gamma rays, and neutrinos released during each of the individual reactions. The total energy yield of one whole chain is 26.73 MeV.

Energy released as gamma rays interact with electrons and protons and heat the interior of the Sun. The kinetic energy of fusion products adds energy to the plasma in the Sun. The fusion process keep the core of the Sun hot and prevents it from collapsing under its own weight, as it would if the Sun were to cool down.

Neutrinos do not interact significantly with matter and therefore do not heat the interior. They can escape the Sun fairly quickly and their signatures are observed in neutrino-capture devices on Earth. However, currently the observed solar neutrino flux is half-one third of the expected neutrino flux, that constitute the famous neutrino problem.

Above the core, one has the radiative zone located below the convection

zone and extends to about 70 % of radius of the Sun outwards from the core. It has temperature about 2 million K and density about 200 kg m^{-3}. The core's energy is emitted in the form of high-frequency γ rays and neutrinos. Because neutrinos are so tiny, they can easily pass through the solar radiation zone and beyond without being impeded. In this layer the energy is transported by photons that are continuously absorbed and emitted by electrons and ions. It takes an average of 171,000 years for photons from the core of the Sun to leave the radiation zone. The temperature at the top of the radiative zone is approximately 1.5 million K (Priest, 2014).

Finally, the convection zone is the outer layer of the solar interior and it is located above the radiative zone. In this region the plasma is too cool and the radiation from the radiative zone absorbed by cool ions, leading to the heating of the plasma. In the convective zone, heat and energy are carried outward along with matter in swirling flows called convection cells. Once the cells reach the surface of the Sun (these convective cells, or granules, can be seen already on the surface of the Sun), they cool down, become heavier and sink again inside the convective region, where they start a new cycle. The average temperature of the convective zone is about 5,700 K and has a density of $2\times\ 10^{-4}$ kg m^{-3}.

The magnetic field that dominates the dynamical processes is generated inside the Sun. It is widely accepted that this field is generated by electrical currents acting as a magnetic dynamo inside the Sun. The electrical currents appear as a result of the flow of hot, ionized gases in the convection zone. Since the Sun posses a differential rotation (the equator makes one rotation every 34.3 days, while the poles every 25.05 days), that results in the magnetic field lines getting wound up. Convection carries magnetic field lines towards the surface and they appear either as massive magnetic strictures (sunspots, pores, etc) or in the form of a weaker remnant magnetic field at the boundaries of granules.

1.1.2 Solar Atmosphere

The solar atmosphere is the only solar region that can be visualised and analysed in great detail and the place where photons escape into the space directly. The solar atmosphere can be divided into three distinct layers: the photosphere, chromosphere and corona, each with its own properties.

The photosphere is the visible layer of the Sun and can seen by naked eye. Its name comes from the Greek word that translated means 'sphere of light'.

The photosphere has thickness of about 500 km and its temperature decays with radial distance to approximately 4,300 K from its value of 6,600 K at the base of the photosphere. The granules cover the entire photosphere and they are the consequence of hot outflowing plasma. Granules have a diameter about 0.3 to 2 Mm and a lifetime between 5 and 10 minutes (Priest, 2014). Hirzberger et al. (2010) found the granules have intensity between 5 to 15 % and about 32 % in white light and near- UV, respectively. The magnetic field in the photosphere layer has different strength and it appears in different forms. Lagg et al. (2010) confirmed strong magnetic field located in the supergranule boundaries and these count for about less than 5 % of the magnetic strength of the entire photosphere. On the other hand, the weaker magnetic field found in the interior of supergranular cells has an intensity of 100 - 300 G. (Khomenko et al., 2003). Observations using SOHO/MDI and SDO/HMI instruments show that magnetic field lines tend to congregate at the boundaries of convective cells due to the outward motion of the granular plasma, from the cells' center to their edges (Foukal, 2004; Solanki et al., 2006). Here the field lines are constantly perturbed by the buffeting motion of granules, which is a possible driver for waves seen in the higher solar atmosphere. The photosphere also hosts the sunspots, one of the most studied solar features. Sunspots appear as dark areas and they are the location of the emergence of strong magnetic fields (of the order of kG). Given the strong magnetic field, the kinetic pressure is suppressed, leading to lower temperatures than their surroundings, sunspots have a radius between 10 to 20 Mm. In general a sunspot has a central part (umbra) where the magnetic field is vertical, and a penumbra, that shows a striated pattern and here the magnetic field is more inclined (McIntosh, 1990; Thomas et al., 2002). The low temperature of the photosphere implies that the plasma is mainly neutral and ionisation of neutral H occurs due to collisions. The consequences of weekly ionised photospheric plasma on wave propagation will be discussed later in Chapter 4.

The dynamical behaviour of the plasma can be understood in terms of the so called plasma-β parameter , that can be defined as the ratio of the plasma pressure to the magnetic pressure. The magnitude of this parameter (relative to 1) defines whether pressure or magnetic forces are dominant. In the solar photosphere plasma-$\beta \gg 1$, so the plasma motion is driven mainly by pressure forces. In contrast, in the solar corona plasma-$\beta \ll 1$, meaning that magnetic forces are responsible for the dynamics, stability and the thermodynamical evolution of the plasma.

On top of the photosphere we have the 2,000 km thick chromosphere, which is a highly dynamic layer, where the temperature increases to a few hundred thousand K. This layer is probably the most enigmatic region, as it is the place where the plasma is changing from being a pressure-force dominated to magnetic force dominated, it is the place where the plasma changes from being partially ionised to fully ionised and it is the place where the mechanisms producing the coronal heating are operating. The network field can still be seen at chromospheric temperatures but sunspots are not, although bright regions known as plages are found near sunspot locations (Foukal, 2004). Dark filaments are seen in the plage regions, outlining regions of different polarity and it is likely that magnetic field lines arch over them to connect the different regions (Golub and Pasachoff, 2002). Other chromospheric features are spicules, mottles and fibrils. It is possible that these features are all related, but their appearance is slightly different depending on where they are seen (Foukal, 2004). Spicules are seen on the limb and are considered jets of plasma rising from the chromosphere following magnetic field lines. It is possible that mottles are actually the same structures as spicules but viewed on the disk rather than the limb. In contrast to spicules, which are approximately vertical, fibrils are horizontal and lie parallel to the disk. However, it is still possible that these two features are linked. Spicules are usually observed in quiet regions of the Sun, where the magnetic field is vertical and extends higher into the atmosphere before returning to the surface and connecting to a region of opposite polarity. Fibrils are seen in active regions where the field lines connect to closer regions, leading to the flatter, horizontal shapes (Foukal, 2004). The solar chromosphere is also in partially ionised state, but the ionisation varies greatly with height. While at the base of the chromoshere the plasma is weakly ionised, at its top, the plasma becomes strongly ionised.

The 100 km thick transition region is located between the chromosphere and the corona and it is visible using ultraviolet observations. This layer contains sharp densities gradients and the temperature increases dramatically by two orders of magnitude by reaching approximately 10^6 K.

Finally, the multi-million degree solar corona with low density and pressures expands out in the heliosphere. The solar corona is a very tenuous region that is responsible for the activity of the Sun that is felt on Earth's surface. The temperatures in the solar corona makes the plasma fully ionised. The solar corona can be observed in many wavelength, each of which reveals different features and provides information about the overall structure of the coronal

plasma. Due to the extreme high temperatures in the corona, the plasma primarily emits in the EUV and soft X-ray portions of the spectrum. However, there are also many emission lines in the visible part of the spectrum, which are produced by emission from highly ionized elements (Golub and Pasachoff, 2010). An EUV images of the corona is shown in Figure 1.2.

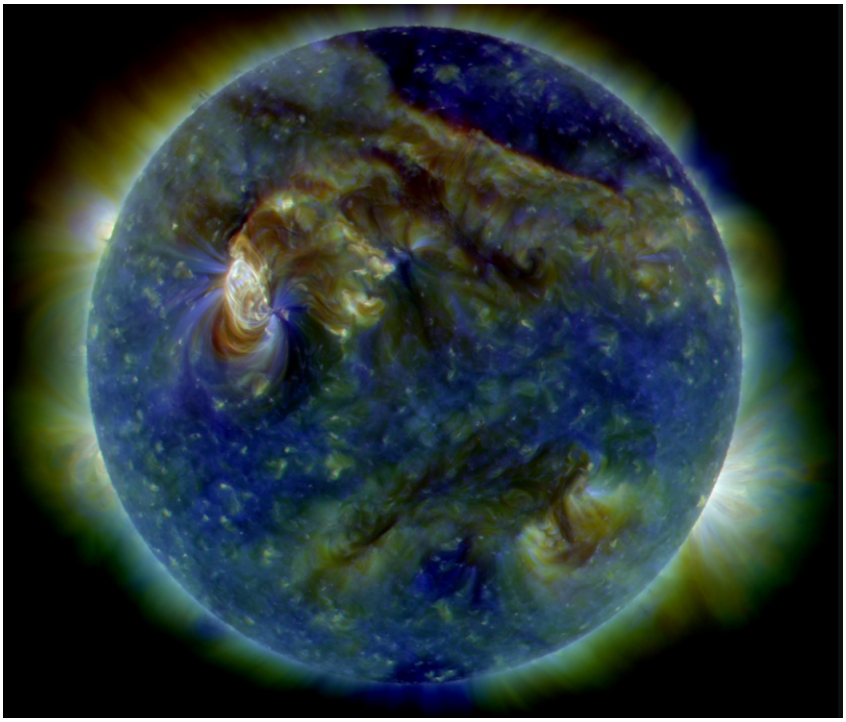

Figure 1.2: An EUV image of the solar corona obtained by superimposing three images in different wavelengths of Extreme Ultraviolet light corresponding to 171 Å, 193 Å and 304 Å. Dark and bright regions denote regions of different temperatures. Credit: Solar Dynamics Observatory/Atmospheric Imaging Assembly (SDO/AIA).

The bright regions coincide with active regions and are formed from many closed magnetic field lines, whereas the dark regions correspond to areas where the field lines are open (Priest, 2014). Although these field lines are usually called open, it is important to remember that they are in fact closed, with one end located in the solar magnetic field and the other in a magnetic region far out in the Solar System. Since the field lines stretch out and away from the Sun, this gives them the appearance of being open. This is in contrast to the closed magnetic field lines that form active regions, which have both ends rooted in the solar magnetic field. The closed magnetic field lines form large coronal loops and join regions of different magnetic polarity.

Coronal loops are magnetic flux tubes, filled with plasma of a higher density than that of the surrounding plasma. Their length varies depending on the

type of loop. Loops connecting active regions are typically up to 700 Mm long while post-flare loops are shorter, with lengths in the region of 100 Mm. An individual loop might only have a lifetime of approximately a day, but a whole loop system can last for several weeks (Priest, 2014).

The open field regions of the corona are called coronal holes and in general they are located at the poles of the Sun. Here magnetic field lines extend out from the Sun into the Solar System. Plasma leaving the Sun along these field lines is known as the solar wind. A consequence of the plasma being removed from the Sun is that the density and temperature in coronal holes are lower than the background coronal values, therefore explaining their dark appearance in images (Aschwanden, 2009). Coronal holes can also appear at other latitudes during times when the solar cycle is at a minimum (Golub and Pasachoff, 2010).

The solar atmosphere is permeated by magnetic field that appears more isolated in the lower part of the atmosphere, but fills up the whole corona. Magnetic field is responsible for the very high temperature of the solar corona, the dynamical and thermal evolution of the plasma. Despite its importance, it is probably the least understood and measured parameter, given the difficulty to measure its magnitude (e.g. the effect of Zeeman splitting of spectroscopic lines does not work in tenuous plasmas), but mainly its structure. One way to address these issues is the indirect study via waves and oscillations, called *magneto-seismology*. Like on Earth, seismology implies the combination of observations with theory to derive quantities that cannot be measured exactly. High resolution observations show that one of the most obvious characteristics of the solar plasma is that it is dynamic on all time and spatial scales. Observations can give information about measurable wave characteristic, such as periods, amplitude, damping times and lengths, frequency, etc. These observations can be combined with theoretical results (dispersion relations, evolutionary equations, etc.) to derive fundamental information such as magnetic field structure and magnitude, heating/cooling functions, transport coefficients, etc. (De Moortel, 2005).

1.1.3 Solar prominences

Prominences are large, cold, bright and dense magnetic features in the solar atmosphere. They are anchored in the photosphere and extend through the corona. They are supported against gravity by the effect of the magnetic field. An example of this kind of structures is shown in Figure 1.3, where the

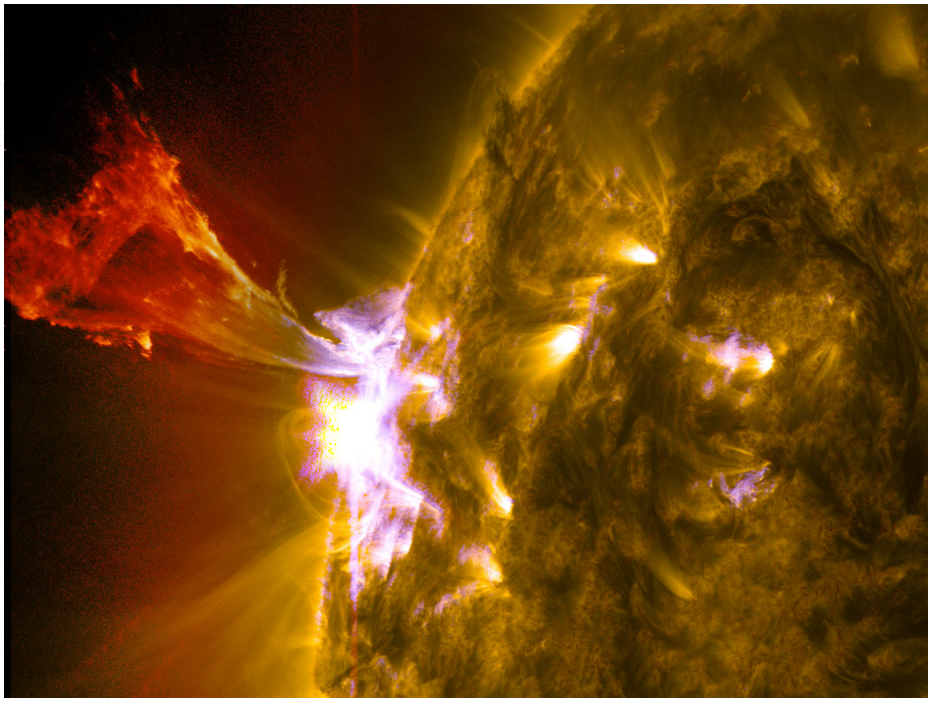

Figure 1.3: Burst of solar material leaps off the left side of the Sun in what's known as prominence eruption. Credit: NASA/SDO/AIA.

plasma can be clearly seen protruding from the limb of the Sun. Prominences extend from the limb of the Sun and appear bright in comparison with the space in the background. They form along the polarity inversion lines (PIL) of the magnetic field, i.e. the lines that divide two regions of opposite magnetic field polarity in the photosphere, but the precise mechanism of its formation is still under active research. Their temperatures are typically one hundred times lower than those found in the corona, of the order of 10^4 K, a reason why the prominence plasma is partially ionized, being made up of hydrogen and helium (Gilbert et al., 2007). In contrast, prominences are between one hundred and one thousand times denser than the corona, with densities of the order of 10^{-12} to 10^{-10} kg m^3. Their heights are of the order of 10^4 km, their widths vary between 4 and 3×10^4 kilometers and their lengths are of the order of 10^5 km. When seen on the solar disk prominences are called filaments where they appear to be dark features as they absorb the background coronal radiation emitted in the EUV lines by the hydrogen and helium resonance continua. Although prominences protrude the multi-million degree corona, their temperature does not change thanks to the thermal shield provided by the magnetic field.

Prominences and filaments can be classified in two categories: quiescent and active. Quiescent prominences seem more stable and can have lifetimes of

up to several months, with an average magnetic field of about 10 G.

In contrast, active prominences are associated with sunspot groups and have much shorter lifetimes of the order of minutes to hours. Active prominences posses stronger magnetic fields and they can erupt at the end of their lifetime, ejecting large amount of mass into space as part of a Coronal Mass Ejection (CME), also known as *disparition brusque (DB)*. A more detailed description of the properties of prominences can be found in earlier studies by, e.g. Labrosse et al. (2010), Mackay et al. (2010), Parenti (2014), etc.

The very first observation of a prominence was taken by Ludovico Muratori in 1239, who described it as burning hole. In 1733 Vassenius labelled prominences as reddish clouds in the lunar atmosphere. The very first proper observation of a solar prominence took place during the eclipse of 1842 by French astronomers. The very first photographed prominence dates back to 1860, while the spectrum of prominences was determined in 1868, proving the prominences are gas clouds (Jansenn and Norman Lockyer independently observed bight emission lines of a previously unknown element, later named Helium). Using a coronograph at the Pic-du-Midi Observatory, Lyot observed prominences for the first time in the absence of an eclipse (Tandberg-Hanssen, 1974). Parallel to the sophistication of observations that provided more and more details about the properties of prominences, the theoretical modelling of prominences was developed. Despite major advances in the modelling of these magnificent solar features, we are far from fully understand how they are formed and and how they evolve in time. For a detailed review of the properties of solar prominences we refer readers to earlier studies by Aboudarham et al. (2008), Priest (2012), Romeuf et al. (2007), Tandberg-Hanssen (1974), Tandberg-Hanssen (2013) and Wang and Stenborg (2010).

Nowadays prominences are observed by high cadence Hα measurements provided by space satellites and ground-based telescopes. With the help of instruments like the SST (Swedish 1-m Solar Telescope) or DOT (Dutch Open Telescope), one can see fine structures down to the resolution limit (0.15" for SST or around 100 km). Homogeneous time series are with a similar spatial resolution from the Solar Optical Telescope (SOT) onboard the Hinode satellite. A large variety of fine structures and their dynamics is also seen on TRACE movies, although the spatial resolution is lower, around 1". These images are usually taken with a 171 or 195 Å filter where the hot coronal structures appear simultaneously with cool ones. The same wavelength range was provided by the EIT instrument onboard SOHO, however, with a lower

resolution. At 171 or 195 Å the HeI and HeII absorption dominates over the HI. It was shown theoretically that this opacity is quite comparable to that of the Hα line (Anzer and Heinzel, 2005).

Since prominences are considered to be partially ionised, they serve as an ideal testing bed for validating physical effects in partially ionised plasmas, the subject of the present Thesis.

1.2 Partially Ionised Plasmas

By definition a partially ionised plasma is a system at relatively low temperature where charged particles (positive and negative) and neutrals co-exist and they interact via short and long-range interactions. This interaction between species ensure a collective behavior necessary to form a plasma. Examples of partially ionised plasmas in the Universe include solar and stellar atmospheres, cold neutral and warm neutral regions in the interstellar medium, molecular clouds, protoplanetary disks, Earth's atmosphere, etc. These cover a large spectrum of ionisation degree, from weakly ionsied to strongly ionised.

In partially ionised plasmas the temperature is not high enough to ensure a full ionisation of the plasma (for a H plasma, full ionisation starts for temperatures in excess of a few 10^4 K). The key interaction that takes place in such plasmas is the collision between ions and neutrals, as this is the interaction that ensures an effective momentum transfer and coupling between different species (collisions with electrons do not imply a significant exchange of momentum and energy given the very large difference between the mass of an electron and the mass of ions or neutrals).

Molecular clouds are the densest and coldest structures in the interstellar medium and they are the sites of star formation. The temperatures in molecular clouds is in the range of 10-20 K, while the characteristic number density of particles is $10^2 - 10^6$ cm^{-3}. At this temperature the plasma is very weakly ionised, with an average ionisation fraction of 10^{-7} (Shu, 1992). However, even this very low level of ionisation is important for the evolution of these clouds. In particular, the ion-neutral drift (or ambipolar diffusion) is an important effect in various aspects of cloud dynamics. Ambipolar diffusion was used to construct the so-called *standard model* of magnetically-regulated star formation (Shu et al., 1987; Mouschovias, 1991). Ambipolar diffusion was also considered as a possible mechanism responsible for a number of observed properties in the interstellar medium and the molecular clouds of our galaxy.

Partially ionised plasma effects have also been used to explain the formation of the cores of molecular clouds, the origin of the nearly constant width of filamentary structures and the explanation of the so-called magnetic braking catastrophe in protostellar accretion disks (Dapp and Basu, 2010; Li et al., 2014; Ballester et al., 2018*a*). According to the radio observations, the magnetic field of molecular clouds is of the order of tens of micro Gauss.

The Earth's outer atmosphere is a partially ionized region that can be ionised by photo-ionization generated by the incoming EUV and soft X-ray energy from the Sun, by impact ionization at high latitudes of energetic, precipitating particles or by impact ionization due to meteor ablation which creates a small population of metallic ions. In addition the distribution of ions in the Earth's ionosphere can also be influenced by charge exchange mechanisms between neutrals and ions. The distribution of the number density of various ions and neutral atoms with height in the Earth's upper atmosphere is shown in Figure 1.4 using the computed values by means of the NRLMSISE-2000 model (Picone et al., 2002). The concentrations per unit volume of ions and neutrals and their variation with height can influence the ionosphere since they determine the amount of neutral gas available for photo-ionization at different altitudes, and also, they determine to what depth the solar EUV and X-ray radiation might penetrate. For example, since the density of neutral particles decreases with height means that photons can penetrate to lower heights.

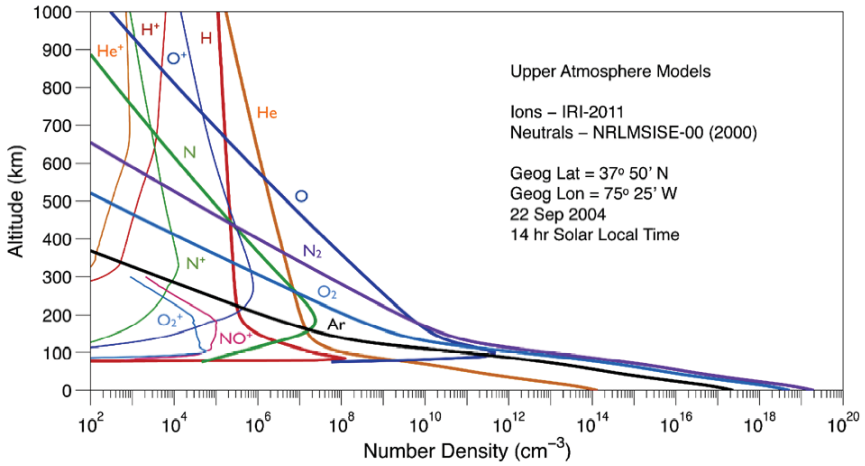

Figure 1.4: The variation of number densities of different ions and neutral atoms in the Earth's upper atmosphere with height. Credit: Pfaff (2012)

The characteristics of ionospheric plasma are influenced by the ion-neutral coupling, displaying an important dynamic interplay between upper atmospheric motions, or winds, and plasma drifts. Thanks to the magnetic field

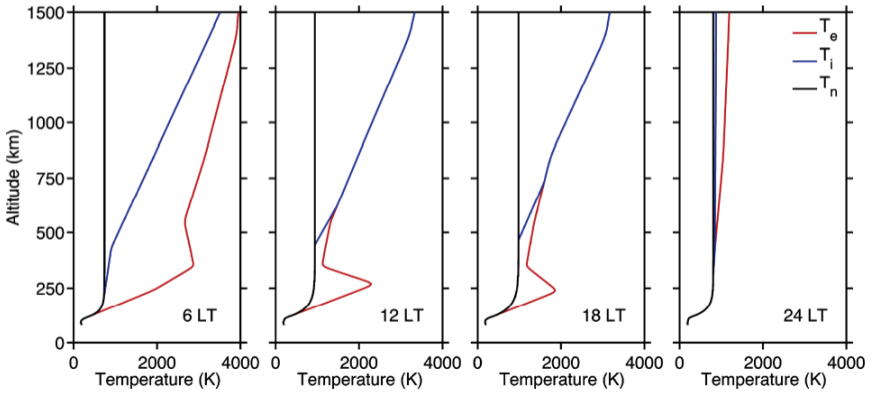

Figure 1.5: The variation of electron, ion and neutral temperatures with height at the Earth's magnetic equator at four different local times. Credit: Pfaff (2012)

around the Earth, charged particles are affected so that strong currents are generated which depend on the local conductivities and collision frequencies, varying with altitude and latitude. Furthermore, as the magnetic field permeates the partially ionised plasma to form the magnetosphere at much higher altitudes, it connects the ionosphere/upper atmosphere to the magnetospheric plasma and solar wind and their sources of energy and momentum, including large electric fields, field-aligned currents, and highly variable particle precipitation. The ionosphere is the ionized component of the Earth's upper atmosphere, covering the height range of approximately 90 to 1000 km. The average ion density of the ionosphere is $10^4 - 10^6$ cm^{-3} and has a temperature that varies with height in the interval 200-500 K. However, the temperature does not only vary with height, it also varies with latitude, being different in the day and night-side of the ionosphere.

The variation of the temperature of electrons, ions and neutral components with height are shown in Figure 1.5 at the magnetic equator at dawn, noon, sunset, and midnight as computed from the IRI model (here shown as 4 different local times (LT)). In the lower ionosphere (covering heights up to 120 km), the average values of the electron, ion, and neutral gas temperatures are very close to each other thanks to the large collisional rate of of particles with neutrals. At higher heights the three temperatures diverge. The electron temperature is highest in the early morning. The neutrals, rotating into sunlight, have yet to warm and the neutral atmosphere is still contracted from the colder, nightside temperature. Hence, the electron-neutral collisions are less frequent. During the day, the neutral atmosphere expands, and the electron-neutral col-

lision frequency, thus, increases at the higher altitudes, reducing the electron temperature. The electron temperature further decreases during the day as it becomes close to the ion temperature due to electron-ion collisions. The temperatures are largest at the higher altitudes where the number densities of particles are low. The enhanced electron temperature near 300 km during the day results from photo-electrons produced within the upper altitude portion of the layer where the neutral atmosphere is less dense. At night, there are no newly-formed photo-electrons and the electron, ion and neutral temperatures quickly converge to similar values via collision processes (for details see Pfaff (2012)).

The characteristic values of the density and temperature make the ionosphere a dense and weakly ionised environment where the frequency of collision between particles is rather low. One interesting effect occurs up to a height of 200 km. The collisional frequency between electrons and neutrals is lower than the electron gyro-frequency, while the collisional frequency of ions and neutrals is higher than the ion gyro-frequency, meaning that only electrons are magnetised. This region is also the location of very strong currents. A similar phenomena occurs in the solar atmosphere and this will be discussed in details in Chapter 4.

In the solar atmosphere the ionisation varies between the limits corresponding to weak ionisation (photosphere) to a strong ionisation (chromosphere) thanks to the increase in temperature (see Figure 1.6). That means that over a distance of about 2.5 Mm (the thickness of the partially ionised layer in the solar atmosphere) the dominant effect changes with height.

Partial ionisation effects (such as the Hall effect and ambipolar diffusion) have been shown to play important role in the process of chromospheric heating (Khomenko et al., 2014*a*). Given that the collisional frequency of various species are so different (as discussed in Chapter 2), a single fluid description of a plasma is not possible, meaning that a multi-fluid framework is more suitable to describe realistic effects in solar atmospheric plasmas. Recent, high-resolution observations made by HINODE, have revealed that limb prominences show a very active dynamics (Berger et al., 2008) that have been interpreted and modeled in terms of different instabilities (Rayleigh-Taylor, Kelvin-Helmholtz, etc.) which develop in the partially ionised prominence plasma (Soler et al., 2012; Díaz et al., 2012; Khomenko et al., 2014*b*; Ballai et al., 2015). These studies have shown that partial ionisation can have dramatic changes in the evolution of instabilities, including their growth rate.

Partial ionisation effects have been considered in conjunction with magnetic reconnection taking place in the lower part of the solar atmosphere. To explain the observations by Katsukawa et al. (2007), who reported small jet-like transient features in sunspot penumbra (with lifetimes of less than 2 minutes, lengths of 1000-4000 km, and widths of about 400 km), by means of Hinode Ca II H observations, Sakai and Smith (2008) performed 2.5D numerical simulation of two horizontal penumbral filaments using a two fluid partially ionised plasma consisting of a neutral H atom fluid interacting with a charged fluid (protons+electrons). They showed that inclined bidirectional jet-like flows, driven by the magnetic reconnection, propagate along the vertical magnetic flux tube, which exists between the filaments. Their simulation also showed that protons are heated to temperatures that are 25 times of their original temperature. In contrast, the neutral fluid was very weakly heated. These authors proposed that the plasma jets may be a viable explanations for the microjects observed by Katsukawa et al. (2007). Furthermore, it was shown that the reconnection rate of the interacting penumbral filaments is strongly enhanced by an initial velocity of filaments, more precisely the reconnection rate can be increased by a factor of 50 for a photospheric neutral H flow of the order of 10 % of the local sound speed.

Leake et al. (2012) performed multi-fluid simulations of magnetic reconnection in a chromospheric weakly ionized plasma, including ion-neutral scattering collisions, ionization, recombination, optically thin radiative loss, collisional heating, and thermal conduction. Their results show that in the resulting tearing mode reconnection, the neutral and ion fluids become decoupled, creating an excess of ions in the reconnection region and therefore an ionization imbalance. Ion recombination in the reconnection region, combined with Alfvénic outflows can remove ions from the reconnection site, leading to a fast reconnection rate. Murphy and Lukin (2015) performed 2.5D simulations of asymmetric reconnection in weakly ionized partially ionised plasma, where the plasma and field parameters were different in each upstream region. In their simulations the authors also included non-equilibrium effects, the result of which ions can recombine into neutral H and vice-versa. During simulations the ion and neutral flows remained decoupled, but the decoupling was asymmetric. Their results showed a net neutral flow through the current sheet directed from the region of weak magnetic field into the strong field region, which resulted from a large scale neutral pressure gradient Similarly, thanks to the Lorentz force acting on the ions from the strong field region led to the ions

pulling the X-point into the weak field region. Murphy and Lukin (2015) also studied the effect of Hall currents in the efficiency of reconnection and they found that the asymmetry led to the development of a quadrupole magnetic field. These results show the importance of considering partially ionised effects in the process of reconnecting field lines that are able to significantly modify and influence the efficiency of magnetic energy release during reconnection.

Partial ionisation effects have been shown to drastically change the properties of waves, however this will be discussed later, in Chapter 2.

The modelling framework of a partially ionised plasma depends on the frequency domain in which we are interested in. For frequencies that are larger than the ion-neutral collisional frequency, the plasma dynamics will be described within the two-fluid approximation, where separate equations will describe the evolution of charged particles and neutrals oppositely, for frequencies that are below the ion-neutral collisional frequency the plasma dynamics can be described within using a single-fluid approach (Krishan, 2016; Ballester et al., 2018*a*) .

In the solar atmosphere the variation of the ionisation degree is due to the increase in temperature. The variation of the temperature and other physical parameters with height can be obtained from spectroscopic measurements that can lead to atmospheric models, such as the one presented in Figure 1.6 (Avrett and Loeser, 2008), where we plot the variation of the temperature (T), turbulent velocity (V), total H density (n_H), neutral H density (n_{H1}) and electron density (n_e). It is clear that in the photosphere (the first 500 or so km), the neutral number density is much larger than the ion number density (by a factor of 4), while in the chromosphere, the ion number density is larger. At the transition region height the number densities of particles have a sudden drop thanks to the very large temperature increase in this region.

The other solar atmospheric model that we will use in our research is the model developed by Vernazza et al. (1981) (labelled as the VAL model), who used extreme ultraviolet (EUV) observations to determine the height-dependence of physical parameters, similar to the AL model shown in Figure 1.6. Although this model does not give accurate estimations for the number of particles at the top of the chromosphere, nowadays it is one of the most popular models. The temperature and number density of particles provided by this model will be used later in Chapter 3 and 4 to estimate the variation of collisional frequencies with height that allows us to differentiate the dominant dynamics in different regions of the solar atmosphere.

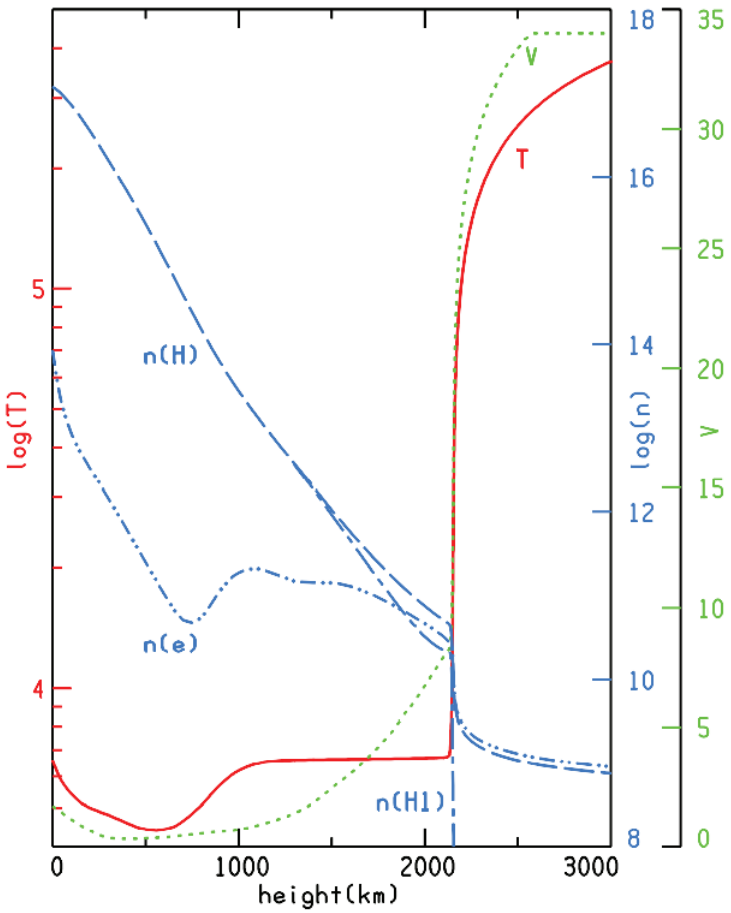

Figure 1.6: The variation of temperature, T, the number densities of electrons, $n(e)$, and neutral H, $n(H)$, with height on logarithmic scale based on the tabulated values of the Avrett and Loeser (AL C7) solar atmospheric model. This picture was taken from Avrett and Loeser (2008).

Another very important parameter for the current Thesis is the collisional frequency of particles and the variation of this frequency with height. Given its importance, we are going to discuss this quantity later in Chapter 2.

Finally, we should mention that partially ionised plasmas appear not only in astrophysical applications. Partially ionised plasmas are very important for confined thermonuclear fusion plasma devices. Partial ionisation effects in this field are considered in two instances: (a) the transformation of an initially dilute neutral gas at room temperature into a fully ionised medium via external heating – the plasma startup, and (b) the influence of neutral molecules in the relatively cool edge region of the fusion plasma on its transport dynamics and stability properties which determine the quality of the confinement and ultimately the prospects of a future fusion reactor.

Very recently partially ionised plasmas received great attention in medicine.

The low temperature of electrons can generate many chemical reactions, such as modifying DNA, proteins, and so on. Research in medical plasmas helped to develop therapeutic strategies for many diseases, such as chronic wounds and MRSA. The plasma was used to treat antibiotic resistance in bacteria by killing the bacteria without harming humans (for more details see, e.g. Morfill et al., 2009; Von Woedtke et al., 2013). Applications of plasmas made up from reactive species and charged particles recently received special attention in biology, where scientists try to explore the impact of cold plasmas on biological cells on macroscopic and microscopic scales. This research could lead to the development of cold plasma-based medical therapies (Laroussi, 2020).

1.3 Thesis outline

The present Thesis constitute a summary of the research I carried in the past years as a PhD student at the University of Sheffield. The Thesis is divided into five Chapters and the results of my scientific research are presented in Chapters 3 and 4. The aim of my research is the investigation of the nature and property of waves propagating in solar atmospheric plasmas in the limits strongly ionised plasma ($\rho_{0n}/\rho_{0i} \ll 1$) and weakly ionised ($\rho_{0n}/\rho_{0i} \gg 1$) plasmas.

This Thesis is structured according to the following Chapters:

- **Chapter 1**: *Introduction into partially ionised plasmas of the solar atmosphere*: this chapter includes the background of my research and a review of the current literature on partially ionised astrophysical plasmas.

- **Chapter 2**: *Mathematical formalism*: here I plan to present the equations that stay at the core of the study of partially ionised plasmas, paying special attention to the governing equations in the multi-fluid approximation. Here I will also discuss the variation of collisional frequency between various species. Since my research aims to study waves in partially ionised plasmas, in this chapter I will review the current state-of-the-art, reviewing the properties of waves and compare them to the properties of waves in fully ionised plasmas.

- **Chapter 3**: *Slow magnetoacoustic waves in gravitationally stratified two-fluid plasmas in strongly ionised limit*: in this chapter, I derive the

system of coupled equations describing the propagation of ion-acoustic and neutral-acoustic waves in space and time in a gravitationally stratified plasma, where the composition of the plasma is dominated by ions (relevant to the upper part of the solar chromosphere). The governing equations are solved as an initial value problem (IVP) using the inverse Laplace transform technique. Solutions are sought in the asymptotic limit, i.e. for large values of time. We investigate the spatial and temporal evolution of waves subject to various types of drivers. We will discuss the nature of cut-off frequencies and how these are modified by the collisions between particles.

- **Chapter 4**: *Waves in partially ionised plasma in the weakly ionised limit*: In this chapter, we study the nature and propagation of waves in a realistic solar atmosphere (using the standard solar atmospheric model developed by Vernazza et al. (1981)). In the weakly ionised limit (relevant to the lower part of the solar atmosphere) the proper description of dynamics requires a multi-fluid approximation. Given the range of frequencies involved in the problem, we could divide the atmosphere into two regions. In the first region all frequencies are above the electron gyro-frequency, meaning that waves can be described in a non-magnetic environment. The second region involves a lower range of frequencies where the collisional frequency of charged particles becomes comparable with the electron gyro-frequency, meaning electrons become magnetised. Due to the relative motion of charged particles, strong currents will develop that could contribute to the chromospheric heating problem. We will apply a normal mode analysis for each region and obtain the dispersion relation of waves. The dispersion relations are solved numerically and their propagation characteristics will be investigated in terms of their propagation direction relative to the background magnetic field.

- **Chapter 5**: *Conclusions and future research prospect*: this chapter will contain the discussion of my results and suggestions on how my research can be expanded in the future.

CHAPTER 2
Mathematical formalism and particle collisions

Partially ionised plasmas are made up from electron, positive ions, and neutrals that interact through collisions. Since collisions play a key role in describing the dynamics at frequency ranges comparable to the collisional frequencies, the mathematical formalism of describing dynamics in partially ionised plasmas differs from the usual magnetohydrodynamics (MHD) approximation, valid for fully ionised plasmas. In this chapter I will introduce the multi-fluid equations that will be used in subsequent studies, I will discuss the problem of collisions between various particles and their collisional frequencies and will review the current understanding of waves in partially ionised solar plasmas.

2.1 Multi-fluid description of partially ionised plasmas

A description of the thermodynamic state and dynamics of plasma is based on a number of conservation laws all rooted in the statistical description of a plasma as an ensemble of particles under the influence of internal and external forces. As such, the most fundamental model developed is the kinetic description, where various parameters are understood as distributions. The dynamics of various species is obtained by solving the Boltzmann transport equation. Macroscopic quantities such as number densities, velocities, pressures can be obtained by integrating the distribution function of particles equation over velocity space. Although it is probably the most accurate description of the plasma, the kinetic theory involves complex mathematics. Many of the results prescribed by the kinetic theory can be obtained using, e.g. the MHD theory, which is based on macroscopic functions rather than distribution functions. In the MHD theory the plasma is considered as a fluid (a continuous medium), meaning that characteristic length scales are much larger than the

cyclotron radius of particles. The plasma is considered to be in thermodynamical equilibrium, i.e. characteristic times are much larger than the collisional time between the particles and length scales are longer than the mean free path. In general the MHD approximation is a low-frequency approximation, which means that the frequency at which it operates is much smaller than the gyro-frequencies of the electrons and ions, as well as the corresponding plasma frequencies defined as (assuming a hydrogen plasma)

$$\Omega_{Be,i} = \frac{|e|B}{m_{e,i}}, \quad \omega_{pe,i} = \left(\frac{n_{e,i}e^2}{\epsilon_0 m_{e,i}}\right)^{1/2}, \tag{2.1}$$

where e is the electron electric charge, B is the magnetic field, $m_{e,i}$ is the electron or ion mass, $n_{e,i}$ is the electron or ion number density and ϵ_0 is the electric permitivity of free space. The gyro-frequency is the frequency at which the charged particles gyrate around magnetic field lines and the plasma frequencies are the rates at which the charged particles react to changes in the electrostatic potential. It is clear that for a quasi-neutral H plasma

$$\frac{\Omega_{Be}}{\Omega_{Bi}} = \frac{m_i}{m_e} = \mu \approx 1836, \quad \frac{\omega_{pe}}{\omega_{pi}} = \mu^{1/2}. \tag{2.2}$$

The kinetic and fluid descriptions of a plasma are related, since the equations that describe the evolution of the fluid can be derived from the kinetic theory by taking velocity moments of the Boltzmann equation (Braginskii, 1965; Khomenko et al., 2014*a*). The existence of low frequency waves driven by magnetic tension predicted by the theoretical study by Alfvén (1949) can be considered to be the advent of ideal MHD, which later was evidenced later in laboratory plasma by, e.g. Lundquist (1949) and Jephcott (1959). Since then Alfvén waves were shown to propagate in various astrophysical plasmas, such as the Earth's atmosphere (Chmyrev et al., 1988), in planetary ionospheres (Berthold et al., 1960; Gurnett and Goertz, 1981), the interstellar medium (Arons and Max, 1975; Balsara, 1996), and in the solar atmosphere (Murawski and Musielak, 2010; Mathioudakis et al., 2013; Zaqarashvili et al., 2013; Ballai, 2020).

However, the mathematical formalism of ideal MHD is not accurate for higher frequency waves, which in the solar atmosphere could be driven by small-scale magnetic activity in the chromospheric network and reconnection of field lines (Axford and McKenzie, 1992; Tu and Marsch, 1997) or by cascading from low frequencies in the corona (Isenberg and Hollweg, 1983; Tu, 1987).

Ideal MHD assumes a simplified approach by treating the plasma as a fully ionized fluid, ignoring the effects related to neutral particles, neglecting the Hall term in the induction equation and considering all ionized species together as a single fluid. Such approximations are reasonable when the frequencies of the oscillations are much lower than the collision frequencies between the different species in the plasma. A plasma can be considered as a single fluid when the collisional coupling between various species is very strong. However, as we will show later, this approximation is not always accurate for solar plasmas.

When one deals with frequencies that are comparable with the collisional frequency of various constituent species (or, equivalently, when the relaxation time of collisions between species is comparable to the period of the waves), each species may react to perturbations in different time-scales and the collisional coupling is weaker, meaning that a multi-fluid description of the plasma is needed. The multi-fluid approach consists in a set of equations for each species of the plasma, with additional terms that describe the interactions between them. Traditionally, a multi-fluid model may be applicable up to frequencies of the order of the cyclotron frequencies. For an even higher frequency domain (of the order of the electron or ion plasma frequencies), a kinetic approach is needed. The current Thesis will discuss the dynamical behaviour of the plasma in the multi-fluid approach, characteristic to various regions in the solar atmosphere.

The equations that compose such model are detailed in this Chapter. However, before embarking in presenting these equations, it is necessary to discuss one of the key ingredients of the multi-fluid approach: the collisions between particles, as a mean of coupling mechanism and energy and momentum exchange between species.

2.2 Collision between particles in partially ionised plasmas

In partially ionised plasmas there are six basic types of particles that can interact: photons, electrons, ground-level atoms (or molecules), excited atoms (or molecules), positive ions and negative ions. Photons are characterised by their energy, $\epsilon_\nu = h\nu = hc/\lambda$, where ν is photon frequency, c is the speed of light, λ is the wavelength of a photon and h is Planck's constant. Photons are generated during recombination processes when an an energetic electron

is captured by a positive ion and the energy excess between the energy of the electron and the energy necessary to bond the electron is emitted as a photon. A photon can also be generated when an electron of an atom in excited state to a lower orbit. During the fall from high energy to low energy, the electron emits a photon with very specific characteristics. For example, the photon born during a decay of an electron from the $n = 3$ to the $n = 2$ energy level of a H atom emits a photon of wavelength of 656.28 nm in air that constitutes the famous Hα emission of the Balmer series, widely used in solar physics observations. While the energy of a bound electron is quantified, the energy of a free electron energy is given by its kinetic energy, $\epsilon_e = m_e w^2/2$, where w is the translation speed (often used on conjunction with the thermal speed). Free electrons are important for the process of ionisation and recombination, but also for the thermalisation of the plasma. In our analysis we will not deal with photons and excited atoms/molecules, meaning that we will neglect all photo-ionisation processes and all atoms will be considered to be in the ground state. Since we consider a H plasma, the positive ions will be just simply protons.

Collisions in partial ionised plasmas can be categorised whether these preserve the energy and momentum of colliding particles (elastic collisions) or not (inelastic collisions). During inelastic collisions the number density of the plasma's components is not conserved, leading to an ionisation non-equilibrium (see, e.g. Mitchner and Kruger Jr, 1973; Ballai, 2019). However, the consideration of inelastic collisions is beyond the scope of the present Thesis, and, therefore, will not be discussed.

Collisions between particles allow the ionised gas to be treated as a fluid. There are many types of collisions taking place in plasma, the most important for our purposes being the collisions between particles leading to an effective momentum transfer. Secondly, neutral atoms can lose or gain electrons through collisions (also called collisional ionisation) leading to ionisation, and its converse process called recombination. We should mention here that the ionisation process can occur only when the energy of the incoming particle is larger than the ionisation energy of electrons (for a H atom the ionisation energy is approximately 13.6 eV for an electron on the lowest orbit, and decreasing according to an $\sim n^{-2}$ law for higher orbit, where here n denotes the atomic energy level). Finally, collision between an ion and a neutral particle in which an electron is transferred, making the ion a neutral particle and the neutral particle an ion leads to the process of charge exchange that can be described by reactions of the type $A + A^+ \rightarrow A^+ + A$. Despite the collision

transfer, the momentum transfer (change of the speed of both particles) is usually small. Raizer (1991) showed that the charge exchange process is very fast and there is no energy exchange meaning that the particles have the same energy. In addition, the cross section and collision frequency related to charge exchange are larger than elastic scattering cross section and elastic collision frequency. (see Figure 2.1 for He, Ne and Ar).

Collisions between particles will take place if these interact through long and short range collisions, meaning that the collision of charged particles would involve a different model than the collision between charged particles and neutrals. A vigorous description of collisions between particles would require a cumbersome statistical physics description involving the Fokker-Planck formalism and the collision operators, however this is beyond the scope of present study. Instead, we refer to the works by Braginskii (1965) and Mitchner and Kruger Jr (1973) for a detailed presentation of this topic. Here we will restrict ourselves to just briefly describing the physical context, giving the expressions of the collisional frequencies between particles.

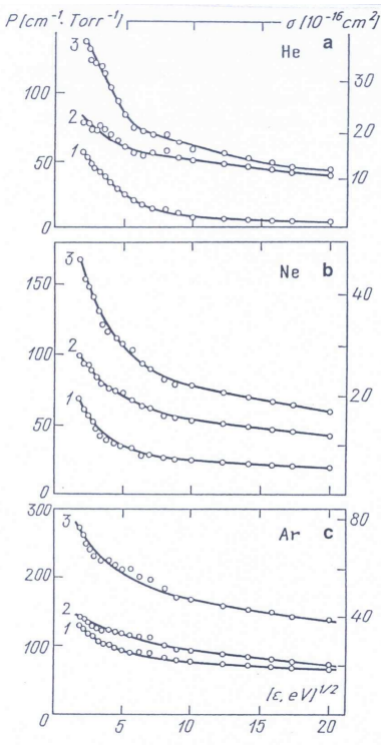

Figure 2.1: Collisional cross sections of atomic He, Ne and Ar. The curves labelled by 1 denote the collisional cross section corresponding to elastic scattering, the label 2 denote the same quantity but in the case of a charge exchange collisions, and label 3 denote the sum of them. Here 1 eV= 11,604 K. This plot was taken from Raizer (1991).

2.3 Collisional Frequencies

In a partially ionised plasma the collisions can be categorised into mutual collisions (collisions of particles of the same type) and inter-particle collisions (collisions of a particle with particles of a different species). Mutual collisions (e-e, i-i, n-n) do not imply transfer of energy and momentum between species, therefore these are important only for the internal energy of a particular species. In contrast, inter-particle collisions are essential for the transfer of energy and momentum and to the coupling of different fluids. In what follows, and throughout the present thesis, we will focus only on the later type of collisions.

The collision between charged particles (electron and ions) is controlled by electrostatic (Coulomb) forces and involve long-range collisions. On the other hand, the collision between neutrals and charged particles is a short-range collision that is described within the traditional dynamics approach (Krishan, 2016). Collisional frequency (or its inverse, the collisional time) is a physical quantity that can quantify the importance of particular type of collision. The collision frequency is the average number of collisions undergone by each particle per unit time, and so the average collision frequency in a stationary state depends on the velocity distribution functions of the colliding particles. In inhomogeneous plasmas, the collisions of particles affect the transport processes.

Considering species having the same temperature, the binary collisional frequencies between species α and α' can be given as (Zhdanov, 1962)

$$\nu_{\alpha\alpha'} = \frac{4}{3} n_{\alpha'} \left(\frac{8 k_B T}{\pi m_{\alpha\alpha'}} \right)^{1/2} \sigma_{\alpha\alpha'}, \tag{2.3}$$

where $n_{\alpha'}$ is the number density of species α', $\sigma_{\alpha\alpha'}$ is the collisional cross-section of the two species, k_B is the Boltzmann constant, T is temperature and $m_{\alpha\alpha'}$ is the reduced mass of colliding particles, defined as

$$m_{\alpha\alpha'} = \frac{m_\alpha m_{\alpha'}}{m_\alpha + m_{\alpha'}}.$$

Given that $m_n \approx m_i \gg m_e$, it is clear that

$$\frac{m_e m_i}{m_e + m_i} = \frac{m_e m_n}{m_e + m_n} \approx m_e, \quad \frac{m_i m_n}{m_i + m_n} \approx \frac{m_i}{2}.$$

Since our research interest is restricted to elastic collisions where the momen-

tum is conserved, we will consider that

$$m_\alpha n_\alpha \nu_{\alpha\alpha'} = m_{\alpha'} n_{\alpha'} \nu_{\alpha'\alpha}.$$

2.3.1 The electron collisional frequencies

Given their very low mass (compared to the mass of ions and neutrals), electrons cannot transfer much of their thermal energy as heat to the heavier plasma components, therefore the role of electrons in collisions is to ensure that the thermal equilibrium for the ensemble of particles is reached quickly. However, the collisions of electrons with the other particles has other, important, consequences for the electrical and thermal conductivity of the plasma. Coulomb collisions result in very poor energy transfer between electrons and ions. The rate of energy transfer is roughly m_e/m_i slower than the e-i collision frequency. Thanks to the huge difference between masses of electrons and ions, in case of stationary ions, the electron path is deviated as a result of the Coulomb potential of ions.

For the collision between charged particles, an electron will be affected by a neighbouring ion if the Coulomb potential is of the order (or more than) the electron thermal energy $3k_BT/2$. This defines a Coulomb interaction distance, r_C, e.g.

$$\frac{e^2}{4\pi\epsilon_0 r_C} \approx \frac{3}{2} k_B T,$$

With the help of this distance (often called the distance of the closest approach) we can define the collisional cross-section of collision between electrons and ions as

$$\sigma_{ei} = \pi r_C^2 \ln\Lambda \approx \pi \left(\frac{e^2}{6\pi\epsilon_0}\right)^2 \frac{1}{k_B^2 T^2} \ln\Lambda,$$

where

$$\ln\Lambda = 23.4 - 1.16 \log_{10} n_e + 3.45 \log_{10} T,$$

is the Coulomb logarithm, with n_e measured in cm^{-3} and T in K. The Coulomb logarithm is needed in the expression of the collisional cross section to account for the truncation related to small angle scattering, inherent in Coulomb-type collisions. Under solar atmospheric conditions the Coulomb logarithm takes values between 10 and 25.

With the help of this cross section, the collisional frequency between elec-

trons and ions becomes (Spitzer, 1962)

$$\nu_{ei} = \frac{4}{3} n_i \sigma_{ei} \left(\frac{8 k_B T}{\pi m_e} \right)^{1/2}, \tag{2.4}$$

where, m_e is the electron mass.

The electron-ion collisional cross-section is inversely proportional to the electron thermal speed, meaning that fast electrons contribute more to the relative motion rather than to the momentum transfer, since their collisionality is relatively low. Thus, it is natural that a fully ionised plasma at high temperature (e.g. solar corona) is nearly collisionless.

The collision between electrons and the neutral species is a head-on type of collision and the collisional frequency for this interaction can be given as

$$\nu_{en} = \frac{4}{3} n_n \sigma_{en} \left(\frac{8 k_B T}{\pi m_e} \right)^{1/2}, \tag{2.5}$$

where n_n is number density of neutrals and σ_{en} the collisional cross section between electrons and neutrals. In a recent study, Vranjes and Krstic (2013) calculated the electron-neutral cross section and the collision frequency of an electron colliding with other species in terms of the electron energy (temperature) and this variation is shown in Figure 2.2.

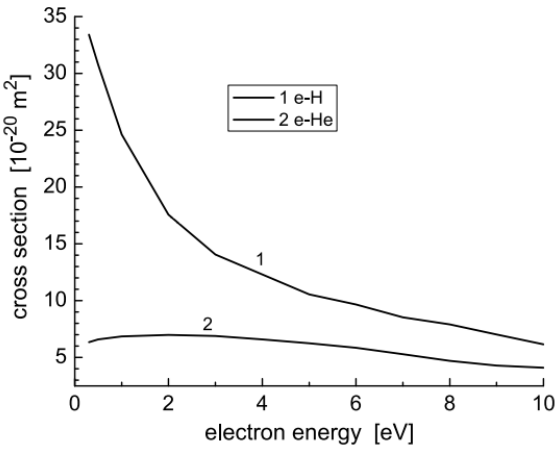

Figure 2.2: The collisional cross-section for electrons colliding with the neutral H (the curve labelled by "1" and He (the curve labelled by "2") in terms of the energy of electrons. Credit: Vranjes and Krstic (2013)

It is clear that for the energy relevant to the solar photosphere/cromosphere the collisional cross section between electrons and the neutral hydrogen has a dramatic change, however, in our study we consider the representative value

of $\sigma_{en} = 10^{-19}$ m^2.

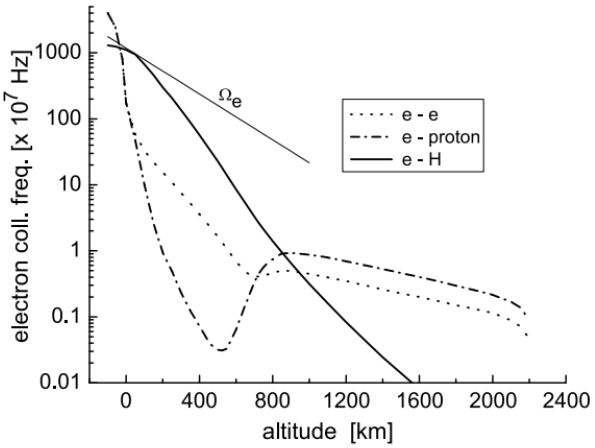

Figure 2.3: The collisional frequency (on logarithmic scale) for the collision of electrons with electrons (dotted line), with protons (dashed-dotted line) and neutral hydrogen (thick solid line) in terms of height in the solar atmosphere. The thin solid line represents the variation of the electron gyro-frequency assuming a simple, exponentially decaying magnetic field in the quiet Sun. Credit: Vranjes and Krstic (2013)

With the help of the collisional cross-section Vranjes and Krstic (2013) calculated the collisional frequency of electrons with other species and the variation of this quantity with height in the solar atmosphere is given by Figure 2.3.

Here we can see that at the base of the solar atmosphere the collisional frequency of ions with protons is above the electron gyro-frequency and it has a minimum around the base of the chromsophere.

2.3.2 The ion collision frequency

The collisions between ions and neutral hydrogen takes place between two massive particles (compared to electrons). The study by Stancil et al. (1998) considered the problem of collisions between these particles taking into account the quantum mechanical indistinguishability of the projectile and target. The variation of the cross-section of ion-neutral collisions for different types of collisions with the ion energy is shown in Figure 2.4. For our study we will concentrate only on the curve labelled by "2", as this corresponds to the type of interaction we are interested in. The oscillatory pattern in the cross-section is a consequence of quantum effects, which are present only at lowest collision energies (i.e. the photosphere and chromosphere).

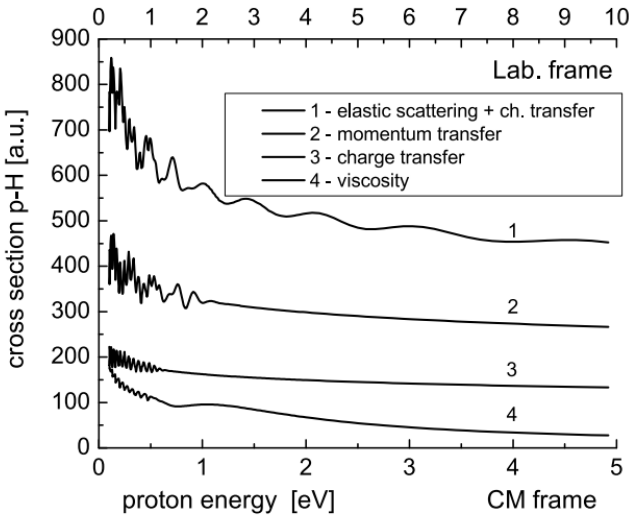

Figure 2.4: Integral cross section of ion-neutral collision in different interactions labelled by different numbers. Here 1 a.u.= 2.8×10^{-21} m^2. Adapted from Vranjes and Krstic (2013).

Following the results by Zhdanov (1962), the ion-neutral collisional frequency can be written as

$$\nu_{in} = \frac{4}{3} n_n \sigma_{in} \left(\frac{16 k_B T}{\pi m_i} \right)^{1/2}, \tag{2.6}$$

where σ_{in} is the ion-neutral collisional cross-section. Based on the results by Vranjes and Krstic (2013), for the collisional cross-section between ions and neutrals we adopt the characteristic value of 10^{-18} m^2 in the solar photosphere and 5×10^{-19} m^2 in the solar chromosphere.

2.4 Governing equations for a multi-fluid plasma

The investigation of the dynamics in a multi-fluid plasma requires the combination of the hydrodynamic equations that describe the evolution of each species in the plasma with Maxwell's equations, which prescribe the evolution of electromagnetic fields, and thermodynamic equation of state of each species. We assume that each species is in thermodynamic equilibrium, meaning that the distribution of particles for each species α obeys a Maxwellian distribution

$$f_\alpha = n_\alpha \left(\frac{m_\alpha}{2\pi k_B T_\alpha} \right)^{3/2} \exp\left(-\frac{m_\alpha \tilde{v}_\alpha}{2 k_B T_\alpha} \right), \tag{2.7}$$

where n_α, m_α, and T_α are the number density, mass and temperature of the species α. The quantity $\tilde{v}_\alpha$ is the random part of the velocity, defined as $\tilde{v}_\alpha = v_\alpha - u_\alpha$, where u_α is the average velocity. Given the much lower mass of electrons, the distribution function of ions and neutrals is much narrower than the distribution function of electrons.

The set of governing equations are obtained by taking velocity moments of the Boltzmann equation, and integrating over velocity space. Given the complexity of calculations and because these are not within the scope of the present Thesis, the details of these derivations are not given, instead we refer the interested reader to the study by Khomenko et al. (2014*a*).

The equation for the mass conservation (also known as mass continuity equation) for each species, can be given as

$$\frac{D\rho_\alpha}{Dt} + \rho_\alpha \nabla \cdot \mathbf{v}_\alpha = 0, \tag{2.8}$$

where $D/Dt = \partial/\partial t + \mathbf{v} \cdot \nabla$ is the convective derivative and $\rho_\alpha = n_\alpha m_\alpha$ is the mass density of the species α. This equation also stipulates that in equilibrium mass cannot be created or destroyed. In an ionisation non-equilibrium plasma the zero on the right-hand side of the above equation is replaced by the rates of ionisation and recombination that takes place during the investigated time-scale (Maneva et al., 2017; Ballai, 2019).

The equilibrium of forces acting on a unit volume plasma element in ionisation equilibrium is described by the momentum equations written for each species in the form

$$\rho_\alpha \frac{D\mathbf{v}_\alpha}{Dt} = -\nabla p_\alpha + \rho_\alpha \mathbf{g} + q_\alpha n_\alpha (\mathbf{E} + \mathbf{v}_\alpha \times \mathbf{B}) + \sum_{\alpha \neq \alpha'} \mathbf{P}_{\alpha\alpha'}, \tag{2.9}$$

where p_α is the kinetic pressure of species α (assumed isotropic), $\mathbf{g}$ is the constant gravitational acceleration, q_α is the elementary charge ($-e$ for electrons and e for ions), $\mathbf{E}$ and $\mathbf{B}$ are the electric and magnetic fields, respectively.

The collisional term in the above equation ($\mathbf{P}_{\alpha\alpha'}$) describing the momentum exchange between the species α and α' will play a key role in our research. For binary collisions between the species α and $\alpha\prime$ the general form can be given as (Zhdanov, 1962)

$$\mathbf{P}_{\alpha\alpha'} = -n_\alpha m_{\alpha\alpha'} \nu_{\alpha\alpha'} (\mathbf{v}_\alpha - \mathbf{v}_{\alpha'}), \tag{2.10}$$

where n_α is the number density of species α, $\nu_{\alpha\alpha'}$ is the collisional frequency

between the two species discussed earlier in Section 2.3.

The last relation that can be derived from the Boltzmann equation is the energy conservation equation that can be written as

$$\frac{D}{Dt}\left(\frac{p_\alpha}{\rho_\alpha^\gamma}\right) = 0, \tag{2.11}$$

where γ is the ratio of specific heats, or the adiabatic index (taken to be $5/3$ for monoatomic H). The above equation implies that there are no additional energy sources and/or sinks in the system. Strictly speaking, all transport mechanisms considered in our Thesis results in some sort of energy loss, however these terms will appear as squares of perturbed quantities, which in the linear approximation employed by us, will be considered negligibly small. For a detailed derivation of the terms that could appear in the right-hand side of the above equation, (see, e.g. Ballester et al., 2018*a*; Braileanu et al., 2019).

2.5 Maxwell's Equations

Maxwell's equations is a set of four electrodynamics equations that describe the characteristics and development of electric and magnetic fields. These relationships may be represented in a variety of theoretically comparable ways, but the differential formulation, which is provided by the following equations, is the most helpful for the purposes of our Thesis:

$$\nabla \times \mathbf{B} = \mu_0 \mathbf{J} + \frac{1}{c^2}\frac{\partial \mathbf{E}}{\partial t}, \tag{2.12}$$

$$\nabla \cdot \mathbf{B} = 0, \tag{2.13}$$

$$\frac{\partial \mathbf{B}}{\partial t} = -\nabla \times \mathbf{E}, \tag{2.14}$$

$$\nabla \cdot \mathbf{E} = \frac{\rho^*}{\epsilon_0}, \tag{2.15}$$

where $\mathbf{J}$ is the current density, $\rho^* = \sum_\alpha q_\alpha n_\alpha$ is the charge density, μ_0 and ϵ_0 are the magnetic permeability and electric the permittivity of free space, and $c = 1/\sqrt{\mu_0 \epsilon_0}$ is the speed of light.

Equation 2.12 is known as Ampére's law, and it stipulates that the magnetic field can be produced by an electric current and time changing electric field. Since the speed of light is much larger than plasma velocity we will deal with, the second term in right hand side of equation 2.12 (called the dis-

placement current) is neglected. One important consequence of neglecting the displacement current is that the model employed by us will not consider the presence of electromagnetic waves.

Equation 2.13 is the solenoidal equation and imposes the impossibility to have magnetic monopoles, and that the total magnetic flux through a closed surface is zero. This equations also prescribes the topology of the magnetic field so that the magnetic field lines are closed.

Equation 2.14 is the Faraday's law and it states that the time varying magnetic field can create an electric field. Finally, equation 2.15 is the Gauss's Law and specifies that an electric field may be induced by charge density and the electric flux through a surface is proportional to the total charge enclosed by the surface. Contrary to the magnetic field, the electric field lines are directed in a radial direction and they are open.

2.6 Generalised Ohm's law and the induction equation

In ideal MHD, the electric field becomes a secondary variable that is obtained from Ohm's law for a perfectly conducting fluid. According to this law the electric field in a frame moving with the fluid vanishes, meaning that if $\mathbf{E}'$ is the electric field in a co-moving reference system, then

$$\mathbf{E}' = \mathbf{E} + \mathbf{v} \times \mathbf{B} = \mathbf{0} \longrightarrow \mathbf{E} = -\mathbf{v} \times \mathbf{B}.$$

Ohm's law states that the electric field is proportional to electric current, also there is an additional electric field if the plasma moving with velocity $\mathbf{v}$ in the presence of magnetic field. The generalised Ohm's law can be calculated using the momentum equation (2.9) written for electrons. Neglecting gravitational effects, this equation can be written as

$$\rho_e \frac{\partial \mathbf{v}_e}{\partial t} + \nabla \cdot (\rho_e \mathbf{v}_e \mathbf{v}_e) + \nabla p_e = -e n_e (\mathbf{E} + \mathbf{v}_e \times \mathbf{B}) + \sum_{s \neq e} \mathbf{P}_{es}. \tag{2.16}$$

Since the mass of electrons is very small, the variations of momentum of electrons are considered to be negligible, therefore, the first two terms of the above equation can be neglected. As a consequence, the electric field can be expressed

as

$$\mathbf{E} = -\mathbf{v}_e \times \mathbf{B} - \frac{\nabla p_e}{e n_e} + \frac{1}{e n_e} \sum_{s \neq e} \mathbf{P}_{es}. \tag{2.17}$$

The electron velocity can be eliminated from this equation using the expression of current defined as $\mathbf{J} = e n_e (\mathbf{v}_i - \mathbf{v}_e)$, so

$$\mathbf{v}_e = \mathbf{v}_i - \frac{\mathbf{J}}{e n_e}.$$

Let us now write the collisional term as $\mathbf{P}_{es} = \alpha_{es}(\mathbf{v}_s - \mathbf{v}_e)$, where the quantity α_{es} is the friction coefficients between electrons and the other species, s. As a result, the electric field becomes

$$\mathbf{E} = -\mathbf{v}_i \times \mathbf{B} + \frac{\mathbf{J} \times \mathbf{B}}{e n_e} - \frac{\nabla p_e}{e n_e} + \eta \mathbf{j} + \frac{1}{e n_e} \sum_{s \neq e} \alpha_{es}(\mathbf{v}_s - \mathbf{v}_i). \tag{2.18}$$

The quantity η is the resistivity coefficient (or magnetic diffusivity) and it is defined as

$$\eta = \frac{1}{(e n_e)^2} \sum_{s \neq e} \alpha_{es},$$

and describes the Ohmic diffusion due to the collision of electrons with ions and neutrals. Finally, combining the above equation with the Faraday's and Ampére's law, we arrive at the induction equation

$$\frac{\partial \mathbf{B}}{\partial t} = \nabla \times \left[\mathbf{v}_i \times \mathbf{B} - \frac{(\nabla \times \mathbf{B}) \times \mathbf{B}}{e n_e \mu_0} - \frac{\eta}{\mu_0} \nabla \times \mathbf{B} - \frac{1}{e n_e} \sum_{s \neq e} \alpha_{es}(\mathbf{v}_s - \mathbf{v}_i) \right] + \\ + \nabla \times \left(\frac{\nabla p_e}{e n_e} \right). \tag{2.19}$$

The first term in the right-hand side of the above equation is the convective term. If only this term is taken into account, the resulting expression corresponds to the induction equation of a perfectly conducting fluid or ideal induction equation where the magnetic field lines move with the fluid, i.e. they are said to be "frozen" in the plasma. As a result, only motion transverse to the magnetic field lines can modify the existing magnetic field.

All subsequent terms in equation 2.19 describe a departure from the ideal, frozen-in situation. The second term on the right-hand side is the well-known Hall term. When this term is important, ions are not completely frozen to the magnetic field and may have a different dynamics than electrons. When a perturbation is applied to the plasma, the smaller inertia of electrons can

cause these particles to follow more easily the perturbations of the magnetic field, compared to ions. In fully ionized plasmas, the Hall term describes a differentiation in the properties of the left-handed and right-handed circularly polarized waves. This effect grows when the wave frequency approaches the cyclotron frequencies of ions but can be neglected when the frequency of oscillations is much smaller. In general the Hall term introduces a new length-scale into the problem that is of the order of the ion inertial length (or ion skin depth). Therefore, the Hall term introduces an additional dispersion of waves. In partially ionized plasmas, the presence of neutrals increases the importance of Hall's effect, specially in weakly ionized plasmas (Pandey and Wardle, 2006).

The next term on the right-hand side of equation 2.19 is the resistive term and its relevance can be determined by carrying out a dimensional analysis of the convective and resistive term. Assuming that the characteristic values of speeds, magnetic fields and lengths are denoted by v_0, B and L, then the convective and resistive terms scale as

$$\left|\nabla \times \mathbf{v}_i \times \mathbf{B}\right| \sim \frac{v_0 B}{L}, \quad \left|\nabla \times \left(\frac{\eta}{\mu_0}\nabla \times \mathbf{B}\right)\right| \sim \frac{\eta B}{\mu_0 L^2}.$$

The ratio of these two scalings results in the magnetic Reynolds number, R_m, defined as

$$R_m = \frac{\mu_0 L v_0}{\eta}.$$

Resistive effects are important in a plasma if the resistive term becomes comparable to the convective term, i.e. when $R_m \sim 1$. Since the resistivity coefficient in solar plasmas is typically very small, important resistive effects appear for small values of L (or steep gradients), i.e. large wavenumbers, as discussed later in the present Thesis when dealing with waves in weakly ionised plasmas.

The next term in the induction equation describes an attenuation of the magnetic field due to the velocity difference in the species and it is a term that appears strictly in partially ionised fluids. Finally, the last term on the right-had side of the induction equation is the Biermann battery term and it is relevant only in those cases when there is a strong electron pressure gradient. The battery term was recently used in the study by Khomenko et al. (2017) to show that in the presence of strong electron pressure, local imbalances in the partially ionized solar photospheric plasmas can generate micro Gauss fields, that superimposed on the dynamo amplification, leads to the generation of quiet Sun magnetic fields of a similar strength to those from solar observations. However, in general, under solar physics conditions, the Biermann battery term

is neglected.

2.7 Prefect Gas Law

Finally the equations that describe the dynamics in partially ionised plasmas can be closed by a relation that connects the thermodynamic quantities, such as pressure, temperature and number density. In reality the interaction between particles can introduce alterations that would imply the treatment of the plasma as a non-ideal gas. It is known that at intermediate pressures and low temperatures, attractive forces pull the particles together so the pressure is less than for an ideal gas under the same set of conditions. At low pressure and high temperatures (as in the solar atmosphere) these effects are far weaker, therefore the use of ideal gas laws for each species is perfectly justified, and they read

$$p_e = p_i = n_i k_B T, \quad p_n = n_n k_B T. \tag{2.20}$$

These relations can be derived using the kinetic theory of gases (Khomenko et al., 2014*a*).

2.8 From three-fluid to two-fluid description

In reality, the use of the right multi-fluid approximation to describe the dynamical state of the plasma depends very much on the relative strengths of collisions between particles. While in the solar photosphere the use of a three-fluid plasma is perfectly justified (see Chapter 4), in the chromosphere the very strong coupling of charged particles renders the plasma to be a two-fluid system, where the fluid of charged particles can interact with the neutral fluid (see Chapter 3). The physical reasoning for each working framework will be given later.

In the solar chromosphere the collisional coupling between charged particles is much higher than with neutrals, therefore, it makes sense to treat the charged particles as one single fluid that can interact with the neutral fluid (for justification based on the VAL IIIC solar atmospherics model, see Chapter 4). This assumptions considerably simplifies the mathematical model. Since the present Thesis employs the equations relevant to a two-fluid description, it is natural to introduce these equations.

The mass, momentum, and energy equations for electrons and ions can be combined to arrive to the equations describing the charged species, here

denoted by the index "c". Consequently, the continuity equation of electron and ion particles can be reduced to

$$\frac{D\rho_c}{Dt} + \rho_c \nabla \cdot \mathbf{v}_c = 0, \tag{2.21}$$

where $\rho_c = \rho_e + \rho_i$ is the total density of charged particles and

$$\mathbf{v}_c = \frac{\rho_e \mathbf{v}_e + \rho_i \mathbf{v}_i}{\rho_e + \rho_i},$$

is the center of mass velocity.

Let us recall that the momentum equations for electrons and ions read

$$\rho_e \frac{D\mathbf{v}_e}{Dt} = -\nabla p_e + \rho_e \mathbf{g} - e n_e (\mathbf{E} + \mathbf{v}_e \times \mathbf{B}) + P_e, \tag{2.22}$$

$$\rho_i \frac{D\mathbf{v}_i}{Dt} = -\nabla p_i + \rho_i \mathbf{g} + e n_e (\mathbf{E} + \mathbf{v}_i \times \mathbf{B}) + P_i. \tag{2.23}$$

Since we are dealing with a quasi-neutral plasma ($n_e = n_i$), the equation for the velocity of the center of mass can be rewritten as

$$\mathbf{v}_c = \frac{m_e \mathbf{v}_e + m_i \mathbf{v}_i}{m_e + m_i} \approx \mathbf{v}_i + \frac{m_e}{m_i} \mathbf{v}_e, \tag{2.24}$$

where we took into account that $m_e \ll m_i$.

When the convective derivatives on the left-hand sides of equations 2.22 and 2.23 are expanded, one has to add together the nonlinear terms $\rho_e(\mathbf{v}_e \cdot \nabla)\mathbf{v}_e$ and $\rho_i(\mathbf{v}_i \cdot \nabla)\mathbf{v}_i$.

We can rewrite equation 2.24 in terms of $\mathbf{v}_i$ and then substitute this expression into the sum of the nonlinear terms to obtain $\approx m_i(\mathbf{v}_c \cdot \nabla)\mathbf{v}_c$. In all our subsequent calculations this term will be neglected, since we are restricting our analysis to linear, small amplitude, motion.

Adding together equations 2.22 and 2.23, and using the expression of the center of mass velocity, we obtain the momentum equation for the charged particles in the form

$$\rho_c \frac{D\mathbf{v}_c}{Dt} = -\nabla p_c + \mathbf{J} \times \mathbf{B} + \rho_c \mathbf{g} + \rho_{0c}(\nu_{en} + \nu_{in})(\mathbf{v}_c - \mathbf{v}_n), \tag{2.25}$$

where $p_c = p_e + p_i$ is the total pressure of the charged fluid and the current density, $\mathbf{J}$, was defined earlier. For neutral fluid, the momentum equation

transforms into

$$\rho_{0n}\frac{\partial \mathbf{v}_n}{\partial t} + \nabla p_n = \rho_n \mathbf{g} - \rho_{0n}\nu_{nc}(\mathbf{v}_n - \mathbf{v}_c). \tag{2.26}$$

The Ohm's law can be obtained by multiplying equation 2.22 by m_e and equation 2.23 by m_i. Neglecting gravitational effects and taking into account that since $m_e \ll m_i$, the terms related to the inertia of electrons are negligibly small, we arrive at

$$\mathbf{E} + \mathbf{v}_c \times \mathbf{B} + \frac{1}{en_i}\nabla p_e = \frac{m_i}{n_i}\mathbf{J} \times \mathbf{B} + \frac{\rho_{0c}}{en_i}(\nu_{ei} + \nu_{en})(\mathbf{v}_c - \mathbf{v}_n). \tag{2.27}$$

By using Faraday's law, the above equation reduces to the well-known induction equation

$$\frac{\partial \mathbf{B}}{\partial t} = \nabla \times (\mathbf{v}_c \times \mathbf{B}) - \nabla \times (\eta \nabla \times \mathbf{B}) + \nabla \times \left(\frac{c\nabla p_e}{en_i}\right)$$
$$- \nabla \times \left(\frac{\mathbf{j} \times \mathbf{B}}{en_e}\right) + \nabla \times \left[\frac{c\alpha_{en}(\mathbf{v}_c - \mathbf{v}_n)}{en_i}\right]. \tag{2.28}$$

The meaning of the terms in the induction equation are similar to the ones presented already earlier (see equation 2.19).

Finally, the energy equation of charge species reduces to

$$\frac{D}{Dt}\left(\frac{p_c}{\rho_c^{\gamma}}\right) = 0. \tag{2.29}$$

The governing equations of two fluid approximation are the continuity equations 2.8 and 2.21, the momentum equations 2.25 and 2.26, the induction equation 2.28 and the energy equations 2.11 and 2.29.

2.9 Waves in Partially Ionised Plasma

Although the plethora of waves able to propagate in partially ionised plasma is far richer that in the case of fully ionised plasmas, here we will restrict our attention only to Alfvén and magnetoacoustic waves, highlighting the major differences in the properties of waves compared to their fully ionised counterparts. In general the studies we are going to review employed a single or a two-fluid approximations.

Waves in plasmas appear as a response of a restoring force (magnetic tension, pressure force, gravity, etc.) to a perturbation. Each type of the restoring

force (or their combination) will generate its own type of waves, with different properties.

2.9.1 Alfvén Waves

When the restoring force to plasma disturbances is the magnetic tension, magnetic waves are able to propagate along the magnetic field lines. These waves are known as the Alfvén waves, and they have been predicted by Hannes Alfvén (Alfvén, 1942).

Alfvén waves are transversal waves that do not perturb the plasma density. In general is rather difficult to detect them, because they can only be seen in solar spectra in the emission coming from atoms in the solar atmosphere. However, recent high-resolution observations provided evidence for their existence in solar plasmas (e.g. Jess et al., 2009; McIntosh et al., 2011; Srivastava et al., 2017; Kohutova et al., 2020; Stangalini et al., 2021, etc.). Majority of these observational studies overlooked the fact that Alfvén waves observed in the lower layers of the solar atmosphere might be affected by partial ionisation. The study by Ballai (2020) has shown, for the first time, how torsional Alfvén waves can be used to determine the ionisation degree of the plasma.

Alfvén waves in partially ionised plasmas show a much more complicated picture than their counterparts in fully ionised plasmas. In a fully ionised plasma Alfvén waves can be described within the framework of ideal MHD, where the magnetic field is frozen into the conducting charged fluid. In partially ionised plasmas the magnetic field is not frozen into any of the electron or ion fluid. The Hall term breaks the degeneracy of the electron and ion fluid. The governing equations describing the dynamics in partially ionised plasmas are dissipative in nature (due to the collisional coupling between species), so these waves are rather short lived waves, propagating with frequencies that are comparable with the collisional frequency between particles.

Unlike in fully ionised plasmas, Alfvén waves propagating in partially ionised plasma possess a cut-off wavenumber. Using a single and two-fluid approximation Zaqarashvili et al. (2012) and Soler et al. (2013*a*) derived the dispersion relation of Alfvén waves propagating in a homogeneous partially ionised plasma along a magnetic field oriented in the z-direction by applying a normal mode analysis in the form

$$s^3 + i\,(1+\chi)\,\nu_{ni}\omega^2 - k_z^2 c_A^2 s + \nu_{ni} k_z^2 c_A^2 = 0, \tag{2.30}$$

where $\chi = n_n/n_i$ and the variable s is defined as $s = -i\omega$, with ω being the frequency of waves, k_z the longitudinal waveneumber and $v_A = B_0/\sqrt{\mu_0\rho_0}$ is the Alfvén speed.

Equation 2.30 is a cubic polynomial, whose discriminant, Λ_d, is given by

$$\Lambda_d = -k_z^2 v_A^2 \left[4\nu_{ni}^4(1+\chi)^3 - (\chi^2 + 20\chi - 8)\nu_{ni}k_z^2 v_A^2 + 4k_z^4 v_A^4\right]. \tag{2.31}$$

Depending on the sign of Λ_d, different type of solutions can be found, so that $\Lambda_d < 0$ corresponds to a regime where the dispersion relation admits a real and two complex roots, while when $\Lambda_d > 0$, the dispersion relation has three distinct real roots. The location when the nature of the solutions changes, corresponds to $\Lambda_s = 0$, results in two values of the wavenumber, and their expressions are given by

$$k_z^{\pm} = \frac{\nu_{ni}}{v_A}\left[\frac{\chi^2 + 20\chi - 8}{8(1+\chi)^3} \pm \frac{\chi^{1/2}(\chi-8)^{3/2}}{8(1+\chi)^3}\right]^{-1/2}. \tag{2.32}$$

The analysis by Soler et al. (2013*a*) showed that the two values of the wavenumber ($k_z^{\pm}$) correspond to the two cut-off values.

When $k_z > k_z^-$ the magnetic tension makes ions to oscillate almost freely, since the friction force is not strong enough to transfer significant inertia to neutrals. In this case, disturbances in the magnetic field affect only the ionized fluid as in the case of classic Alfvén waves in fully ionized plasmas. On the other hand, when $k_z < k_z^+$, the ion-neutral coupling is strong enough for neutrals to be nearly frozen into the magnetic field. When the system is perturbed, neutrals are dragged by ions almost instantly and both species oscillate together as a single fluid. When the wavenumber is between the two cut-off values, the disturbance in the magnetic field decays before the ion-neutral coupling has had time to transfer the restoring properties of magnetic tension to the neutral fluid. Therefore, neutral-ion collisions are mainly used to attenuate the magnetic field perturbations, however, they do not ensure an efficient transfer of inertia to neutrals.

In the absence of collisions the dispersion relation 2.31 reduces to

$$\omega^2 - k_z^2 v_A^2 = 0, \tag{2.33}$$

which is dispersion relation of Alfvén wave in ideal fluid.

The same authors compared the analytical and numerical solutions by solving the dispersion relation 2.30 numerically and they confirmed that the nu-

merical result is agreement with analytical one (see Figure 2.5, the solid line related to numerical result while symbols related to analytical result).

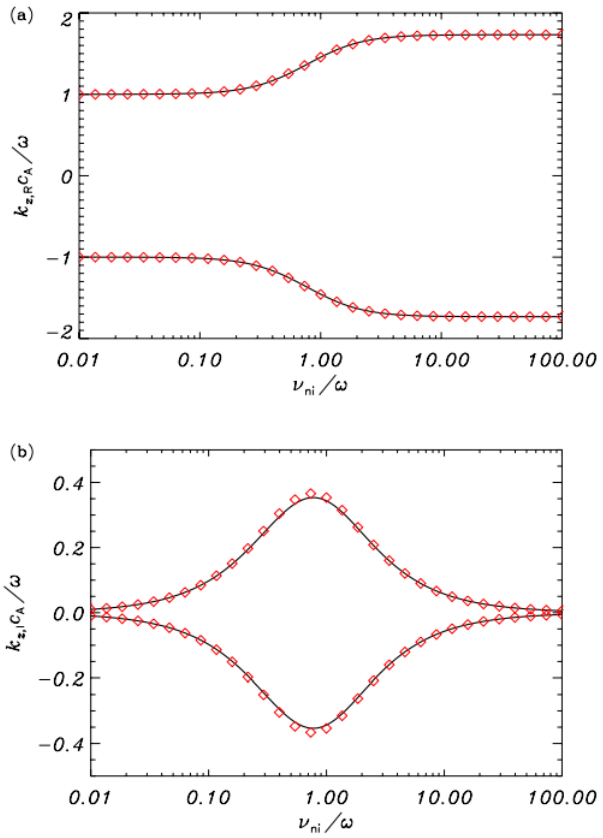

Figure 2.5: The variation of analytical and numerical results of dispersion relation 2.30 when $\chi = 2$ in terms of the dimensionless collisional frequency between neutrals and ions. The two panels display the variation of the real (upper panel) and imaginary parts (lower panel) of the solutions, respectively. Solid lines correspond to the numerical results, while symbols correspond to the analytic approximations. This figure was adapted from Soler et al. (2013*a*).

These figures show that the damping rates derived in the two-fluid approach reach a peak near the ion-neutral collision frequency and then decrease for higher frequencies unlike the single-fluid approach, where the damping increases linearly with increasing frequency, as shown in the study by Zaqarashvili et al. (2011*a*).

The study by Soler et al. (2013*a*) also performed an initial value study of Alfvén waves and they showed that these waves decay with a damping time

$$t_d \approx \frac{1}{\nu_{in}} \frac{k_z^2 v_A^2 + (1+\chi)\nu_{ni}^2}{k_z^2 v_A^2 + (1+\chi)^2 \nu_{ni}^2},$$

which confirms the result that damping times are (in the first order approx-

imation) of the order of the collisional frequency between particles. Furthermore, in the weakly collisional limit, the vorticity perturbations of the ionized and neutral fluids are decoupled from each other. Excited waves propagating weakly damped along the field oscillate with a frequency $k_z v_A$, and a damping time proportional to $1/\nu_{ni}$. On the other hand, disturbances in the neutral fluid are evanescent in time because, due to the weak coupling between particles, there is no driving force for the motions in the neutral fluid.

In the limit of strong collisions the oscillations in the two fluids tend to couple each other (almost like a single fluid), propagating with a frequency $k_z v_A/\sqrt{1+\chi}$ and decay exponential in time with a decay time proportional to $(\nu_{in}+\nu_{ni})^{-1}$.

Later, Ballai (2019) studied the properties of Alfvén waves in a partially ionised plasma in ionisation non-equilibrium. His results suggest that ionisation non-equilibrium waves could damp even in the collisionless limit, and this result can have serious consequences for the evolution of Alfvén waves in plasmas where the collision between particles is very weak (solar wind, Earth's atmosphere, etc). Furthermore, Ballai (2020) investigated the diagnostic of plasma ionisation using torsional Alfvén waves. Using observational data he found that the number of neutrals in the solar prominence fibrils is about 5×10^{10} cm^{-3}.

Alfvén waves in partially ionised plasmas have also been studied within the context of plasma heating. Dong and Paty (2011) found that the non-resonant Alfvén waves in partially ionized plasma are important for heating as long as the ion-neutral collisional frequency becomes comparable to the ion cyclotron frequency.

2.9.2 Magnetoacoustic Waves

Magnetoacoustic waves in partially ionised plasmas can be divided into two types, similar to their fully ionised counterparts: fast and slow. However, the number of modes and the way they couple is very specific to the partially ionised plasma environment. Magnetoacousic modes are driven by the combination of pressure forces and magnetic tension. In the absence of magnetic field the slow wave disappears and fast wave reduces to sound wave.

Forteza et al. (2007) studied the propagation of linear waves in single-fluid partially ionized plasma considering the effect of ambipolar diffusion. These authors found that the most affected wave is the fast wave, which damps more heavily and this strongly depends on the ionisation degree of the plasma.

Later, Carbonell et al. (2010) investigated the same problem in the presence of plasma flows, modelling the propagation and damping of waves in solar prominences. Their results show that the strong damping of fast and Alfvén waves depends on the joint action of flow and resistivity. The damping lengths of adiabatic fast and slow waves are strongly affected by partial ionisation. The properties of adiabatic fast waves are similar to the properties of Alfvén waves. In the case of non-adiabatic slow waves, the wavelength and damping length are comparable with the values obtained from the observations of prominence oscillations.

Later, Ballester et al. (2018*b*) addressed the problem of heating or cooling in optically thin partially ionised plasmas. In this case the period, damping time and cut-off wavenumber of Alfvén waves became time dependent quantities. The attenuation rate of waves was shown to be different in a cooling or heating process. Although the properties of slow waves in a cooling partially ionised plasma are very similar to the slow waves in fully ionised plasma, the period and damping time of these waves in both plasmas are completely different when the plasma is heated. The temporal behaviour of the Alfvén and fast wave is very similar in the cooling case, but in the heating case, an important difference appears in the temporal damping of waves.

Magnetoacostic waves have also been studied in two-fluid approximation, i.e. when the frequency of waves is comparable with the collisional frequency between particles. In this framework there are two slow waves associated to charged particles and neutrals, and one fast mode. The existence of this richer spectrum compared to fully ionised plasmas is very easy to understand. Slow waves are acoustic in nature, connected to the compressibility of the plasmas. That is why, it is natural to have two slow waves. In contrast, fast waves are Alfvénic in nature, meaning that these waves are connected to the charged species, i.e. the species that is affected by the presence of the magnetic field. Of course, the properties of these waves are not strictly linked to a species, instead their properties are modified by the existence of the other species.

Zaqarashvili et al. (2011*b*) investigated the MHD waves in two-fluid plasma under solar atmospheric conditions. The authors applied the Fourier analysis for the system of two-fluid MHD equations, which resulted in a seventh order dispersion relation describing the 3 pairs of waves propagating in opposite direction and one entropy, non-propagating mode. In the case of parallel propagation, taking $\chi = 0.5$, these authors found that the three waves are propagating only for large wavenumbers with strong damping rate. The slow

mode associated to neutrals disappears for small wavenumbers, because at strong coupling between ions and neutrals, the two fluids behave like a single fluid (see Figure 2.6).

In the low frequency two-fluid approximation, the frequencies and damping rate are similar to single-fluid approximation while they are different in high frequency two-fluid description. They also found that the maximum damping rate of fast waves is larger than the ion-neutral collisional frequency. The authors confirmed that the damping rate of slow mode in low plasma β regime is the same one was obtained by Braginskii (1965) (see Figure 2.7).

The problem of wave propagation in two-fluid plasmas has been reconsidered later by Soler et al. (2013*b*). These authors determined the modification of the waves' frequency due to the collision between particles and then studied the frictional damping during ion-neutral collisions. Using a normal mode analysis, the two-fluid MHD equations were reduced to the system of coupled equations

$$\left(\omega^4 - \omega^2 k^2 (c_i^2 + v_A^2) + k_z^2 k^2 c_i^2 v_A^2\right) \Delta_i = -i\nu_{in}\omega^3(\Delta_i - \Delta_n)$$

$$+ \frac{i\nu_{in}}{\omega + i(\nu_{ni} + \nu_{in})} v_A^2 k_z^2 k^2 (c_i^2 \Delta_i - c_n^2 \Delta_n), \tag{2.34}$$

$$(\omega^2 - k^2 c_n^2)\Delta_n = -i\nu_{ni}\omega(\Delta_n - \Delta_i), \tag{2.35}$$

where $k^2 = k_x^2 + k_y^2 + k_z^2$, $c_i = \gamma p_i/\rho_i$, $c_n = \gamma p_n/\rho_n$ and the quantities Δ_i and Δ_n are describing the compressibility of the charged and neutrals fluids, and are given by

$$\Delta_i = \nabla \cdot \mathbf{v}_i = ik_x v_{x,i} + ik_y v_{y,i} + ik_z v_{z,i},$$

$$\Delta_n = \nabla \cdot \mathbf{v}_n = ik_x v_{x,n} + ik_y v_{y,n} + ik_z v_{z,n}.$$

The authors studied analytically the solutions of the dispersion relation in the two limiting cases corresponding to the uncoupled plasma (collisions between particles is neglected), and the case of strongly coupled plasma, where the collisional frequencies tend to infinity. In the uncoupled case the solutions of the dispersion relation are the acoustic mode corresponding to neutrals, and two magnetoacoustic modes (slow and fast) associated to the charged species. In the strongly coupled case there are only two propagating waves, i.e. the modified slow and fast magnetoacoustic modes. The mode corresponding to the neutral species is absent because they became entropy modes. The neutral acoustic mode and the charged magnetoacoustic modes interact in the presence

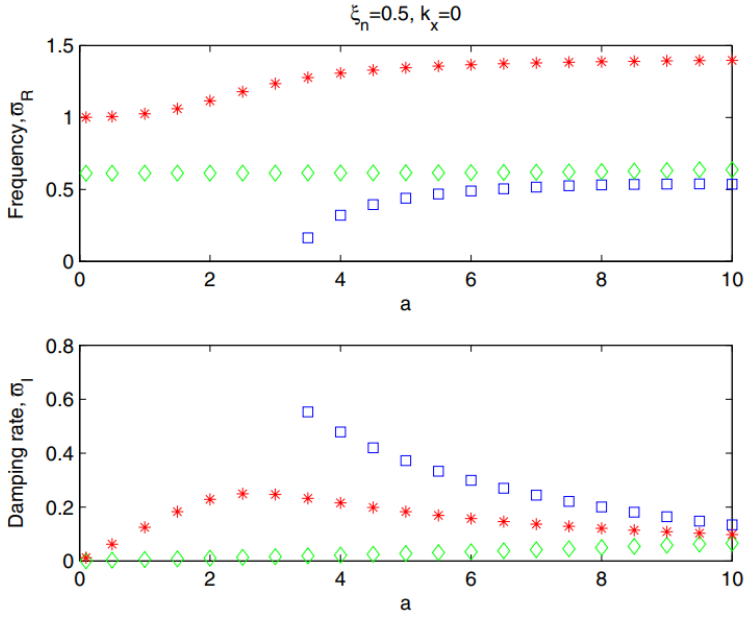

Figure 2.6: The magnetoacoustic modes propagating along the magnetic field, when $\chi = 0.5$. The red asterisks and green diamonds correspond to fast and slow modes associated to ions. Blue squares denote the slow mode associated to neutrals that appear only for large wavenumbers. The two panels show the real and imaginary parts of the solutions. This figure was taken from Zaqarashvili et al. (2011*b*).

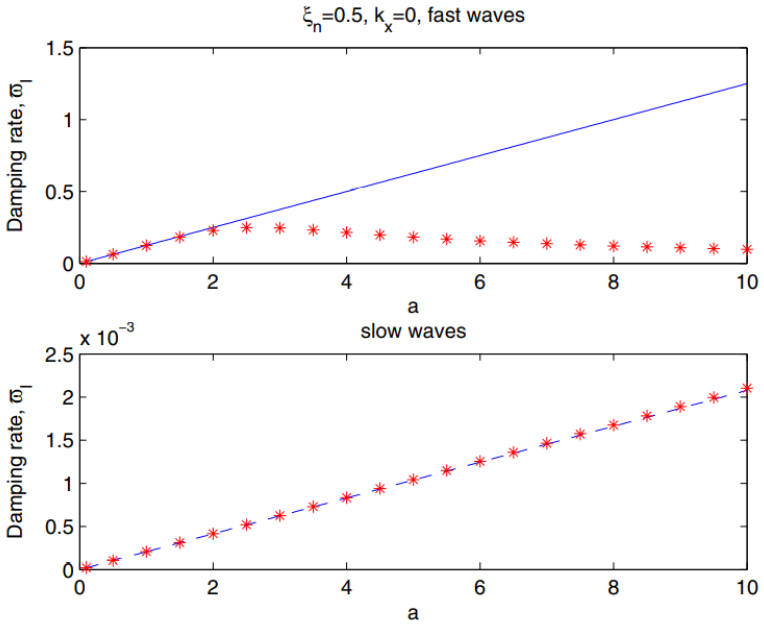

Figure 2.7: The damping rate for fast and slow modes. Red asterisks related to the dispersion relation while blue lines related to the solutions of Braginskii. This figure was adapted from Zaqarashvili et al. (2011*b*).

of ion-neutral collisions. The two resulting modes in the strongly coupled regime have mixed properties and are influenced by the physical conditions in the two fluids, in particular by the relative magnitude of characteristic speeds and the ionisation degree of the plasma.

Magnetoacoustic waves are damped by the ion-neutral collisions in a rather differentiated way. As a typical example of the variation of the frequencies of waves in terms of the collisional frequency of waves (normalised by kc_i) propagating parallel to the equilibrium magnetic field is shown in Figure 2.8 for the particular value of ion plasma-$\beta_i = 0.04$. The slow magnetoacoustic wave and the neutral acoustic wave interact strongly, with a visible change of the character of the waves depending on the value of the ionisation factor, χ. When $\chi \ll 1$, the neutral acoustic mode has a cut-off and the classic slow mode becomes the modified slow mode in the limit of large $\bar{\nu}/kc_{\rm i}$, where $\bar{\nu}$ is averaged collision frequency. This situation is reversed when $\chi \geq 1$, so that the solution that is cut-off is the classic slow mode while the neutral acoustic mode is the solution that becomes the modified slow mode. The behave of the fast magnetoacoustic wave in the low-β_i limit is very similar to that of the Alfvén waves studied since in this limit fast waves behave as Alfvén waves for parallel propagation to the magnetic field. Fast magnetoacoustic waves are non-propagating in a short interval of $\bar{\nu}/kc_{\rm i}$ when the collisional frequency is approximately equal to kc_i, where fast waves become entropy waves.

The study by Soler et al. (2013*b*) also classified the frequencies of slow and fast waves depending on the relative magnitude of characteristic speeds in the high collisional limit, showing the very complex nature of magnetoacoustic waves in partially ionised plasmas (see Table 2.1). These results show that depending on the relative magnitude of the Alfvén and the two sounds speeds, but also the ionisation degree of the plasma, the properties of waves can change and the propagation speed of magnetoacoustic modes are influenced by the ionisation degree of the plasma.

In the next chapters we will assume that all species have the same temperature, so that $T_e = T_i = T_n = T$. This assumption is in line with the physical requirement that a system will tend towards a state of equipartition of energy and uniform temperature that maximises the system's entropy. As a result, any local modification of temperature (and increase in the thermal speed of particles) is smoothed out after a few collisional times, i.e. over times that are smaller than the period of waves (very often this time is called the equilibration time) and any modifications in the distribution of particles is reduced in time,

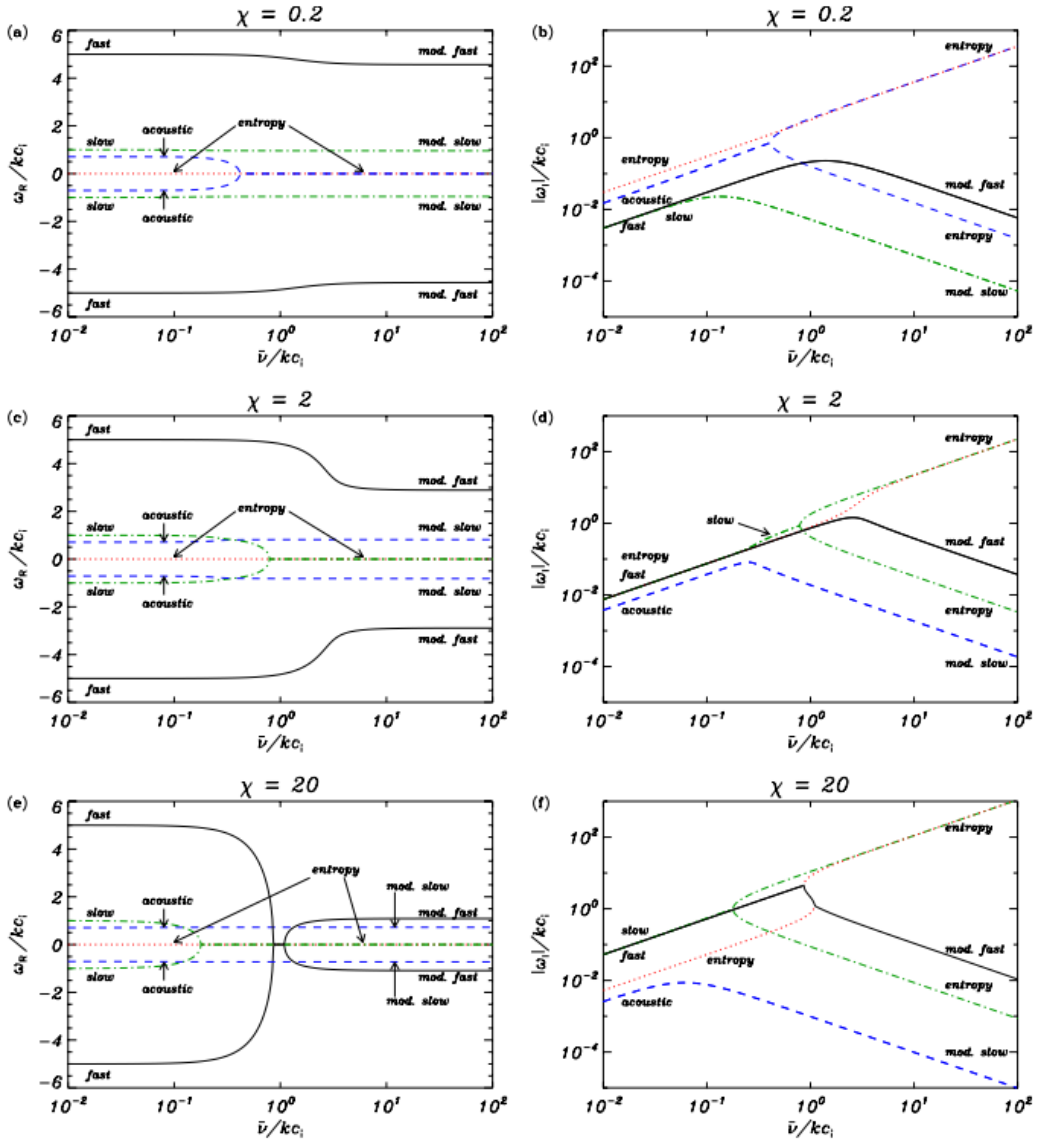

Figure 2.8: Real (left) and imaginary (right) parts of the frequency of the magnetoacoustic waves in terms the averaged collision frequency (in logarithmic scale) for parallel propagation to the magnetic field, with $\beta_i = 0.04$. Panels (a) and (b) correspond to a strong ionisation ($\chi = 0.2$), panels (c) and (d) are for intermediate ionisation ($\chi = 2$, and finally, panels (e) and (f) represent the case of weak ionisation ($\chi = 20$). All frequencies are expressed in units of kc_i. Credit: Soler et al. (2013*b*).

leading to a Maxwellian distribution. Since for the hydrogen plasma assumed here the mass of ions and neutrals are nearly identical, ions rapidly exchange energy with neutrals and tend to reach a thermal equilibrium with neutrals. Indeed, the amount of energy that is exchanged between ions and neutrals can be at most $m_i m_n/(m_i + m_n)^2 \approx 0.25$ times of their energy, making the process of thermalisation through collision very effective. In contrast, during

the collision between electrons and hydrogen neutral atoms, electrons are able to transfer only $m_e m_n/(m_e + m_n)^2 \approx 5.4 \times 10^{-4}$th part of their energy and it requires approximately 1850 collisions to reach the equipartition of energy between electrons and neutrals, and consequently, equality of their temperature. For a typical strongly ionised plasma where $T = 10^4$ K plasma and a neutral number density of $n_n = 2 \times 10^{15}$ m^{-3} (as discussed in Chapter 3) the collisional frequency between electrons and neutrals is approximately 39 s^{-1}, meaning that in about 47 seconds the electron and neutral population reach a thermal equilibrium.

Let us estimate the equilibration time between ions and neutrals in a strongly ionised plasma. In the absence of flows and other spatial inhomogeneities, the evolution of the temperature is given by the energy equations written for the two species

$$\frac{dT_i}{dt} = \nu_{in}(T_n - T_i),$$

$$\frac{dT_n}{dt} = \nu_{ni}(T_i - T_n).$$

Assuming that the temperatures of the two species at the start of our investigation are $\hat{T}_i$ and $\hat{T}_i$, the temporal evolution of the temperatures with time (see Soler et al., 2013*b*) is given by

$$T_i = T_f - (\hat{T}_n - \hat{T}_i)\frac{\nu_{in}}{\nu_{in} + \nu_{ni}} e^{-(\nu_{in}+\nu_{ni})t},$$

$$T_n = T_f + (\hat{T}_n - \hat{T}_i)\frac{\nu_{ni}}{\nu_{in} + \nu_{ni}} e^{-(\nu_{in}+\nu_{ni})t},$$

where

$$T_f = \frac{\nu_{in}\hat{T}_n + \nu_{ni}\hat{T}_i}{\nu_{in} + \nu_{ni}},$$

is the final temperature the two species will tend to through collision. We can easily estimate the time (t_f) required for the two species to reach 99% of the common temperature as

$$t_f = \frac{1}{\nu_{ni}\,(1 + \nu_{in}/\nu_{ni})} \ln\left[10^2 \frac{(\hat{T}_i - \hat{T}_n)}{\hat{T}_i + \hat{T}_n \nu_{in}/\nu_{ni}}\right].$$

Given the relationship between the two collisional frequencies we can write t_f

as

$$t_f = \frac{1}{\nu_{ni}\,(1+n_n/n_i)}\left[\ln 10^2 \frac{(\hat{T}_i-\hat{T}_n)}{\hat{T}_i+\hat{T}_n n_n/n_i}\right].$$

Finally, taking into account that in the present study we deal with strongly ionised plasma for which $n_i \gg n_n$, the above relation simplifies to

$$t_f \approx \frac{1}{\nu_{ni}}\left[4.6+\ln\left(1-\frac{\hat{T}_n}{\hat{T}_i}\right)\right].$$

For an order of magnitude estimate let us consider that $\hat{T}_i = 3\hat{T}_n$, and $\nu_{ni} = 10\ \mathrm{s}^{-1}$. As a result, the time needed for the two species to reach 99% of the thermal equilibrium is 0.4 seconds, i.e. thermal equilibrium between the massive particles is settled, indeed, very quickly. This conclusion is in line with the results obtained by earlier studies, e.g. Zaqarashvili et al. (2011*b*); Soler et al. (2013*b*); Oliver et al. (2016).

In a weakly ionised plasma ($n_n \gg n_i$) as discussed in Chapter 4 the equilibration time in the case of collisions between ions and neutrals reads

$$t_f = \frac{1}{\nu_{in}}\left(4.6+\ln\left|\frac{\hat{T}_i}{\hat{T}_n}-1\right|\right),$$

where, as before, $\hat{T}_i$ and $\hat{T}_n$ are the temperatures of the ion and neutral fluids and ν_{in} is the ion-neutral collisional frequency. For an order of magnitude estimate let us consider that $\hat{T}_i = 3\hat{T}_n$, and $\nu_{in} = 5\times 10^6\ \mathrm{s}^{-1}$. As a result, the time needed for the two species to reach 99% of the thermal equilibrium is 10^{-8} seconds, i.e. thermal equilibrium between the massive particles is settled, indeed, very quickly, much quicker than in the upper part of the atmosphere, thanks to the very high collisional frequency. A similar conclusion can be drawn after analysing the time required to reach the equilibrium temperature between electrons and neutrals (where t_f is now of the order of ν_{en}^{-1}). Therefore, assuming equal temperatures in such plasma is a realistic assumption.

Behavior of the Modified Fast and Slow Waves		
Velocities	Modified Fast Wave	Modified Slow Wave
$c_A^2 \gg c_i^2 \gg \chi c_n^2$	I-E IMW, $\omega^2 \approx k^2 c_A^2$	I-E GAW, $\omega^2 \approx k^2 c_i^2 \cos^2\theta$
$c_A^2 \gg c_i^2 \sim \chi c_n^2$	Effective IMW, $\omega^2 \approx \frac{k^2 c_A^2}{1+\chi}$	Effective GAW, $\omega^2 \approx \frac{k^2(c_i^2+\chi c_n^2)}{1+\chi}\cos^2\theta$
$c_A^2 \gg \chi c_n^2 \gg c_i^2$	N IMW, $\omega^2 \approx \frac{k^2 c_A^2}{\chi}$	N GAW, $\omega^2 \approx k^2 c_n^2 \cos^2\theta$
$\chi c_n^2 \gg c_A^2 \gg c_i^2$	N IAW, $\omega^2 \approx k^2 c_n^2$	N GMW, $\omega^2 \approx \frac{k^2 c_A^2}{\chi}\cos^2\theta$
$c_i^2 \gg c_A^2 \gg \chi c_n^2$	I-E IAW, $\omega^2 \approx k^2 c_i^2$	I-E GMW, $\omega^2 \approx k^2 c_A^2 \cos^2\theta$
$c_i^2 \gg \chi c_n^2 \gg c_A^2$	I-E IAW, $\omega^2 \approx k^2 c_i^2$	I-E GMW, $\omega^2 \approx k^2 c_A^2 \cos^2\theta$
$c_i^2 \sim \chi c_n^2 \gg c_A^2$	Effective IAW $\omega^2 \approx \frac{k^2(c_i^2+\chi c_n^2)}{1+\chi}$	Effective GMW, $\omega^2 \approx \frac{k^2 c_A^2}{1+\chi}\cos^2\theta$
$\chi c_n^2 \gg c_i^2 \gg c_A^2$	N IAW, $\omega^2 \approx k^2 c_n^2$	N GMW, $\omega^2 \approx \frac{k^2 c_A^2}{\chi}\cos^2\theta$

Table 2.1: Characteristics of fast and slow waves in partially ionised plasmas (together with their approximate frequencies) in the highly collisional limit in terms of the relative magnitude of characteristic velocities. Adapted from Soler et al. (2013*b*). Note: E, I, N, IMW, IAW, GMW, and GAW denote electron, ion, neutral isotropic magnetic wave, isotropic acoustic wave, guided magnetic wave, and guided acoustic wave, respectively.

CHAPTER 3

Slow magnetoacoustic waves in gravitationally stratified two-fluid plasmas in strongly ionised limit [1]

3.1 Introduction

One of the key characteristics of solar atmosphere is that in the lower regions (photosphere and chromosphere) the plasma is partially ionised, where neutral atoms, electrons and positively charged ions can interact through collisions. The ionisation degree of the plasma depends mainly on temperature, however, as shown by Heinzel et al. (2015) in the case solar prominences, the ionisation degree also depends on density and pressure. Existing solar atmospheric models predict a very low ionisation degree in the deep photosphere (where for every ion there are approximately 10^4 neutrals), and increases with height due to the increase of temperature (Vernazza et al., 1981; Fontenla et al., 1990).

The different species of particles present in the plasma interact through collisions and the frequency of the collisions also decreases with height due to the decrease of density of particles with height (a quantitative description is presented in Chapter 2). Although collisions between various species are important for various aspects related to partially ionised plasmas such as thermalisation of the plasma, various ionisation/recombination processes, appearance of thermal layers for shock waves in partially ionised plasmas, etc. (Shanmugasundaram and Murty, 1978; Mathers, 1980; Terradas et al., 2015; Martínez-Gómez et al., 2018; Ballai, 2019; Kuźma et al., 2020), the short-range collisions between neutrals and charged particles are of key importance as only this physical mechanism ensures that neutrals are a constituent part of the plasma. The collisions between electrons and the ions/neutrals help in the Maxwellisation of the electron population but is not affecting considerably the energy and momentum of massive particles.

[1] This Chapter is based on the study by Alharbi et al. (2021), published in MNRAS.

Unfortunately the characteristics of current ground-based and space-borne observational facilities are not suitable for the direct observation of waves with frequencies of the order of the collisional frequencies in partially ionised plasmas, as these waves require a time cadence that currently cannot be achieved. Nevertheless, waves and instabilities in partially ionised plasmas, together with their effects and consequences, have been largely explored theoretically and numerically. For a recent review on the progress of research on dynamical processes in solar and astrophysical plasmas (see Ballester et al., 2018*a*).

The theoretical investigation of waves in partially ionised plasmas under solar conditions has received recently an increased attention. More and more studies started to take into account the realistic model of a solar atmosphere, where the plasma is not hot enough to ensure a full ionisation. We should mention here that the consideration of partial ionisation effects depends on the range of frequencies we are interested in. If the frequency of waves we plan to investigate is much smaller than the collisional frequency of particles, the dynamics can be described within the framework of usual magnetohydrodynamics (MHD). Since current observational capabilities are mostly centered onto this regime, the observation of waves outside the MHD regime can be achieved only indirectly. Although the observation of high-frequency waves is still nearly impossible, several attempts have been made to evidence the effect of partial ionisation in solar lower atmosphere. Due to an imperfect collisional coupling between massive particles (ions and neutrals), there is an imbalance in the velocity of these species and this has been evidenced through a simultaneous measuring of the Doppler shift in the Fe II ion and neutral Fe I lines over the same volume of plasma in the sunspot penumbra (Khomenko et al., 2015). Later, Khomenko et al. (2016) found non-negligible differences in He I and Ca II velocities in solar prominences. Gilbert et al. (2007) compared He I and Hα data in multiple solar prominences in different phases of their life cycle and detected the drainage effect across the prominence magnetic field with different timescales for He and H atom. Later, de la Cruz Rodriguez and Socas-Navarro (2011) have reported misalignment in the visible direction of chromospheric fibrils that were attributed to the large ambipolar diffusion, that is, when the ion-neutral collisional frequency drops, the magnetic field can slip through the neutral population. This observational result has been later confirmed through numerical simulations by Martínez-Sykora et al. (2016) using advanced radiative MHD simulations. Finally, some observations have found evidence for higher frequency waves with periods as short as 45 s (0.15

Hz) in spicules (Okamoto and De Pontieu, 2011). Transition region spectral lines often show significant broadening beyond the thermal width of the order of 20 km s^{-1} in exposure times as short as 4 s (De Pontieu et al., 2015). If this non-thermal broadening were to be caused by waves, wave frequencies could be significantly higher than 1 Hz.

The framework used to describe the dynamics of waves in partially ionised plasmas depends on the frequency range of interest. For wave frequencies that are of the order of the collisional frequency between ions and neutrals we can employ a model where charged and neutrals particles are treated as separate, but interacting, fluids. Waves propagating in partially ionised plasmas differ qualitatively and quantitatively from their counterpart in fully ionised plasmas. As shown earlier, the spectrum of possible waves is larger as now, in addition to the ion-related modes, there are also acoustic modes associated to neutrals.

The study of waves in inhomogeneous plasma is not an easy task as inhomogeneities can change dramatically the property of waves and the coefficients of equations that describe the evolution of perturbations will be dependent of the coordinate. The damping of Alfvén waves in gravitationally stratified plasmas and their contribution to the heating of chromospheric plasma has been studied by a number of authors. Leake et al. (2005) used a single-fluid plasma approximation in the presence of Cowling resistivity and they found a very clear frequency-dependent damping of waves for chromospheric heights of 1000-2500 km above the solar surface. According to these authors Alfvén waves with frequencies below 0.01 Hz are unaffected by dissipative effects and propagate through the partially ionised plasma with little diffusion. In contrast, Alfvén waves with frequency above 0.6 Hz are completely damped. The research in this topic has been extended later by Tu and Song (2013), who carried out a numerical investigation of the two-fluid approximation, where collisions between various species (neutrals, electrons and positive ions) have been considered. The results of this analysis show that thanks to the density gradient, Alfvén waves are partially reflected throughout the chromosphere and more strongly at higher altitudes. Waves were observed to be damped in the lower chromosphere dominantly through Joule dissipation, producing heating strong enough to balance the radiative loss for the quiet chromosphere without invoking anomalous processes or turbulences. These authors also found that there is an upper cutoff frequency, depending on the background magnetic field, above which waves are completely damped. For a magnetic field of 100 G, the determined cut-off (or critical) frequency was found to be 0.12

Hz (Soler et al., 2019, 2021). A numerical analysis of the variation of the cut-off frequency with height has recently been made by Wójcik et al. (2019) assuming a two-fluid plasma.

When applied to chromospheric situations the study by Soler et al. (2013*b*) revealed that wavelengths smaller than 10^3 m are affected by two-fluid effects in the presence of strong magnetic fields. However, their approach is an eigenvalue problem, meaning that the temporal evolution of waves cannot be studied. Furthermore, they neglected gravitational stratification, meaning that important effects such as the presence of frequency cut-offs could not be studied. In the present Chapter we plan to address both of these shortcomings.

Here we will derive the evolutionary equations describing the spatial and temporal evolution of slow sausage modes attached to each species, i.e. waves that propagate such that the symmetry axis of the magnetic flux does not change. Solutions of the governing equations, assuming a strong ionisation thermal equilibrium is obtained. For mathematical progress we will consider asymptotic solutions corresponding to large values of time.

3.2 Assumptions and mathematical background

Before we embark on describing the evolution of slow guided waves in a gravitationally stratified plasma we need to make a few assumptions that will simplify our analysis. First of all we assume that during the typical time-scales involved in wave description the plasma remains in ionisation equilibrium, i.e. no additional ions are created by ionisation or neutrals due to recombination. This assumption is rather restrictive as typical time-scales associated to ionisation and recombination often can be comparable to period of waves. A treatment of waves in partially ionised non-equilibrium plasma can be found in the study by Ballai (2019).

Waves will propagate in a vertically unbounded magnetic cylinder and the magnetic field is parallel to the symmetry axis of the flux tube in the positive z-direction. For simplicity, the environment of the flux tube is non-magnetic.

To reduce the complexity of our analysis we will assume that the flux tube of cross-sectional area $A(z,t)$ is thin, i.e. waves propagating in the flux tube have wavelengths much larger than the radius of the tube (also known as the slender tube approximation). In this limit waves will not "sense" the boundary of waveguide. Due to the gravitational stratification, the dispersion relation of slow waves in a fully ionised plasma becomes $\omega^2 \approx k^2 c_T^2 + \omega_c^2$ (Roberts and

Webb, 1978), where k is wavenumber, $c_T^2 = c_S^2 v_A^2/(c_S^2 + v_A^2)$ is cusp speed and ω_c is the cut-off frequency of waves that depends on characteristic speeds and gravitational acceleration. As a result, the frequency of waves is increased compared to the unstratified case and waves become dispersive, which means that waves with longer wavelength will propagate faster. In the opposite case, when the wavelength of waves is comparable (or smaller) to the radius of the flux tube we are dealing with a thick flux tube, where the properties of waves are considerably changed. The propagation characteristics of slow sausage waves in a thick flux tube in a fully ionised plasma has been investigated by Pardi et al. (2014).

Since we aim to study the propagation of longitudinal waves, we can consider only the longitudinal velocity components of the species involved in the problem.

We assume that the length scales of variables that describe the dynamical and thermodynamical state of the plasma are much longer than the scattering mean free path, so that the concept of fluid is applicable. We are going to employ a two-fluid approximation where neutrals and charged species will interact through collisions. Although the interaction between electrons and neutrals also takes place, we are going to limit ourselves to the collisions between the massive particles, i.e. ions and neutrals as this interaction is mainly responsible for the collisional coupling between species. For simplicity we are going to label the charged species as "ions". Physical quantities related to this fluid are labeled by an index i and the parameters of the neutral fluid will be labelled by an index n. We should mention here that the charged particles (ions and electrons) all have a common velocity since differences in the divergence of the ion and electron velocities would lead to charge separation and strong electric fields opposing the charge separation. This assumption will be relaxed in the following Chapter, where the charged particles will have a distinct and different dynamics.

The system of equations describing the linear dynamics of the two-fluid plasma is given by

$$\frac{\partial}{\partial t}(\rho_{0i} A + \rho_i A_0) + \frac{\partial}{\partial z}(\rho_{0i} A_0 v_i) = 0, \tag{3.1}$$

$$\frac{\partial}{\partial t}(\rho_{0n} A + \rho_n A_0) + \frac{\partial}{\partial z}(\rho_{0n} A_0 v_n) = 0, \tag{3.2}$$

$$\rho_{0i}\frac{\partial v_i}{\partial t} + \frac{\partial p_i}{\partial z} + \rho_i g + \alpha_{in}(v_i - v_n) = 0, \tag{3.3}$$

$$\rho_{0n}\frac{\partial v_n}{\partial t}+\frac{\partial p_n}{\partial z}+\rho_n g+\alpha_{in}(v_n-v_i)=0, \tag{3.4}$$

$$\frac{\partial p_i}{\partial t}+v_i\frac{dp_{0i}}{dz}=c_{Si}^2\left(\frac{\partial \rho_i}{\partial t}+v_i\frac{\partial \rho_{0i}}{\partial z}\right), \tag{3.5}$$

$$\frac{\partial p_n}{\partial t}+v_n\frac{dp_{0n}}{dz}=c_{Sn}^2\left(\frac{\partial \rho_n}{\partial t}+v_n\frac{\partial \rho_{0n}}{\partial z}\right). \tag{3.6}$$

Mathematical details of the governing equations can be found in earlier studies by Defouw (1976) and Herbold et al. (1985). The above system of equations has to be supplemented by the two conditions

$$B_0A+BA_0=0, \quad p_i+p_n+\frac{B_0}{\mu_0}B=\pi(z,t), \tag{3.7}$$

expressing the conservation (in a linearised way) of the magnetic flux, and the total pressure at the boundaries of the flux tube. The quantities with an index '0' denote equilibrium values. In the above equations ρ_i, v_i and p_i are the density, longitudinal velocity component and pressure of charged particles (ions and electrons), ρ_n, v_n and p_n are the corresponding quantities for neutral species, $g = 274$ m s^{-2} the constant gravitational acceleration, and the sound speed associated with the two species are defined as

$$c_{Si}=\left(\frac{\gamma p_{0i}}{\rho_{0i}}\right)^{1/2}, \quad c_{Sn}=\left(\frac{\gamma p_{0n}}{\rho_{0n}}\right)^{1/2},$$

with γ being the usual ratio of specific heats. In equation 3.7 B_0 and B are the equilibrium and perturbed magnetic field, A_0 and A are the equilibrium cross-section area of the tube and the associated perturbation, while in the pressure balance equation $\pi(z,t)$ is the external pressure. For completeness, we should mention that, strictly speaking, the energy conservation equations for the two species should have contained a term that describes the energy lost due to the collisional friction between particles, however, since this term is nonlinear (proportional to the square of $(v_i - v_n)$), these will be neglected and the energy conservation is described by an adiabatic equation written for each fluid.

During the propagation of waves particles will undergo collisions with other particles. Neglecting mutual collisions between particles of the same type, the frictional coefficients between the colliding ions and neutrals is α_{in} and is given by

$$\alpha_{in}=\rho_i\nu_{in}=\rho_n\nu_{ni}, \tag{3.8}$$

where ν_{in} and ν_{ni} are the frequencies of ion-neutral and neutral-ions collisions defined earlier (see equation 2.6). Although normally the collisional frequencies are also height dependent, we are going to treat these quantities as constants and we are going to evaluate them for particular solar parameters, at particular height.

The collisions between the massive particles in the system acts as a dissipative term and waves will be expected to decay due to the collisions. Using the standard atmospheric models it can be shown that up to a height of approximately 2 Mm, $\nu_{in} > \nu_{ni}$, however, after this height, this inequality reverses due to the decrease in the number of neutrals thanks to the ionisation driven by the increase in temperature.

Due to the gravitational stratification equilibrium quantities will have a height-dependence. In a hydrostatic equilibrium the variation of the pressure with height for the two constituent fluids is given by

$$p_{0i}(z) = p_{0i}(0)e^{-\gamma_i(z)}, \quad p_{0n}(z) = p_{0n}(0)e^{-\gamma_n(z)}.$$

The dimensionless quantities $\gamma_i(z)$ and $\gamma_n(z)$ are given by

$$\gamma_i(z) = \int_0^z \frac{1}{H_i(z')}dz', \quad \gamma_n(z) = \int_0^z \frac{1}{H_n(z')}dz'$$

where

$$H_i(z) = \frac{RT_i(z)}{\tilde{\mu}_i g}, \quad H_n(z) = \frac{RT_n(z)}{\tilde{\mu}_n g}$$

are the gravitational pressure scale heights for ions and neutrals, R is the gas constant, $\tilde{\mu}_i$ and $\tilde{\mu}_n$ are the mean atomic weights and T_i and T_n are the temperature of the ion and neutral fluid (such that the mean translational kinetic energy or fluid particle in a frame moving with the fluid is $(3/2)k_BT_i$ and $(3/2)k_BT_n$, respectively). We should stress out that T_i stands for the temperature of the charged fluid, therefore it is the sum of the temperatures corresponding to ions and electrons. For simplicity we assume that the plasma is isothermal, meaning that the temperatures do not depend on height. As a result, the scale-heights are also constant, so the height-variation of the two pressures are simply given by

$$p_{0i} = p_{0i}(0)e^{-z/H_i}, \quad p_{0n} = p_{0n}(0)e^{-z/H_n}.$$

Using the ideal gas law the equilibrium densities of the two species also vary according to similar laws. One important implication of the isothermal limit

is that the sound speeds for the two species will be constant and the two scale-heights will be simply $H_i = c_{Si}^2/\gamma g$ and $H_n = c_{Sn}^2/\gamma g$.

As a consequence of the variation of pressure and density with height, the equilibrium is reached if the magnetic field and the magnetic flux tube's cross section area vary with height according to (for explanation see, e,g, Roberts and Webb (1978))

$$B_0(z) = B_0(0)e^{-z/2H_i}, \quad A_0(z) = A_0(0)e^{z/2H_i}.$$

With this particular choice of the magnetic field even the Alfvén speed, defined as,

$$v_A(z) = \frac{B_0(z)}{(\mu_0 \rho_{0i}(z))^{1/2}},$$

becomes also height-independent.

Our calculations will be further simplified by considering that temporal changes in the environment (the plasma outside the magnetic flux tube) take place over time scales that are much longer than any characteristic times scales of interest occurring inside the flux tube (very often this is also called the rigid boundary approximation). As a result every term that contains a time derivative of the external pressure, $\pi(z,t)$ will be neglected.

The propagation of slow waves in an unbounded plasma has been investigated previously in great detail as an eigenvalue problem by Zaqarashvili et al. (2011*b*) and Soler et al. (2013*b*) for varying collisional rate between ions and neutrals. While in the collisionless limit the two slow modes propagate with the ion cusp speed, and neutral sound speed, respectively, in the collisional case the propagation speed of slow waves becomes complex due to their interaction. In the weakly ionised and very low plasma-beta regime these authors found that the neutral slow waves are affected by a frequency cut-off, while the slow mode associated to ions becomes the modified slow mode

$$\omega^2 \approx k^2 \frac{c_{Si}^2 + \chi c_{Sn}^2}{1+\chi},$$

where χ is defined as $\chi = \rho_{0n}/\rho_{0i}$. When $\chi \ll 1$, the propagation speed of ion slow waves becomes essentially $\omega^2 \approx k^2 c_{Si}^2$.

Since we aim to analyse the spatial and temporal evolution of waves, we will not discuss explicitly the role of collisions as in the study by Soler et al. (2013*b*), instead we will assume a fixed value of the collisional frequency that is representative for the region of the solar atmosphere where our analysis is

valid. In our study we will also assume that the parameter χ is much less than one, and this parameter can be used as an expansion parameter to simplify the mathematics. Accordingly, the density ratio, χ, can be written as

$$\chi = \frac{\rho_{0n}(z)}{\rho_{0i}(z)} = \frac{\rho_{0n}(0)}{\rho_{0i}(0)} \exp\left[-z\left(\frac{1}{H_n} - \frac{1}{H_i}\right)\right] = \chi_0 e^{-z/h}. \tag{3.9}$$

Clearly the condition $\chi \ll 1$ means not only that $\chi_0 \ll 1$, but also that $h > 0$, i.e. $H_i > H_n$. This assumption is based on the relative variation of the neutral density compared to the density of ions with height according to the AL C7 atmospheric model (Avrett and Loeser, 2008). In Figure 3.1 we compare the predictions of the VAL IIIC atmospheric model (Vernazza et al., 1981) shown by red line, with the AL C7 model shown by the blue line. Clearly the two models show a good similarity up to heights of about 2 Mm. The large discrepancy following this height is due to more extensive set of chromospheric observations included in the solar atmospheric model developed by Avrett and Loeser (2008).

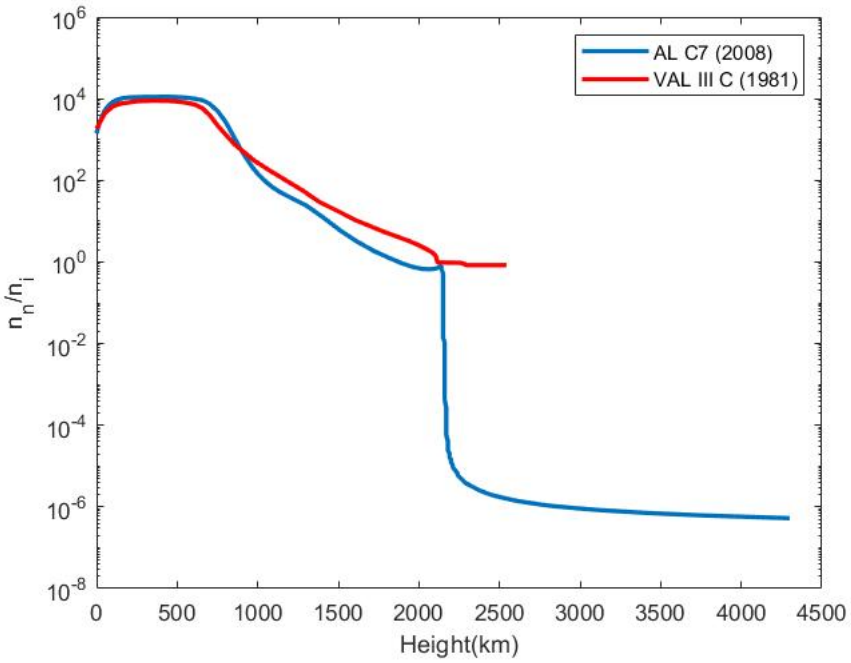

Figure 3.1: The variation of the ratio of number densities of neutrals and ions with height based on the VAL III C atmospheric model (Vernazza et al. (1981), red line) and the AL C7 atmospheric model (Avrett and Loeser (2008), blue line).

It is clear that, while in the photosphere the density ratio can be even of the order of 10^4, for chromospheric heights the density ratio is very small, and,

therefore, our assumption is justified.

3.3 Evolutionary equations

The governing equations 3.1 – 3.6 together with the particular choice of equilibrium parameters and the two conservation relations can be reduced to a system of coupled differential equations for the longitudinal velocity components of the two fluids of the form

$$\frac{\partial^2 v_i}{\partial t^2} - c_T^2 \frac{\partial^2 v_i}{\partial z^2} + \alpha_1 \frac{\partial v_i}{\partial z} + \alpha_2 v_i = 0, \tag{3.10}$$

$$\frac{\partial^2 v_n}{\partial t^2} - c_{Sn}^2 \frac{\partial^2 v_n}{\partial z^2} + \alpha_3 \frac{\partial v_n}{\partial z} + \alpha_4 v_n + \nu_{ni} \frac{\partial v_n}{\partial t} = - \frac{c_{Sn}^2 c_T^2}{v_A^2} \frac{\partial^2 v_i}{\partial z^2} + \alpha_5 \frac{\partial v_i}{\partial z} + \alpha_6 v_i, \tag{3.11}$$

where $c_T^2 = c_{Si}^2 v_A^2/(c_{Si}^2 + v_A^2)$ is the cusp speed related to ions. The above two relations describe the evolution of two slow magnetoacoustic modes propagating with the cusp speed and neutral sound speed, respectively. We should note that due to the relative low number of neutrals ion-acoustic modes will propagate (to leading order) unaffected by collisions, while the propagation of neutral-acoustic modes is strongly affected by collisions with ions and their dynamical behaviour is driven by ions through the set of terms on the right-hand side of equation 3.11.

The coefficients that appear in the above two equations are given by

$$\alpha_1 = \frac{c_T^2}{2H_i}, \quad \alpha_2 = \frac{\gamma - 1}{\gamma^2 H_i^2} \left[c_{Si}^2 - c_T^2 \left(1 - \gamma/2\right) \right], \tag{3.12}$$

$$\alpha_3 = \frac{c_{Sn}^2}{H_n} \left(1 - \frac{H_n}{2H_i} \right), \quad \alpha_4 = \frac{c_{Sn}^2 (\gamma - 1)}{2\gamma H_n H_i}, \tag{3.13}$$

$$\alpha_5 = \frac{c_{Sn}^2 c_T^2 (\gamma - 1)}{\gamma H_n v_A^2} \left(1 - \frac{H_n}{H_i} \right), \quad \alpha_6 = \frac{c_{Sn}^2 \alpha_1}{\gamma^2 H_n v_A^2} (\gamma^2 - 3\gamma + 2). \tag{3.14}$$

Equations 3.10 and 3.11 describing the evolution of the two waves can be brought into a simpler form by introducing the reduced function for ions and neutrals of the form

$$v_i(z,t) = Q_i(z,t) \exp(\lambda_i z), \quad v_n(z,t) = Q_n(z,t) \exp(\lambda_n z).$$

As the quantities λ_i and λ_n can be arbitrary, we can choose their values so

that first-order derivatives with respect to the spatial coordinate, z, vanish. Therefore, by choosing

$$\lambda_i = \frac{1}{4H_i}, \quad \lambda_n = \frac{1}{4H_i} - \frac{1}{2H_n}, \tag{3.15}$$

the evolutionary equations 3.10 and 3.11 can be reduced to

$$\frac{\partial^2 Q_i}{\partial t^2} - c_T^2 \frac{\partial^2 Q_i}{\partial z^2} + \omega_i^2 Q_i = 0, \tag{3.16}$$

$$\begin{aligned} &\frac{\partial^2 Q_n}{\partial t^2} - c_{Sn}^2 \frac{\partial^2 Q_n}{\partial z^2} + \Omega_n^2 Q_n + \nu_{ni} \frac{\partial Q_n}{\partial t} = \\ &= \left(-\frac{c_{Sn}^2 c_T^2}{v_A^2} \frac{\partial^2 Q_i}{\partial z^2} + \delta Q_i \right) \exp\left(-\frac{z}{2\gamma h} \right), \end{aligned} \tag{3.17}$$

where now the coefficients ω_i^2, Ω_n^2 and δ are given by

$$\omega_i^2 = \left(\frac{9}{4} - \frac{2}{\gamma} \right) \omega_{Ai}^2 - \omega_{Ai}^2 \frac{\beta\gamma}{2+\beta\gamma} \left(\frac{3}{2} - \frac{2}{\gamma} \right)^2,$$

$$\Omega_n^2 = \frac{c_{Sn}^2}{2c_{Si}^2} \omega_{Ai}^2 + \omega_{An}^2 + \frac{c_{Sn}^2}{4\gamma H_i H_n} (\gamma - 2),$$

and

$$\delta = \frac{c_{Sn}^2}{v_A^2(2+\gamma\beta)} \left[\omega_{Ai}^2 \left(\frac{1}{2} - \frac{2}{\gamma} + \frac{2}{\gamma^2} \right) + \frac{2c_{Si}^2}{c_{Sn}^2} \omega_{An}^2 \left(1 - \frac{2}{\gamma} + \frac{1}{\gamma^2} \right) + \right.$$

$$\left. \frac{c_{Si}^2}{H_i H_n} \left(\frac{1}{4} - \frac{3}{2\gamma} + \frac{1}{\gamma^2} \right) \right],$$

with $\beta = 2c_{Si}^2/(\gamma v_A^2)$ is the usual plasma-β parameter associated to ions, and $\omega_{Ai} = c_{Si}/(2H_i)$ and $\omega_{An} = c_{Sn}/(2H_n)$ are the acoustic cut-off frequency for ions and neutrals.

The significance of the quantity ω_i in equation 3.16 becomes clear once a normal mode analysis is applied to this equation and consider that the function $Q_i(z,t)$ has a plane-wave dependence of the form $Q_i(z,t) \sim e^{i(kz-\omega t)}$. The resulting dispersion relation can be rearranged into the form

$$k^2 = \frac{\omega^2 - \omega_i^2}{c_T^2}. \tag{3.18}$$

Propagating waves are possible only when the wavenumber, k, is real and this condition is satisfied if $k^2 > 0$, i.e. $\omega^2 > \omega_i^2$. Therefore, waves will propagate

only if their frequencies are larger than the cut-off value ω_i, so the stratified solar atmosphere acts as a frequency filter, where only high frequency waves propagate. When $\omega < \omega_i$ waves will be evanescent with an e-folding length of $c_{Si}/\sqrt{\omega_i^2 - \omega^2}$. The acoustic cut-off arises when ion-acoustic waves cannot propagate vertically because the wavelength is comparable with the density scale-height; consequently there is insufficient inertia on the low-density side of a compression to resist the acceleration of plasma, thereby cancelling too much of the pressure gradient to permit adequate subsequent compression of the surroundings, essential for causing the perturbation to propagate in a wave-like way. The dynamics operates on the vertical component of the motion, and is most effective for motion that is purely vertical.

Equation 3.18 can also be written as

$$\frac{d^2 Q_i}{dz^2} + \frac{\omega^2 - \omega_i^2}{c_{Si}^2} Q_i = 0,$$

meaning that propagating/evanescent waves correspond to $d^2Q_i/dz^2 < 0$ and $d^2Q_i/dz^2 > 0$, respectively.

A similar treatment for neutral-acoustic modes is not possible, and we will return to this aspect later. We should note here that in the strongly ionised limit the value of the ion cut-off frequency agrees (qualitatively) with the cut-off frequency for a fully ionised plasma, derived by, e.g. Rae and Roberts (1982).

The system of coupled equations 3.16 and 3.17 describe the propagation of ion-acoustic and neutral-acoustic waves in space and time. All the coefficients that appear in homogeneous part of these equations are constants. The two partial differential equations will be solved as an initial value problem (IVP), where we aim to study the asymptotic evolution of waves.

3.4 Asymptotic behaviour of guided slow waves

In order to discuss the asymptotic behaviour of waves for large values of time we will need to solve the initial value problem associated with the two evolutionary equations 3.16 and 3.17. As a consequence of the thermal equilibrium discussed in Chapter 2, the relationship between the sound speeds associated with the two constituent fluids becomes

$$c_{Si}^2 = \frac{\gamma(p_{0i} + p_{0e})}{\rho_{0i}} = \frac{\gamma k_B (T_i + T_e)}{m_i} = \frac{2\gamma k_B T_n}{m_n} = \frac{2\gamma p_{0n}}{\rho_{0n}} = 2c_{Sn}^2.$$

Using this result, the ratio of the propagation speed of waves associated to neutral and charged species takes the form

$$\frac{c_{Sn}^2}{c_T^2} = \frac{c_{Sn}^2}{c_{Si}^2}\left(1 + \frac{c_{Si}^2}{v_A^2}\right) = \frac{1}{2}\left(1 + \frac{\gamma\beta}{2}\right) \approx \frac{1}{2}, \tag{3.19}$$

where we used the consideration that our investigation is valid for the low plasma-beta case. The above result shows that the wave associated to charged particles propagates with a speed that is roughly twice the propagation speed of neutral-acoustic mode. Another straightforward implication of the above assumption is that the gravitational scale-height of ions (H_i) is twice the scale height corresponding to neutrals (H_n), i.e. the density decrease of neutrals with height is faster than for ions. In addition, the reduced scale-height, h, defined by equation 3.9, becomes $h = 2H_n$.

Because the two modes always appear together the above consideration raises an important aspect. Since the neutral acoustic modes are trailing the ion acoustic modes, the former waves will propagate in an environment that is already modified by the ion acoustic mode and this materialises partly in a modified temperature and density that results from the perturbations caused by the ion acoustic modes. The passage of the ion acoustic mode will also modify the density of ions, and through collisions, the density of neutrals will also be modified. However, in the present study we will assume that these changes are insignificant and, therefore, will be neglected. It is likely that the correctness of our assumption can be checked only by rigorous numerical investigation.

3.4.1 Ion-acoustic modes

Let us recall that the evolutionary equation for the charged fluid was obtained to be given by the Klein-Gordon equation

$$\frac{\partial^2 Q_i}{\partial t^2} - c_T^2 \frac{\partial^2 Q_i}{\partial z^2} + \omega_i^2 Q_i = 0. \tag{3.20}$$

We are going to consider the spatial positive domain and the solution of the above equation will be sought subject to the initial conditions $Q_i(z,0) = \partial Q_i(z,0)/\partial t = 0$. In addition, we require that waves will vanish at $z \to \infty$, i.e. $Q_i(z \to \infty, t) = 0$.

The IVP problem can be studied by means of the Laplace transform. Ac-

cordingly, we introduce the Laplace transform of the function $Q_i(z,t)$ as

$$\Psi_i(z,s) = \mathcal{L}[Q_i(z,t] = \int_0^\infty Q_i(z,t)e^{-st}\, dt. \tag{3.21}$$

As a result, the Klein-Gordon equation for ions reduces

$$s^2\Psi_i(z,s) - c_T^2\frac{d^2}{dz^2}\Psi_i(z,s) + \omega_i^2\Psi_i(z,s) = 0, \tag{3.22}$$

that has to be solved subject to the boundary condition $\Psi_i(z \to \infty, s) = 0$. The above equation can rearranged as

$$\frac{d^2}{dz^2}\Psi_i(z,s) - \frac{s^2+\omega_i^2}{c_T^2}\Psi_i(z,s) = 0, \tag{3.23}$$

whose general solution can be simply written as

$$\Psi_i(z,s) = C_1 \exp\left(\frac{z}{c_T}\sqrt{s^2+\omega_i^2}\right) + C_2 \exp\left(-\frac{z}{c_T}\sqrt{s^2+\omega_i^2}\right), \tag{3.24}$$

where C_1 and C_2 are arbitrary constants. Clearly, the first term will not satisfy the required boundary condition, therefore we choose $C_1 = 0$. Let us consider that at $z = 0$ the wave is driven by a function $Q_i(0,t) = \mathcal{A}_0(t)$ and its Laplace transform is $\Psi_i(0,s) = a_0(s)$. After applying this condition to the general solution, we obtain

$$\Psi_i(z,s) = a_0(s) \exp\left(-\sqrt{\frac{s^2+\omega_i^2}{c_T^2}}z\right). \tag{3.25}$$

Now, the function $Q_i(z,t)$ can be obtained by applying the inverse Laplace transform to the function given by equation 3.25. Since we have to compute the inverse Laplace transform of a product, we will use the convolution theorem. In finding the value of the inverse Laplace transform we will closely follow the method outlined by Sutmann et al. (1998).

In order to find the inverse Laplace transform of equation 3.25 we use the identity (Bateman, 1954)

$$\mathcal{L}^{-1}\left[\frac{e^{-a\sqrt{s^2+\omega_i^2}}}{\sqrt{s^2+\omega_i^2}}\right] = \begin{cases} J_0\left(\omega_i\sqrt{t^2-a^2}\right), & \text{for } t > a \\ 0, & \text{for } 0 < t < a, \end{cases} \tag{3.26}$$

where J_0 is the zero-th order Bessel function. Let us define the function

$$I = \frac{e^{-a\sqrt{s^2+\omega_i^2}}}{\sqrt{s^2+\omega_i^2}} = \int_a^\infty J_0\left(\omega_i\sqrt{t^2-a^2}\right)e^{-st}dt. \tag{3.27}$$

We differentiate both sides of equation 3.27 with respect a, so that

$$\frac{dI}{da} =$$

$$-\omega_i a\int_a^\infty \frac{J_0'\left(\omega_i\sqrt{t^2-a^2}\right)}{\sqrt{t^2-a^2}}e^{-st}dt - e^{-as} = -\exp\left(-a\sqrt{\omega_i^2+s^2}\right). \tag{3.28}$$

We can use the identity $J_0'(x) = -J_1(x)$, and substitute a by $t_i = z/c_T$ to obtain

$$\exp\left(-t_i\sqrt{\omega_i^2+s^2}\right) = \exp(-st_i) - \omega_i t_i\int_{t_i}^\infty \frac{J_1\left(\omega_i\sqrt{t^2-t_i^2}\right)}{\sqrt{t^2-t_i^2}}e^{-st}dt. \tag{3.29}$$

Now, introducing equation 3.29 into equation 3.25, we find that

$$\Psi_i(z,s) = a_0(s)\exp(-st_i) - a_0(s)\omega_i t_i\int_{t_i}^\infty \frac{J_1\left(\omega_i\sqrt{t^2-t_i^2}\right)}{\sqrt{t^2-t_i^2}}e^{-st}dt. \tag{3.30}$$

Note that the z-dependence of the above function is ensured through the expression of t_i, which was introduced to simplify the notation. Let us define the function

$$Z_i(z,t) = -\omega_i t_i\frac{J_1\left(\omega_i\sqrt{t^2-t_i^2}\right)}{\sqrt{t^2-t_i^2}}H\left(t-t_i\right), \tag{3.31}$$

where the $H(t-t_i)$ is the Heaviside step function defined as

$$H(t-t_i) = \begin{cases} 1, & \text{for } t > t_i \\ 0, & \text{for } 0 < t < t_i, \end{cases}$$

With the help of the second shifting theorem applied in connection to the first term on the right-hand side of equation 3.30, we obtain

$$a_0(s)\exp(-st_i) = \mathcal{L}\left[\mathcal{A}_0\left(t-t_i\right)H\left(t-t_i\right)\right]. \tag{3.32}$$

As a result, equation 3.30 becomes

$$\Psi_i(z,s) = \mathcal{L}\left[\mathcal{A}_0(t-t_i)H(t-t_i)\right] + \mathcal{L}\left[\mathcal{A}_0(t)Z_i(z,t)\right]. \tag{3.33}$$

Using the convolution theorem, the second term in right-hand side of above equation can be written as

$$\mathcal{L}\left[\mathcal{A}_0(t)Z_i(z,t)\right] = \mathcal{L}\left[\int_0^t \mathcal{A}_0(t-\tau)Z_i(z,\tau)d\tau\right]. \tag{3.34}$$

Since the original function $Q_i(z,t)$ can be determined as the inverse Laplace transform of the function $\Psi_i(z,s)$ given by equation 3.33, eventually we we obtain

$$Q_i(z,t) = \mathcal{A}_0\left(t-t_i\right)H\left(t-t_i\right) + \int_0^t \mathcal{A}_0(t-\tau)Z_i(z,\tau)d\,\tau. \tag{3.35}$$

3.4.2 Neutral-acoustic modes

The equation that describes the spatial-temporal evolution of these waves is given by equation 3.17. It is clear that the evolution of these waves (described by the left-hand side of equation 3.17 is driven by ions. In contrast to ions, where in the first order of approximation the collisions with neutrals can be neglected, in the case of neutrals the collisions with ions will play an essential role, and this effect is described by the last term on the left-hand side of equation 3.17. This equation is an inhomogeneous partial differential equation and solutions can be obtained by determining the complementary solution and a particular solution that is driven by the form of the inhomogeneous term. The complementary solution can be obtained after solving the equation

$$\frac{\partial^2 Q_n}{\partial t^2} - c_{Sn}^2\frac{\partial^2 Q_n}{\partial z^2} + \Omega_n^2 Q_n + \nu_{ni}\frac{\partial Q_n}{\partial t} = 0. \tag{3.36}$$

The above equation is the well-known telegrapher's equation that can be easily reduced to a Klein-Gordon equation. Accordingly, let us introduce a new function so that $Q_n(z,t) = q_n(z,t)e^{-\nu_{ni}t/2}$ As a result the equation that describes the complementary solution of neutral-acoustic modes becomes

$$\frac{\partial^2 q_n}{\partial t^2} - c_{Sn}^2\frac{\partial^2 q_n}{\partial z^2} + \left(\Omega_n^2 - \frac{\nu_{ni}^2}{4}\right)q_n = 0. \tag{3.37}$$

It can be shown that the quantity $\Omega_n^2 - \nu_{ni}^2/4$ is always negative. Again, using a normal mode analysis similar to the method employed in the case of ion-acoustic modes, it becomes clear that neutral-acoustic modes propagate with no cut-off.

Now, let us write the governing equation for the neutral-acoustic mode in the form

$$\frac{\partial^2 q_n}{\partial t^2} - c_{Sn}^2 \frac{\partial^2 q_n}{\partial z^2} - \omega_n^2 q_n =$$

$$= \left(-\frac{c_{Sn}^2 c_T^2}{v_A^2} \frac{\partial^2 Q_i}{\partial z^2} + \nu_{ni} \frac{\partial Q_i}{\partial t} + \delta Q_i \right) e^{\nu_{ni} t/2} e^{-z/4\gamma H_n}, \tag{3.38}$$

where $\omega_n^2 = \nu_{ni}^2/4 - \Omega_n^2$. Next, we apply the Laplace transform to the above equation and denote the Laplace transform of the function q_n as

$$\Psi_n(z,s) = \int q_n(z,t) e^{-st}\, dt.$$

Using the expression of $\Psi_i(z,s)$ given by equation 3.25 we can write the governing equation for neutrals as

$$\frac{\partial^2 \Psi_n}{\partial z^2} - \frac{s^2 - \omega_n^2}{c_{Sn}^2} \Psi_n = f(z,s), \tag{3.39}$$

where, with the help of the shifting theorem, the inhomogeneous part, $f(z,s)$ is given by

$$f(z,s) = \left\{ -\frac{1}{v_A^2} \left[\left(s - \frac{\nu_{ni}}{2} \right)^2 + \omega_i^2 \right] + \frac{\nu_{ni}}{c_{Sn}^2} \left(s - \frac{\nu_{ni}}{2} \right) + \frac{\delta}{c_{Sn}^2} \right\} \times$$

$$a_0 \left(s - \frac{\nu_{ni}}{2} \right) exp \left[-t_i \sqrt{\left(s - \frac{\nu_{ni}}{2} \right)^2 + \omega_i^2} - \frac{z}{4\gamma H_n} \right]. \tag{3.40}$$

The solution of the homogeneous part of the equation 3.39 that satisfies the condition at infinity becomes

$$\Psi_n^{hom} = B_1 \exp \left[-\frac{z}{c_{Sn}} \sqrt{s^2 - \omega_n^2} \right], \tag{3.41}$$

and the value of the constant B_1 will be chosen such that its value will be the Laplace transform of the driver at $z = 0$. For simplicity we will assume that the waves associated to both fluids are initiated by the same driver, therefore we will write $B_1 = a_0(s)$.

To find the inverse Laplace transform of the homogeneous solution we use

the identity (Bateman, 1954)

$$\mathcal{L}^{-1}\left[\frac{e^{-a\sqrt{s^2-\omega_n^2}}}{\sqrt{s^2-\omega_n^2}}\right] = \begin{cases} I_0\left(\omega_n\sqrt{t^2-a^2}\right), & \text{for } t > a, \\ 0, & \text{for } 0 < t < a, \end{cases}$$

where $I_0(x)$ is the modified Bessel function of order zero. Now let us define the function

$$J = \frac{e^{-a\sqrt{s^2-\omega_n^2}}}{\sqrt{s^2-\omega_n^2}} = \int_a^\infty I_0(\omega_n\sqrt{t^2-a^2})e^{-st}\,dt. \tag{3.42}$$

After differentiating the above function with respect to a, we obtain

$$\frac{dJ}{da} = -e^{-a\sqrt{s^2-\omega_n^2}} = -a\omega_n\int_a^\infty \frac{I_0'(\omega_n\sqrt{t^2-a^2})}{\sqrt{t^2-a^2}}e^{-st}\,dt - e^{-as},$$

where *dash* denotes the derivative of the function $I_0(x)$ with respect to its argument. Using the identity $I_0'(x) = I_1(x)$ and replacing a by $t_n = z/c_{Sn}$ we obtain

$$\exp\left(-t_n\sqrt{s^2-\omega_n^2}\right) = \omega_n t_n\int_{t_n}^\infty \frac{I_1(\omega_n\sqrt{t^2-t_n^2})}{\sqrt{t^2-t_n^2}}e^{-st}dt + e^{-st_n}. \tag{3.43}$$

It can be easily shown that in the low beta approximation $t_i \approx t_n/\sqrt{2}$. Let us define the function

$$Z_n(z,t) = \omega_n t_n\frac{I_1(\omega_n\sqrt{t^2-t_n^2})}{\sqrt{t^2-t_n^2}}H\left(t-t_n\right).$$

As a result, the solution of the homogeneous part of the governing equation for neutral-acoustic slow waves becomes

$$q_n(z,s) = a_0(s)e^{-st_n} + a_0(s)\mathcal{L}\left[Z_n(z,t)\right].$$

After applying the inverse Laplace transform and the convolution theorem, the solution becomes

$$q_n(z,t) = \mathcal{A}_0\left(t-t_n\right)H\left(t-t_n\right) + \int_0^t \mathcal{A}_0(t-\tau)Z_n(z,\tau)\,d\tau. \tag{3.44}$$

In order to determine the particular solution of the evolutionary equation for neutrals, we will need to calculate the inverse Laplace transform of the

expression

$$D(z,s) = a_0\left(s - \frac{\nu_{ni}}{2}\right) K(s) e^{-z/4\gamma H_n} \exp\left[-t_i\sqrt{(s-\nu_{ni}/2)^2+\omega_i^2}\right], \quad (3.45)$$

where the function $K(s)$ is defined as

$$K(s) = \frac{-\frac{\beta\gamma}{4}\left[\left(s-\frac{\nu_{ni}}{2}\right)^2+\omega_i^2\right] + \nu_{ni}\left(s-\frac{\nu_{ni}}{2}\right) + \delta}{s^2 - \omega_n^2 - c_{Sn}^2\left[\frac{1}{4\gamma H_n} + \frac{1}{c_T}\sqrt{\left(s-\frac{\nu_{ni}}{2}\right)^2+\omega_i^2}\right]^2}.$$

The above relation shows that we will need to deal with the inverse Laplace transform of a triple product, therefore we will use the triple convolution formula. According to the standard definition if $F(s)$, $G(s)$ and $H(s)$ are the Laplace transforms of the functions $f(t)$, $g(t)$ and $h(t)$, then

$$\mathcal{L}^{-1}\left[F(s)G(s)H(s)\right] = \int_0^t \left[f(t-\tau)\int_0^\tau g(\tau-\zeta)h(\zeta)d\zeta\right]d\tau.$$

Since the inverse Laplace transform of the exponential term in equation 3.45 has already been obtained (see equation 3.34), the only task here will be to derive the inverse Laplace transform of the function $K(s)$. This function has two simple poles at the zeros of the denominator, therefore the inverse Laplace transform can be obtained as the sum of the residues at the two poles. It is easy to see that the denominator is singular at

$$\Gamma_{1,2} = \frac{-\nu_{ni} \pm \mathcal{G}}{1 - g/2\omega_i c_T}, \quad (3.46)$$

where

$$\mathcal{G} = \left[\nu_{ni}^2 - \left(2 - \frac{g}{\omega_i c_T}\right)\left(\Omega_n^2 - \frac{g^2}{16c_{Sn}^2} - \frac{\omega_i^2}{2} - \frac{\omega_i g}{2c_T}\right)\right]^{1/2}.$$

It can be shown that for typical chromospheric conditions $\mathcal{G}$ is real, therefore both roots, $\Gamma_{1,2}$, are real and negative. As a result, the inverse Laplace transform of the function $K(s)$ becomes

$$\mathcal{L}^{-1}[K(s)] = \frac{i\pi\left(1 - g/2\omega_i c_T\right)}{\mathcal{G}} e^{\nu_{ni}t/2}\left(y_1 e^{\Gamma_1 t} - y_2 e^{\Gamma_2 t}\right), \quad (3.47)$$

with

$$y_j = \delta - \frac{\beta\gamma}{4}\left(\omega_i^2 + \Gamma_j^2\right) + \nu_{ni}\Gamma_j, \quad j = 1, 2.$$

Taking into account the inverse Laplace transform of all terms that appear in

the expression of $D(z,s)$ given by equation 3.45 after a lengthy, but straightforward calculation we can obtain the the particular solution of equation 3.38. However, since the expression of the whole particular solution is far too long and the expression of this solution will not be used in the present form, we choose to give the detailed solution once the asymptotic expression for large values of time is derived.

The asymptotic solution of these equations refers to the case of large values of time, i.e. for values of time for which $t \gg z/c_T$. Given the relationship between the propagation speed of the two modes, this condition includes the condition we impose for neutral-acoustic modes.

3.4.3 Oscillations driven by a sinusoidal pulse

We choose to drive the system (both species) with a harmonic pulse of the form $\mathcal{A}_0(t) = V_0 e^{-i\omega t}[H(t) - H(t-P)]$, where $P = 2\pi/\omega$. This driver acts for a duration P, after which is stopped. The driver acts at $z = 0$. In what follows we are going to discuss separately the asymptotic solution for both species.

In the case of ion-acoustic modes the spatial and temporal evolution of the reduced speed, $Q_i(z,t)$ is given by equation 3.35. Given the specific driver we have

$$\mathcal{A}_0(t-t_i) = V_0[H(t-t_i) - H(t-t_i-P)]e^{i\omega(t-t_i)}.$$

Since we are interested in the asymptotic behaviour of waves it is clear that $t \gg t_i$, which implies $t \gg (t_i + P)$. As a result both Heaviside functions become unity, and the first term of equation 3.35 becomes zero. Further, the second term of equation 3.35 can be written as

$$Q_i(z,t) = V_0 \int_0^t H(t-\tau)e^{-i\omega(t-\tau)}Z_i(z,\tau)d\tau -$$

$$-V_0 \int_0^t H(t-\tau-P)e^{-i\omega(t-\tau)}Z_i(z,\tau)d\tau.$$

It is clear that the first term cancels because all the values of τ have to be in the interval $(0,t)$, for which the Heaviside function is zero. Using the Heaviside function, the reduced speed, Q_i can be written as

$$Q_i(z,t) = -V_0 \int_{t-P}^t e^{-i\omega(t-\tau)}Z_i(z,\tau)d\tau.$$

In order to make analytical progress we will rewrite the convolutive integral

such that

$$\int_{t-P}^{t} \dots d\tau = \int_{t-P}^{\infty} \dots d\tau - \int_{t}^{\infty} \dots d\tau.$$

In order to estimate the value of these integrals we should keep in mind that the asymptotic analysis is valid provided $t \gg t_i$ or $\tau \gg t_i$ for which the Bessel function $J_1(x)$ for large arguments can be written as

$$J_1(x) \approx \frac{2}{\sqrt{\pi x}} \left[\cos\left(x - \frac{3\pi}{4} \right) + \mathcal{O}\left(\frac{1}{x} \right) \right].$$

After some straightforward calculations (for details see Sutmann et al., 1998, Appendix B) we eventually obtain

$$Q_i(z,t) = V_0 \sqrt{\frac{2\omega_i}{\pi}} \frac{1}{\omega^2 - \omega_i^2} \frac{2t_i}{t^{3/2}} \sin\left(\frac{\omega_i P}{2} \right) \times$$

$$\left[\omega_i \sin\left(\omega_i (t - P/2) - \frac{3\pi}{4} \right) - i\omega \cos\left(\omega_i (t - P/2) - \frac{3\pi}{4} \right) \right]. \tag{3.48}$$

Clearly this solution describes a wave whose transient part that oscillates with the cut-off frequency, ω_i, but this decays in time as $t^{-3/2}$. As a result, an observer situated at a given height, z_0, would observe a damped slow wave propagating with the cut-off frequency ω_i and free oscillations (the steady solution) are not present.

Now let us return to neutral acoustic modes, whose evolutionary equation is given by equation 3.38. First, let us investigate the asymptotic form of the homogeneous solution given by equation 3.44. Again, assuming the same harmonic driver of the form $\mathcal{A}_0(t) = V_0 e^{-i\omega t}[H(t) - H(t-P)]$ situated at $z = 0$ we have

$$\begin{aligned} q_n(z,t) = V_0 e^{-i\omega(t-t_n)}[H(t-t_n) - H(t-P-t_n)] + \\ + V_0 \int_0^t H(t-\tau) e^{-i\omega(t-\tau)} Z_n(z,\tau)\, d\tau - \\ - V_0 \int_0^t H(t-\tau-P) e^{-i\omega(t-\tau)} Z_n(z,\tau)\, d\tau. \end{aligned} \tag{3.49}$$

Similar to the discussion presented in the case of ion-acoustic slow modes the contributions of the first two terms of the above equation are zero. As a result after taking into account the restriction imposed by the Heaviside function, the homogeneous part of the equation of q_n is given by

$$q_n(z,t) = -V_0 \int_{t-P}^{t} e^{-i\omega(t-\tau)} Z_n(z,\tau)\, d\tau.$$

Since we are investigating the asymptotic behaviour of waves for large values of time, we can write that this corresponds to $\tau \gg t_n$, which means that our equation reduces to

$$q_n(z,t) = -V_0 e^{-i\omega t} \int_{t-P}^{t} \frac{I_1(\omega_n \tau)}{\tau} e^{i\omega\tau}\, d\tau. \tag{3.50}$$

For large arguments the modified Bessel function can be written as

$$I_1(\omega_n \tau) \approx \frac{e^{\omega_n \tau}}{(2\pi\omega_n \tau)^{1/2}}.$$

Therefore the evolutionary equation for the homogeneous part of the governing equation for neutrals becomes

$$q_n(z,t) = -\frac{V_0 e^{-i\omega t}}{\sqrt{2\pi\omega_n}} \int_{t-P}^{t} \frac{e^{(\omega_n + i\omega)\tau}}{\tau^{3/2}}\, d\tau. \tag{3.51}$$

The integral in the above relation can be given approximately (see Appendix A.1). As a result the evolution of the homogeneous part of $q_n(z,t)$ becomes

$$q_n(z,t) = -\frac{V_0(\omega_n - i\omega)e^{\omega_n t}}{\sqrt{2\pi\omega_n} t^{3/2}(\omega_n^2 + \omega^2)} \left[1 - e^{(\omega_n + i\omega)P}\right], \tag{3.52}$$

where we used the approximation

$$\frac{1}{(t-P)^{3/2}} \approx \left(1 + \frac{3}{2}\frac{P}{t}\right) \frac{1}{t^{3/2}} = \frac{1}{t^{3/2}} + \mathcal{O}\left(t^{-5/2}\right). \tag{3.53}$$

Now taking into account the relationship between $q_n(z,t)$ and $Q_n(z,t)$ we can find that the homogeneous solution of the evolutionary equation for neutrals becomes

$$Q_n^{hom} = -V_0 \sqrt{\frac{\omega_n}{2\pi}} \frac{\omega_n - i\omega}{\omega_n^2 + \omega^2} \frac{e^{(\omega_n - \nu_{ni}/2)t}}{t^{3/2}} \left[1 - e^{-(\omega_n + i\omega)P}\right]. \tag{3.54}$$

Since $\nu_{ni}/2 > \omega_n$, it is clear that the above solution describes an evanescent wave whose amplitude decays very rapidly due to collisions.

Finally, using the technique presented earlier, the inverse Laplace transform of the inhomogeneous part of equation 3.45 that gives the particular solution of equation 3.38 is

$$Q_n^{inh}(z,t) = \frac{A_2 A_3 V_0}{t^{3/2}} \times$$

$$\left[(\omega\sin\Phi_1 - i\omega_i\cos\Phi_1)\left(\frac{y_1\Gamma_1}{\Gamma_1^2+\omega_i^2} - \frac{y_2\Gamma_2}{\Gamma_2^2+\omega_i^2}\right) -\right.$$
$$-(\omega\sin\Phi_2 - i\omega_i\cos\Phi_2)\left(\frac{y_1\Gamma_1 e^{\Gamma_1 P}}{\Gamma_1^2+\omega_i^2} - \frac{y_2\Gamma_2 e^{\Gamma_2 P}}{\Gamma_2^2+\omega_i^2}\right) -$$
$$-\omega_i(\omega\cos\Phi_1 - i\omega_i\sin\Phi_1)\left(\frac{y_1}{\Gamma_1^2+\omega_i^2} - \frac{y_2}{\Gamma_2^2+\omega_i^2}\right) +$$
$$\left.+\omega_i\,(\omega\cos\Phi_2 - i\omega_i\sin\Phi_2)\left(\frac{y_1 e^{\Gamma_1 P}}{\Gamma_1^2+\omega_i^2} - \frac{y_2 e^{\Gamma_2 P}}{\Gamma_2^2+\omega_i^2}\right)\right], \tag{3.55}$$

where we used the notations

$$A_2 = \frac{\pi e^{-z/4\gamma H_n}\,(1 - g/2\omega_i c_T)\sin(\omega_i P/2)}{\mathcal{G}},$$

$$A_3 = \sqrt{\frac{2\omega_i}{\pi}}\frac{2}{\omega^2-\omega_i^2}t_i,$$

$$\Phi_1 = \omega_i\left(t - \frac{P}{2}\right) - \frac{3\pi}{4}, \quad \Phi_i = \omega_i\left(t - \frac{3P}{2}\right) - \frac{3\pi}{4}.$$

In contrast to the homogeneous solution, the particular solution shows a decaying oscillatory motion with the cut-off frequency of ions. This behaviour is a consequence of the coupling between neutrals and ions, where ions provide the oscillatory background for neutrals and the oscillatory behaviour of neutrals is driven by ions via collisions.

3.4.4 Oscillations driven by a monochromatic driver

We choose to drive the system (both species) with a harmonic and monochromatic source of the form $\mathcal{A}_0(t) = V_0 e^{-i\omega t}$ situated at $z = 0$. In what follows we are going to discuss separately the asymptotic solution for both species.

In the case of ion-acoustic modes the spatial and temporal evolution of the reduced speed, $Q_i(z,t)$ is given by equation 3.35. In order to make analytical progress we will rewrite the convolutive integral such that

$$\int_0^t \ldots d\tau = \int_0^\infty \ldots d\tau - \int_t^\infty \ldots d\tau.$$

As a result the expression of $Q_i(z,t)$ is given by

$$Q_i(z,t) = V_0\left[e^{-i\omega(t-z/c_T)}H\left(t - \frac{z}{c_T}\right) - I_1 + I_2\right], \tag{3.56}$$

where the quantities I_1 and I_2 are given by

$$I_1 = C_0 \int_0^{\infty} \frac{J_1\left(\omega_i \sqrt{\tau^2 - z^2/c_T^2}\right)}{\sqrt{\tau^2 - z^2/c_T^2}} H\left(t - \frac{z}{c_T}\right) e^{i\omega\tau} d\tau,$$

$$I_2 = C_0 \int_t^{\infty} \frac{J_1\left(\omega_i \sqrt{\tau^2 - z^2/c_T^2}\right)}{\sqrt{\tau^2 - z^2/c_T^2}} H\left(t - \frac{z}{c_T}\right) e^{i\omega\tau} d\tau.$$

In the above relations $C_0 = \omega_i (z/c_T) e^{-i\omega t}$. In order to estimate the value of I_1 we make use of the properties given by equation 3.21 and obtain that

$$I_1 = e^{-i\omega t} \left[e^{-i\omega z/c_T} - e^{-i\sqrt{\omega^2 - \omega_i^2} z/c_T} \right]. \tag{3.57}$$

In order to estimate the value of I_2 we should keep in mind that the asymptotic analysis is valid provided $t \gg z/c_T$ or $\tau \gg z/c_T$. In addition, the value of the Bessel function $J_1(x)$ for large arguments can be written as

$$J_1(x) \approx \frac{2}{\sqrt{\pi x}} \left[\cos\left(x - \frac{3\pi}{4}\right) + \mathcal{O}\left(\frac{1}{x}\right) \right].$$

After some straightforward calculations (for details see Sutmann et al., 1998, Appendix B) we can obtain that

$$I_2 = \sqrt{\frac{2\omega_i}{\pi}} \frac{1}{\omega^2 - \omega_i^2} \frac{z}{c_T} \frac{1}{t^{3/2}} \left[\omega_i \sin\left(\omega_i t - \frac{3\pi}{4}\right) + i\omega \cos\left(\omega_i t - \frac{3\pi}{4}\right) \right]. \tag{3.58}$$

Introducing the values of the integrals into the expression of $Q_i(z,t)$ given by equation 3.56, we eventually obtain

$$Q_i(z,t) = V_0 e^{-i\left(\omega t - \sqrt{\omega^2 - \omega_i^2} z/c_T\right)}$$

$$+ V_0 \sqrt{\frac{2\omega_i}{\pi}} \frac{1}{\omega^2 - \omega_i^2} \frac{z}{c_T} \frac{1}{t^{3/2}} \left[\omega_i \sin\left(\omega_i t - \frac{3\pi}{4}\right) + i\omega \cos\left(\omega_i t - \frac{3\pi}{4}\right) \right]. \tag{3.59}$$

Clearly this solution describes a wave whose steady part oscillates with the driving frequency, ω, and a transient part that oscillates with the cut-off frequency, ω_i, but this decays in time as $t^{-3/2}$. As a result, an observer situated at a given height, z_0, would first observe a slow wave propagating with the frequency ω and a speed c_T followed by a wake with decaying amplitude. The amplitude of the wake is always smaller than the amplitude of the wave itself.

Now let us return to neutral acoustic modes, whose evolutionary equation is given by equation 3.38. First, let us investigate the asymptotic form of

the homogeneous solution given by equation 3.44. Again, assuming the same harmonic driver of the form $A_0(t) = V_0 e^{-i\omega t}$ situated at $z = 0$ we have

$$q_n(z,t) = V_0 e^{-i\omega(t-z/c_{Sn})} H\left(t - \frac{z}{c_{Sn}}\right)$$

$$+ D_0 \int_0^\infty \frac{I_1\left(\omega_n \sqrt{\tau^2 - (z/c_{Sn})^2}\right)}{\sqrt{\tau^2 - (z/c_{Sn})^2}} e^{i\omega\tau} H\left(t - (z/c_{Sn})\right) d\tau, \tag{3.60}$$

where,

$$D_0 = \frac{V_0 \omega_n z}{c_{Sn}} e^{-i\omega t}.$$

Since we are investigating the asymptotic behaviour of waves for large values of time, we can write that this corresponds to $\tau \gg z/c_{Sn}$, which means that our equation reduces to

$$q_n(z,t) = V_0 e^{-i\omega t} + D_0 \int_{z/c_{Sn}}^t \frac{I_1(\omega_n \tau)}{\tau} e^{i\omega\tau} d\tau. \tag{3.61}$$

For large arguments the modified Bessel function can be written as

$$I_1(\omega_n \tau) \approx \frac{e^{\omega_n \tau}}{(2\pi\omega_n \tau)^{1/2}}.$$

Therefore the evolutionary equation for the homogeneous part of the governing equation for neutrals becomes

$$q_n(z,t) = V_0 e^{-i\omega t} + \frac{D_0}{\sqrt{2\pi\omega_n}} \int_{z/c_{Sn}}^t \frac{e^{(\omega_n + i\omega)t}}{\tau^{3/2}} d\tau. \tag{3.62}$$

The integral in the above relation can be given approximately (see Appendix A.2). As a result the evolution of the homogeneous part of $q_n(z,t)$ becomes

$$q_n(z,t) = V_0 e^{-i\omega t} + \frac{D_0(\omega_n - i\omega)}{\sqrt{2\pi\omega_n}(\omega_n^2 + \omega^2)} \left[\frac{e^{(\omega_n + i\omega)t}}{t^{3/2}} - \frac{e^{(\omega_n + i\omega)z/c_{Sn}}}{(z/c_{Sn})^{3/2}}\right]. \tag{3.63}$$

Now taking into account the relationship between $q_n(z,t)$ and $Q_n(z,t)$ we can find that the homogeneous solution of the evolutionary equation for neutrals becomes

$$Q_n^{hom} = V_0 e^{-\nu_{ni} t/2} e^{-i\omega t} + V_0 \sqrt{\frac{\omega_n}{2\pi}} \frac{z}{c_{Sn}} \frac{\omega_n - i\omega}{\omega_n^2 + \omega^2}$$

$$\times \left[\frac{e^{(\omega_n - \nu_{ni}/2)t}}{t^{3/2}} - \frac{(e^{\omega_n z/c_{Sn} - \nu_{ni} t/2} e^{-i\omega t})}{(z/c_{Sn})^{3/2}}\right]. \tag{3.64}$$

It is clear that although the above solution describes a wave that oscillates with the driving frequency, ω, its amplitude decays very rapidly due to collisions.

Finally, the inhomogeneous part of the solution can be found by using the results shown in Appendix A.3, which has to be transformed according to the relationship between $q_n(z,t)$ and $Q_n(z,t)$. As a result, the particular solution of the evolutionary equation for neutrals becomes

$$Q_n^{inh}(z,t) = \frac{iA_2V_0\left[\delta - \beta\gamma/4(1+2\Gamma_1^2)\right]e^{-i\omega z/c_T}}{P_1+i\omega_i}\left[e^{\Gamma_1 t} - e^{-i\omega t}e^{-\nu_{ni}t/2}\right]e^{\sqrt{\omega^2-\omega_i^2}z/c_T}$$

$$-\frac{iA_2V_0\left[\delta - \beta\gamma/4(1+2\Gamma_2^2)\right]e^{-i\omega z/c_T}}{P_2+i\omega_i}\left[e^{\Gamma_2 t} - e^{-i\omega t}e^{-\nu_{ni}t/2}\right]e^{\sqrt{\omega^2-\omega_i^2}z/c_T}$$

$$-\frac{iA_2V_0A_3\omega_i}{P_1^2+\omega_i^2}\left[\delta - \frac{\beta\gamma}{4}(1+2\Gamma_1^2)\right]\left\{\frac{e^{-\nu_{ni}t/2}}{t^{3/2}}\left[P_1\sin\left(\omega_i t - \frac{3\pi}{4}\right) - \omega_i\cos\left(\omega_i t - \frac{3\pi}{4}\right)\right]\right.$$

$$\left.-\frac{e^{\Gamma_1 t}}{(z/c_T)^{3/2}}\left[P_1\sin\left(\omega_i\frac{z}{c_T} - \frac{3\pi}{4}\right) - \omega_i\cos\left(\omega_i\frac{z}{c_T} - \frac{3\pi}{4}\right)\right]\right\}$$

$$+\frac{A_2A_3V_0\omega}{P_2^2+\omega_i^2}\left[\delta - \frac{\beta\gamma}{4}(1+2\Gamma_2^2)\right]\left\{\frac{e^{-\nu_{ni}t/2}}{t^{3/2}}\left[P_2\cos\left(\omega_i t - \frac{3\pi}{4}\right) - \omega_i\sin\left(\omega_i t - \frac{3\pi}{4}\right)\right]\right.$$

$$\left.-\frac{e^{\Gamma_2 t}}{(z/c_T)^{3/2}}\left[P_2\cos\left(\omega_i\frac{z}{c_T} - \frac{3\pi}{4}\right) - \omega_i\sin\left(\omega_i\frac{z}{c_T} - \frac{3\pi}{4}\right)\right]\right\}. \qquad (3.65)$$

Similar to the homogeneous solution, the particular solution also shows an oscillatory pattern with a very rapid decay of the amplitude due to collisions. These solutions will be investigated numerically in the next section for particular solar atmospheric values.

3.5 Application to solar atmosphere

In what follows we are going to analyse our results assuming typical solar chromsopheric values for density and temperature. For magnetic field we assume a field strength of 10 G throughout all our investigations.

In order to estimate key parameters that are important for our calculations we are going to consider that the plasma has a temperature of $T = 10^4$ K and the number densities of ions and neutrals are $n_i = 2\times10^{15}$ m^{-3} and $n_n = 2\times10^{13}$ m^{-3}. With these parameters we can estimate that the characteristic speeds will be $c_{Si} = 16.6$ km s^{-1}, $c_{Sn} = 11.7$ km s^{-1} and $v_A = 450$ km

s^{-1}, which would result in a plasma-$\beta = 1.7 \times 10^{-3}$ and a cusp speed on the charged fluid $c_T = 15.58$ km s^{-1}. For the given density and temperature values the collisional frequency between neutrals and ions can be determined with the help of equations 2.6 and 3.8 and results in $\nu_{ni} = 10.48$ s^{-1}. Finally, the gravitational scale-heights connected to ions and neutrals in thermal equilibrium become $H_i = 2H_n = 0.5$ Mm.

Our analysis showed that ion-acoustic modes propagate in the stratified plasma such that their frequency is affected by a cut-off value. Using the definition of this quantity given by equation 3.16 we obtain that for the representative temperature we have chosen, $\omega_i \approx 0.015$ Hz and it varies as $T^{-1/2}$ (we should mention here that the value of the cut-off we would obtain for a fully ionised plasma for the same values of temperature and magnetic field, would be almost identical with the above value thanks to the strongly ionised limit employed by us). In addition, the variation of the cut-off frequency with respect to plasma-beta shows a very weak dependence. It is interesting to note that Leake et al. (2005) found that Alfvén waves have a cut-off frequency of 0.6 Hz. As we proved earlier in Section 3.4.2, neutral-acoustic modes propagate with no cut-off frequency, however employing a normal mode analysis (i.e. assume that perturbations are proportional to the exponential factor $e^{i(kz-\omega t)}$ the homogeneous part of equation 3.38 reduces to $\omega^2 = k^2 c_{Sn}^2 - \omega_n^2$, so the requirement of propagating wave ($\omega^2 > 0$) means that in the case of neutral-acoustic waves the condition $k > \omega_n / c_{Sn} \approx \nu_{ni} / 2c_{Sn}$ has to be satisfied (here the stratification effects are much smaller). Since ω_n depends on collisional frequency, the wavenumber cut-off will be influenced by collisions. For the values of characteristic speeds and collisional frequency determined earlier neutral-acoustic waves will propagate provided their wavenumber is larger than 5×10^{-4} m^{-1}, or their wavelength is shorter than 1.25×10^4 m. Clearly, such small wavelengths are impossible to observe with the current observational facilities. That is why observations can detect only one mode (connected to the charged species), while the neutral-acoustic modes remain sub-resolution modes. Such condition connected to wavenumbers is not imposed on ion-acoustic modes, for these waves the only restriction remains that their frequency has to be larger than the cut-off frequency ω_i.

If the above conditions are not satisfied, neutral-acoustic modes are becoming non-propagating entropy modes, i.e. modes whose frequency is purely imaginary. In the case of these modes all perturbations are zero, except density and temperature perturbations in such a way that the pressure perturbation is

constant. Entropy modes owe their existence to the collisions of neutrals with ions in strongly ionised limit and they play important role in the development and evolution of turbulences in the presence of small spatial scales (see, e.g. Lithwick and Goldreich, 2001; Soler et al., 2013*b*).

Now let us return to the study of the temporal evolution of the two waves. For that we are going to fix the value of height and study the temporal evolution of the reduced velocity for the two waves.

3.5.1 Excitation by a sinusoidal pulse

In Figure 3.2 we plot the temporal evolution of neutral-acoustic (solid line) and ion-acoustic (dashed line) slow mode at a given height ($z = 4$ Mm) as given by the real parts of equations 3.48 and 3.55. Due to the coupling between the two species, both waves oscillate with the same frequency ω_i. It is clear that the neutral-acoustic mode has a larger amplitude and decays slower than the corresponding ion-acoustic modes. The two modes are excited at the $z = 0$ level with the driving frequency $\omega = 0.1$ Hz. Since the lifetime of the driver is limited (here chosen to be $P = 20\pi$ s), the free oscillations associated with the two species are absent, instead both slow modes attenuate. However, we should keep in mind that this attenuation is not due to physical damping (here collisions), instead it is due to dispersion and expansion of the cross section of the magnetic flux tube.

3.5.2 Excitation by monochromatic driver

In Figure 3.3 we plot the temporal evolution of ion-acoustic slow mode at a given height (z = 4 Mm) as given by the real part of equation 3.59. Here the blue line correspond to the first term of this equation and describes a harmonic change of the amplitude of oscillations. This part of the reduced velocity $Q_i(z,t)$ oscillates with the driving frequency chosen to be $\omega = 0.1$ Hz. As we described earlier based on a phenomenological approach, indeed this part of the solution oscillates harmonically with no damping, which is a consequence of a constant driving of waves. The red curve represents the second term of the solution and it shows a very small amplitude oscillations with rapid decay. Obviously, an observer would see the combined effects of these two modes. Since for the chosen atmospheric parameters the two oscillations are in anti-phase, an observer at the chosen height will see an increasing amplitude wave oscillating with a frequency that is combination of the driving frequency and

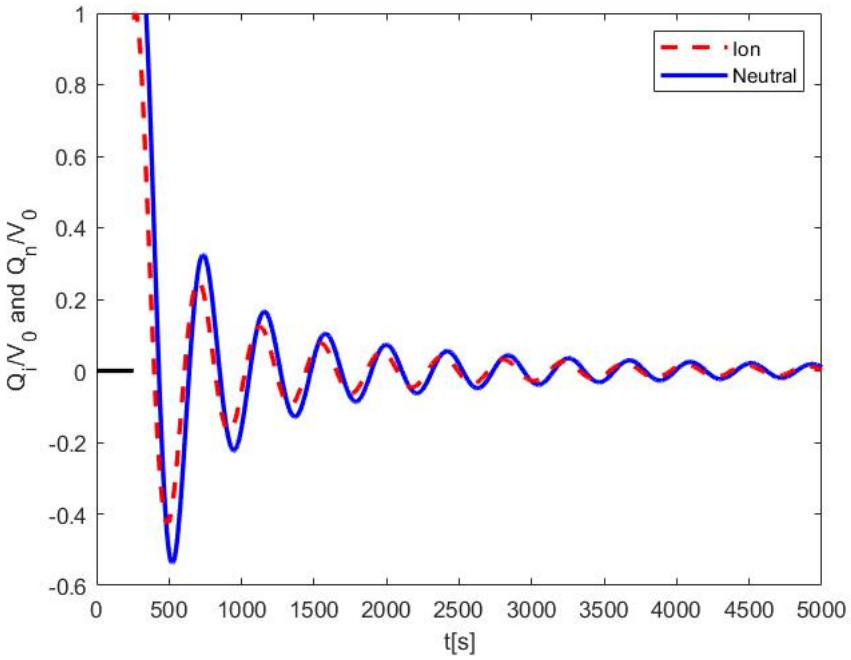

Figure 3.2: The temporal evolution of neutral-acoustic (solid lines) and ion-acoustic (dashed lines) modes at $z = 4$ Mm. The slow sausage modes associated with the two species is driven by a sinusoidal pulse of lifetime P. Both slow modes oscillate with the ion cut-off frequency, ω_i. For an observer situated at the observational height of 4 Mm, wave-like behaviour will be observable only after the delay time $t_i = z/c_T$. The delay time is shown here as a horizontal straight line.

cut-off frequency, followed by a steady oscillation with the frequency ω.

The asymptotic evolution of the slow sausage mode associated to the neutral species is given by equations 3.64 and 3.65. Since these equations contain an exponentially decaying solution with a damping time of $T_d = \nu_{ni}/2$ valid for large values of time, these slow sausage modes will undergo a very rapid decay and their temporal evolution will not be plotted as the amplitudes (even after returning to the original variable, $v_n(z,t)$) we are dealing with are infinitesimally small. This result has serious consequences for observations of waves in the chromosphere, where the degree of plasma ionisation is high. While the slow sausage mode associated to ions has a clear and observable behaviour, the slow sausage modes associated to neutrals become undetectable. This behaviour is likely to remain similar in the case of other kinds drivers that could be imposed at $z = 0$.

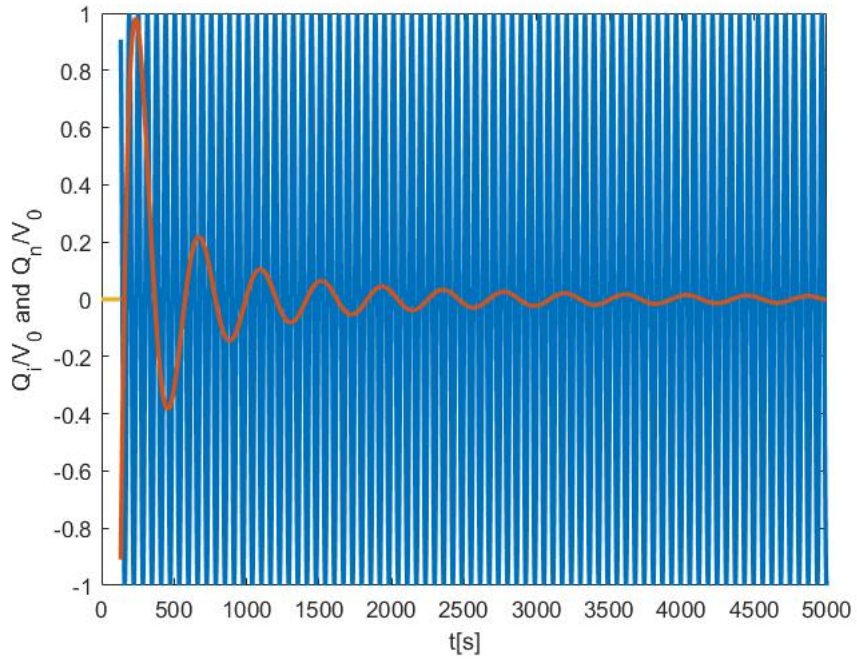

Figure 3.3: The temporal evolution of ion-acoustic modes at $z = 4$ Mm. The blue curves denote oscillations at the driving frequency. The red curve represents the oscillation of the wake with the cut-off frequency, ω_i. For comparison purposes the amplitude of the wake has been multiplied by a factor of 100.

3.6 Conclusions

The present Chapter was devoted to the investigation of the temporal and spatial evolution of slow sausage waves propagating in an expanding magnetic flux tube in a gravitationally stratified atmosphere. The plasma temperatures are typical for the solar chromosphere, where the ionisation degree of the plasma is high, nevertheless the plasma is not fully ionised. Given the very different concentration of neutrals and charged species, the ratio between neutral and charged density is very small and this ratio was used as a small parameter in deriving the evolutionary equation for waves. The plasma was assumed to be isothermal, which implies that all characteristic speeds are constant quantities.

The evolutionary equation for slow sausage waves associated with the two species was derived in the linear limit. While the equation for waves associated with the charged particles is described by a Klein-Gordon equation, for neutrals this becomes the telegrapher's equation. Given the plasmas's high degree of ionisation the collisions have different role for the two species. For ions the collision with neutrals is just a secondary effect (and proportional to the density ratio between neutrals and ions). As a result the equation for ions (in the

leading order) is not affected by collisions. In contrast, the equation for the neutrals species is strongly affected by the collisions between neutrals and ions, causing a strong decay of waves. While the ion-related waves propagate with a cut-off frequency, neutral sausage modes propagate with no frequency cut-off thanks to the collisions between species. In contrast, propagating slow waves associated to neutrals are possible only for wavelengths that are shorter than 12.5 km, that is they are small wavelength waves.

The evolutionary equations have been solved as an initial value problem, imposing a oscillatory pulse and a monochromatic driver and an atmosphere that is unbounded in the z direction. We considered the situation when the signal has already passed through the atmosphere (i.e. we performed an asymptotic analysis valid for $t \gg z/c_T$), which implies that an observer would just observe the wake left behind the pulse. This wake oscillates with the cut-off frequency of the ion population. In other words, steady oscillations are excluded, and the system will oscillate with the transient part of the solution that decays as $t^{-3/2}$. This result is similar to the findings of Kalkofen et al. (1994) and Sutmann et al. (1998).

Slow sausage waves associated with neutrals propagate with no cut-off but given the high degree of coupling with ions, these will impose on neutrals the same behaviour, i.e. the transient solution of neutral slow wave oscillate with the same ion-related cut-off frequency and show the same temporal damping pattern as in the case of ions. It is very likely that in strongly ionised plasmas these waves will have a very rapid decay, even in the absence of the simplifications we imposed to the employed model. That would mean that any possible observation of these waves has to be carried out in an environment where the ionisation degree is moderate. The presence of the cut-off frequency for ion-acoustic waves also implies that for a driving frequency smaller than the cut-off frequency, the ion-acoustic mode becomes evanescent (exponentially decaying), while the slow waves associated with neutrals will still propagate unaffected. This has large ranging consequences for observation of waves in the solar atmosphere. Finally we should mention that when oscillations are driven by a sinusoidal pulse, whose frequency is identical with the ion cut-off frequency, the slow sausage modes associated to the two species will not propagate as these are free oscillations (for details see, e.g. Sutmann et al., 1998).

Any attempt to describe wave propagation in a different plasma and field environments would require a detailed numerical analysis of the coupled system of charged particles and neutrals

CHAPTER 4

Waves in weakly ionised solar plasmas [1]

4.1 Introduction

Study of waves and oscillations in the solar atmosphere received new impetus in the last few decades thanks to a plethora of high-resolution observations showing plasma dynamics on all sort of spatial and temporal scales. Waves proved to be an essential tool for plasma and magnetic field diagnostics when combining theoretical results (dispersion relations, evolutionary equation, polarisation of waves, etc.) with observations (wavelengths, periods, damping time and length, etc.) similar to the seismological techniques on Earth. The solar atmospheric seismology aims to obtain values for physical parameters that cannot be directly or indirectly measured, such as the magnitude and the (sub)resolution of the magnetic field, plasma density, transport coefficients, heating/cooling functions, etc.

In recent years there was a substantial surge in the number of studies of waves where the plasma was considered to be partially ionised, describing a situation one can meet in the lower part of the solar atmosphere where the temperature is not high enough to ensure a complete ionisation of the plasma. In such plasmas the governing equations describing the dynamical and thermodynamical state of the plasma requires a multi-fluid approach, where particles interact via collisions and the frequencies at which changes occur are comparable to the collisional frequencies of particles (Zaqarashvili et al., 2011*b*; Khomenko et al., 2014*a*). A multi-fluid approach not only increases considerably the number of equations (and so the number of waves present in such plasmas) and the complexity of the mathematical description, but also involves some physical aspects that cannot be recovered in a single fluid approximation (e.g. existence of cut-offs, forbidden propagation regimes, plasma filamenta-

[1] This Chapter is based on a paper (Alharbi et al., 2022), submitted for publication to MNRAS

tion, etc.).

The study of waves and instabilities in partially ionised plasmas has shed light on the effect of interaction between particles on the nature and properties of waves, and on the onset and evolution of instabilities. In this respect Zaqarashvili et al. (2011*b*), Soler et al. (2013*b*) and Braileanu et al. (2019) studied the propagation of magnetoacoustic waves in two-fluid plasma, where the two components are the charged particles (positive ions and electrons) and neutrals. Their results showed that in this configuration waves are affected by the collision between particles, leading to a damping of waves. In addition, when considering chromospheric conditions, these studies found that magnetoacoustic waves with wavelengths smaller than 1 km are affected by two-fluid effects in regions with intense magnetic fields, while much shorter wavelengths have to be considered for these effects to be relevant in quiet Sun conditions.

The same two-fluid model has been also considered when analysing Alfvén waves by Soler et al. (2013*a*). These authors found that similar to magnetoacoustic modes, Alfvén waves are also strongly influenced by the collision between particles and the damping of these modes is most efficient when the wave frequency and the collision frequency are of the same order of magnitude. The effect of heavy particles (He atoms) and stratification on the propagation of torsional Alfvén waves was investigated by Zaqarashvili et al. (2013) and their results show that shorter-period (< 5 s) torsional Alfvén waves damp quickly in the chromospheric network due to ion-neutral collision, while longer-period (> 5 s) waves do not reach the transition region as they become evanescent at lower heights in the network cores, meaning that stratification of the plasma has a filtering effect on wave propagation.

The partially ionised solar plasma in the lower part of the solar atmosphere is a very dynamical environment, where the chemical composition of the plasma can change over time scales comparable with the temporal characteristic of waves due to additional ionisation and recombination. These processes confer the plasma a non-equilibrium state. Waves in such plasmas have been modelled numerically and analytically (e.g. Maneva et al., 2017; Ballai, 2019; Braileanu et al., 2019; Zhang et al., 2021) showing that the propagation of waves and the process of plasma heating is seriously affected by non-equilibrium effects. For a comprehensive review on the property of waves in partially ionised plasma (see, e.g. Ballester et al., 2018*a*).

In Chapter 3 we have studied the propagation of guided slow sausage waves in the presence of gravitational stratification in the solar chromosphere, where

the ionisation degree is high. There we used a two-fluid model (neutrals and charged particles), and the small value of the density ratio between neutrals and ions was employed as an expansion parameter. Considering an initial value problem, our analysis showed that while ion-acoustic modes possessed an acoustic cut-off, the slow mode associated with neutrals propagated with no cut-off frequency and the absence of this value was due to the collisions between neutrals and ions.

The above studies considered a two-fluid approach, however, their model choice was not always justified within the framework of solar and space plasmas. In many investigations listed earlier the collisional frequency was considered a free parameter and the analysis focused on the investigation of wave properties when the collisional frequency was varying between the collision-free case and a regime completely dominated by collisions. While such investigations are important to analyse the variation of wave properties over a large parametric space, these have a rather restricted connectivity to real solar physics applications. In the present study we plan to apply observational constrains and construct our model on realistic background.

Our research can be considered to be a continuation (or complementary) of the study described by Chapter 3, but now we focus on the study of waves in weakly ionised limit, corresponding to the lower part of the solar atmosphere.

We will start by constructing our working environment using standard solar atmospheric models and investigate the key properties that are important for our purposes. Later we will introduce the mathematical formalism together with assumptions that are based on observational facts aimed to simplify our treatment as much as possible, yet describing a realistic physical situation. The governing equations describing the evolution of waves are solved and analysed for a simple configuration to elucidate the role of gravitational stratification in the process of wave propagation. A normal mode analysis is employed different frequency regimes in order to study the properties of waves and their propagation characteristics.

4.2 Model restrictions

In order to correctly describe the evolution of waves and their properties, we will need to impose a few physical restrictions derived from observations. The lower part of the solar atmosphere is a layer of the solar atmosphere which is characterised by relatively low temperatures and high densities. This means

that here the plasma is weakly ionised. Various solar atmospheric models predict a ratio of neutral number density to ions of the order of 10^4 (for details see Chapter 3). Since we assume a quasi-neutral hydrogen plasma, the above statement also means that the ratio between the number density of neutrals and electrons is equally very high.

During their motion particles interact through short and long-range collisions, during which the plasma can be thermalised and effective momentum transfer can take place. While electrons have much lower mass than ions and neutrals and they do not contribute significantly to the process of momentum and energy transfer, however, their interaction with massive particles (neutrals and ions) is important because any thermal inhomogeneity will be smoothed out through the electron collisions. Given the high density of particles in the solar photosphere, collisions will play a very important role.

Another important ingredient in our analysis is the magnetic field. The region of our interest corresponding to low level of ionisation, is the region whose magnetic field, its properties and structure, was determined and measured most reliably using various techniques (e.g. spectroscopic measurements, the Zeeman and Hanle-effects, etc.). The magnetic field in the solar photosphere takes various forms. The most prominent structures dominating the active regions and the network are the sunspots and pores (appearing as dark regions), that have field strengths of a few kG. In addition, the quiet Sun is permeated by a weaker field, often forming structures such as small-scale Ω loops, U-loops and turbulent field. Although such features are found everywhere in the photosphere, they are most typical for the quiet Sun, in particular the interiors of supergeranular cells, the internetwork (for a review of the quiet Sun magnetism see, e.g. Almeida, 2003; Khomenko, 2006; Trujillo Bueno et al., 2006; Title, 2007; Solanki, 2009). In our study we will focus on weaker field regions and assume a simple variation of the magnetic field with height.

The formulaic variation of the magnetic field with height is an open question and this depends very much on the nature of the magnetic structure we would like to investigate. Applying the thin flux-tube model and pressure balance equation, Khomenko et al. (2015) proposed a magnetic field variation law with height of the form

$$B_0(z) = B_0(0) \exp\left[-\frac{z}{600}\right], \tag{4.1}$$

where B_0 is the magnetic field at $z = 0$ reference level and the height, z, is measured in km. We should mention here that the choice of the above dependence is somehow arbitrary. Using the same considerations Vranjes and

Krstic (2013) proposed a height variation where the e-folding length was 250 km. The same thin flux tube principle was used by Goodman (2000) who, inspired by a series of considerations made by Parker (1979), assumed a height dependence of the magnetic field of the form

$$B(z) = B_0(0)\exp[-\Gamma(z)],$$

where

$$\Gamma(z) = \frac{m_i g}{2k_B}\int_0^z \frac{dz'}{T(z')},$$

with m_i being the ion mass and $T(z)$ the height-dependent temperature.

Finally, Pillet et al. (1997) proposed a height variation of the magnetic field above the plage region of the form

$$B(z) = B_0(0)\left[\frac{\rho(z)}{\rho(0)}\right]^a,$$

where the value of the constant a is taken to be 0.3 and $\rho(0)$ is the density at height $z = 0$. While the first two relations give an empirical dependence on the height, the last two equations connect the variation of the magnetic field with height to the variation of the temperature and density, respectively. In our study we are going to use the relation proposed by Khomenko et al. (2015) assuming a 100 G magnetic field at the $z = 0$ level. At the $z = 2$ Mm chromospheric height this model predicts a magnetic field of 3.57 G.

With the values of the magnetic field determined using equation 4.1 we can determine the values of the electron and ion gyro (or cyclotron) frequencies defined earlier (see equations 2.1 and 2.2).

The cyclotron frequencies are the frequencies at which the charged particles gyrate around the magnetic field lines and these are going to play an important role in the determination of the nature of the dynamics. The variation of these two important quantities with height is shown in Figure 4.1 by solid green and black lines, respectively (on logarithmic scale). It is clear that in the case of both species the gyro-frequency decays with height.

The second key physical ingredient of our problem is the collision between particles. While collisions between neutral and charged species is a short-range collision (head-on), the collision between charged particles, is a long-range collision, controlled by electrostatic forces. As before, we are going to determine the characteristic values of collisional frequencies based on the tabulated values of number densities of particles and temperature given by

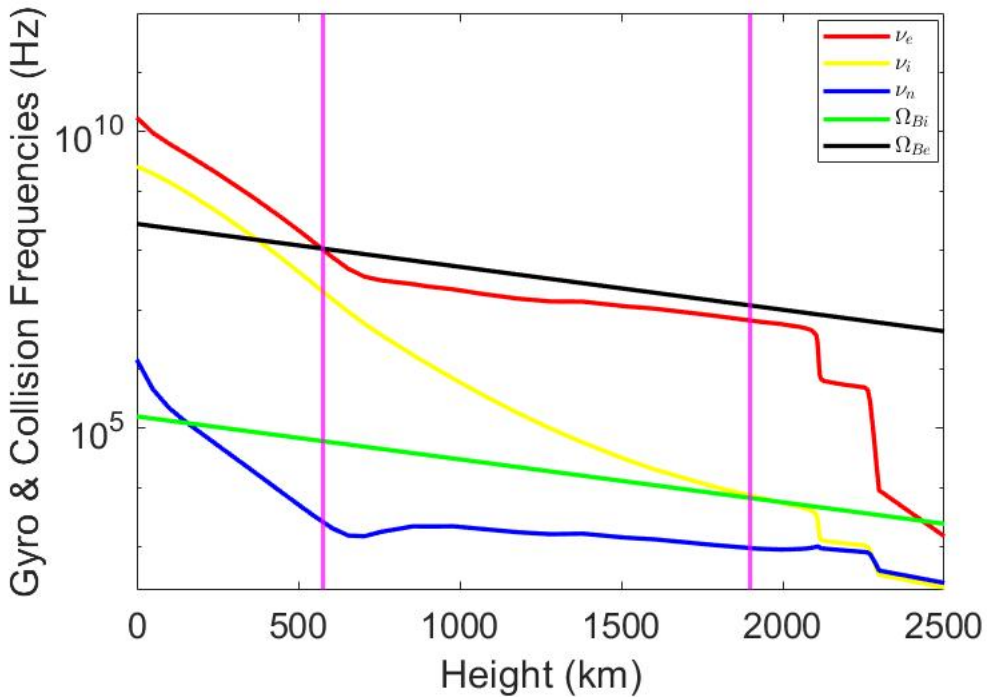

Figure 4.1: The variation of the collisional frequency of various particles and gyro-frequencies with height based on the VAL III atmospheric model (Vernazza et al., 1981). The purple vertical lines are showing the locations where the collisional frequencies of electrons and ions cross the electron and ion gyro-frequencies and these delimitate regions in the solar atmosphere with different dynamics.

the VAL IIIC model (Vernazza et al., 1981). The collisions between various particles are important as these processes ensure an effective transfer of energy and momentum between species, and provide a mechanism for thermalisation of the plasma.

Let us assume that the collision between particles are elastic and no further ionisation/recombination, excitation and charge exchange take place. Considering species having the same temperature, the binary collisional frequencies between species was given as earlier by equation 2.3.

Clearly, due to the height variation of the number densities and temperatures, the collisional frequencies between the three species will also vary with height. To illustrate this we employ the VAL III model (Vernazza et al., 1981) and we plot the total collisional frequencies of particles together with the gyro-frequencies of charged particles with height (see Figure 4.1). In this figure the total collisional frequency denote the collisional frequency of a particular species with the other two species, e.g. $\nu_i = \nu_{ie} + \nu_{in}$. The lines corresponding

to the electron, ion and neutral total collisional frequencies are shown by red, yellow and blue solid lines, respectively.

Figure 4.1 constitutes the physical background of the investigation presented here. We can clearly identify several regions will distinct physics governing the evolution of the plasma (the boundaries of these regions are shown by the purple vertical lines). First of all below heights of approximately 600 km, (Region I) covering the extent of the whole photosphere, the collisional frequencies of both charged species are larger than the gyro-frequencies of both electrons and ions, meaning that in this region particles collide many times within a gyro-period, so magnetic effects can be neglected. In the absence of magnetic forces particles have a simple Brownian motion and the dynamics can be described within the framework of usual hydrodynamics. Above this height (Region II), up to approximately 1900 km, both the collisional frequency of charged species become smaller than the electron gyro-frequency, but they are still larger than the ion gyro frequency, meaning that electrons become magnetised, however, ions are still non-magnetised and they are collisionally coupled to neutrals. That implies that magnetic forces affect only the motion of electrons. Finally, above the height of 1900 km the collisional frequency of both charged species becomes smaller than the ion gyro-frequency, meaning that ions also become magnetised. For completeness, electrons remains unmagnetised as long as the magnetic field is below the critical value

$$B_c \leq \frac{2\pi\nu_e m_e}{e}.$$

Considering a characteristic electron-neutrals collisional frequency of 1.5×10^{10} Hz, the critical magnetic field takes the value of 5.5 kG. Since such magnetic fields are unrealistically high in the quiet solar photosphere, our working framework is valid for any magnetic field. Sunspots are known to have kG magnetic fields, however, there the atmospheric model employed by us is not applicable. The solar photosphere is the region of the solar atmosphere where one can have not only very intense magnetic fields (e.g. sunpots and pores are typical examples where field strength is of the order of a few kG), but also a remnant quiet Sun magnetic field of the order of a few tens of G (Ballai and Forgács-Dajka, 2010).

Another key aspect that can be derived from variation of collisional frequencies of electrons with height (see Figure 4.2) is that starting from the low chromosphere electrons are much more tightly coupled to ions than to neutrals. As a consequence the charged particles can form a single fluid that can interact

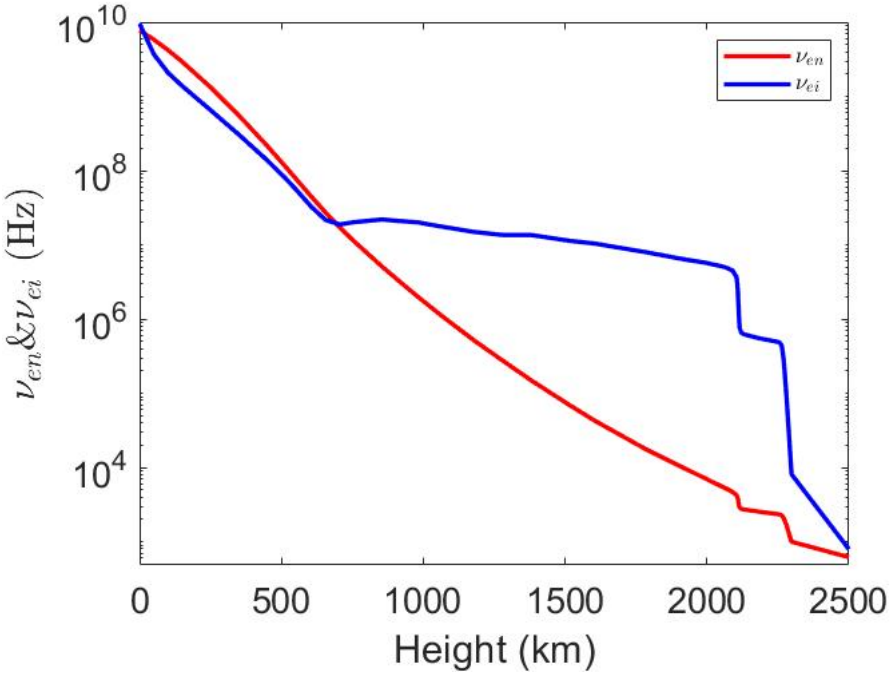

Figure 4.2: The variation of the collisional frequency of electrons with ions (ν_{ei}, blue line) and electrons with neutrals (ν_{en}, red line) with height based on a VAL IIIC solar atmospheric model (Vernazza et al., 1981)

with the neutral fluid. Below this height, the collisional frequencies of electrons and the other species are close to each other, meaning that the plasma dynamics can be described within the framework of a three-fluid plasma.

On the other hand, in Region II electrons are magnetised, however, the collision of electrons with ions and neutrals will not change the dynamics of the system, when the frequency domain is restricted to frequencies of the order of ion-neutral collisional frequency, i.e. the frequency regime described by a two-fluid approximation, where ions and electrons are strongly coupled and form a charged fluid that interacts with the neutral fluid.

Given the relatively low temperature of the lower solar atmosphere, the gravitational scales heights might be comparable with the wavelength of waves, meaning that gravitational stratification could play an important role in the propagation of waves. This aspect will be elucidated later in this paper.

In Chapter 2 we found that a multi-temperature plasma can reach thermal equilibrium very fast, therefore, all sound speeds will be considered equal. In a uni-thermal plasma the sound speeds associated to different species will be equal.

4.3 Governing Equations and Assumptions

The dynamics of waves studied in this paper can be described within the framework of a multi-fluid MHD approximation, where the governing equations describe conservation laws for each species (electrons, ions, neutrals) denoted by the index α ($\alpha = e, i, n$). In the absence of magnetic forces, equations (2.8), (2.9) and (2.11) reduce to

$$\frac{\partial \rho_\alpha}{\partial t} + \nabla \cdot (\rho_\alpha \mathbf{v}_\alpha) = 0, \tag{4.2}$$

$$\rho_\alpha \frac{d\mathbf{v}_\alpha}{\partial t} + \nabla p_\alpha = \rho_\alpha \mathbf{g} + \sum_{\alpha' \neq \alpha} \mathbf{P}_{\alpha\alpha'} + \mathcal{F}, \tag{4.3}$$

$$\frac{d}{dt}\left(\frac{p_\alpha}{\rho_\alpha^\gamma}\right) = 0, \tag{4.4}$$

where $\mathcal{F}$ represents any other force that will be introduced later in Section 4.4, ρ_α, $\mathbf{v}_\alpha$ and p_α are the density, velocity vector and pressure of species α, γ is the adiabatic index, and $\mathbf{P}_{\alpha\alpha'}$ represents the longitudinal momentum transfer between species α and α' (given by equation 2.10), and the summation is made for $\alpha' \neq \alpha$. We should note that, under normal circumstances, the above energy equations should contain a heating term due to collisions between particles, however, these terms are proportional to the squares of velocities (i.e. nonlinear).

4.4 Waves in weakly ionised plasmas

Based on the complex picture revealed by Figure 4.1, it is natural to divide the region containing weakly ionised plasma in different regimes and study the properties of waves for each separate case.

4.4.1 Waves in Region I

The spatial extent of this region is determined by the condition $\nu_e > \Omega_{Be}$. For the chosen magnetic field profile, this region covers the whole photosphere. The fact that magnetic effects can be neglected when concentrating on the dynamics of waves in weakly ionised photospheric plasma, considerably simplifies the modelling because the only waves that can propagate are the acoustic modes. In the present study we are going to study only linear waves, therefore all

governing equations will be linearised.

Since, in the first instance, we would like to elucidate the importance of gravity and the effects connected to this important ingredient, we are going to concentrate on one-dimensional dynamics and consider that perturbations propagate vertically, against the gravitational field. That is why the dynamics of waves in the three-fluid plasma will be given by the linearised system of equations 4.2–4.4 as

$$\frac{\partial \rho_\alpha}{\partial t} + \frac{\partial}{\partial z}(\rho_{0\alpha} v_\alpha) = 0, \tag{4.5}$$

$$\rho_{0\alpha}\frac{\partial v_\alpha}{\partial t} + \frac{\partial p_\alpha}{\partial z} + \rho_\alpha g = \sum_{\alpha' \neq \alpha} P_{\alpha\alpha'}, \tag{4.6}$$

$$\frac{\partial p_\alpha}{\partial t} + v_\alpha \frac{dp_{0\alpha}}{dz} = c_S^2 \left(\frac{\partial \rho_\alpha}{\partial t} + v_\alpha \frac{\partial \rho_\alpha}{\partial z} \right). \tag{4.7}$$

As before, the quantities with an index '0' denote equilibrium values. Since we consider uni-thermal plasma, the sound speeds for all three species will be equal, therefore we will drop the index α from the sound speeds. The quantities $P_{\alpha\alpha'}$ refer only to the longitudinal transfer of momentum between species and the velocity v_α refers to the vertical component of velocity.

Now let us discuss in details the momentum transfer for each species using equation 2.10. In the case of neutrals, the transfer of momentum will have two terms corresponding to the collision of neutrals with electrons and with ions. Accordingly we have

$$P_{ne} = -\frac{8}{3}\sqrt{2} n_e n_n m_e \left(\frac{k_B T}{\pi m_e} \right)^{1/2} \sigma_{ne}(v_n - v_e), \tag{4.8}$$

$$P_{ni} = -\frac{8}{3} n_n n_i m_i \left(\frac{k_B T}{\pi m_i} \right)^{1/2} \sigma_{ni}(v_n - v_i). \tag{4.9}$$

For ions the relevant momentum transfer terms become

$$P_{in} = -\frac{8}{3} n_n n_i m_i \left(\frac{k_B T}{\pi m_i} \right)^{1/2} \sigma_{in}(v_i - v_n), \tag{4.10}$$

and

$$P_{ie} = -\frac{8}{3}\sqrt{2} n_i n_e m_e \left(\frac{k_B T}{\pi m_e} \right)^{1/2} \sigma_{ie}(v_i - v_e). \tag{4.11}$$

Finally, for electrons these expressions become

$$P_{en} = -\frac{8}{3}\sqrt{2} n_e n_n m_e \left(\frac{k_B T}{\pi m_e} \right)^{1/2} \sigma_{en}(v_e - v_n), \tag{4.12}$$

and

$$P_{ei} = -\frac{8}{3}\sqrt{2} n_e n_i m_e \left(\frac{k_B T}{\pi m_e}\right)^{1/2} \sigma_{ei}(v_e - v_i). \tag{4.13}$$

We should point out that since we are dealing with elastic collisions, the momentum conservation requires that $P_{\alpha\alpha'} + P_{\alpha'\alpha} = 0$.

Now let us estimate the magnitude of the two terms for each species. Assuming that velocity perturbations are of the same order we have that

$$\left|\frac{P_{ne}}{P_{ni}}\right| = \mathcal{O}\left(\mu^{-1/2}\frac{\sigma_{ne}}{\sigma_{ni}}\right), \quad \left|\frac{P_{in}}{P_{ie}}\right| = \mathcal{O}\left(\frac{n_n}{n_e}\mu^{1/2}\frac{\sigma_{in}}{\sigma_{ie}}\right),$$

$$\left|\frac{P_{en}}{P_{ei}}\right| = \mathcal{O}\left(\frac{n_n}{n_i}\frac{\sigma_{en}}{\sigma_{ei}}\right). \tag{4.14}$$

Taking into account that we are dealing with a weakly ionised quasi-neutral hydrogen plasma ($n_i = n_e \ll n_n$) and the typical values of collisional cross sections available in the literature, we can show that $P_{ne} \ll P_{ni}$, $P_{in} \gg P_{ie}$ and $P_{en} \gg P_{ei}$. These orderings between momentum transfer rates will help us simplify the momentum equations for the three species.

The plasma is in hydrostatic equilibrium so that for each species we have

$$\frac{dp_{0\alpha}}{dz} = -g\rho_{0\alpha}.$$

In addition, the equilibrium state also satisfies the equations of state, i.e.

$$p_{0j} = \frac{k_B \rho_{0\alpha} T_0}{\tilde{m}_\alpha},$$

where T_0 is the equilibrium values of the temperature, and $\tilde{m}_\alpha$ denotes the mean particle mass for the species α.

As a result, the three simplified momentum equations read

$$\begin{aligned}
\rho_{0n}\frac{\partial v_n}{\partial t} + \frac{\partial p_n}{\partial z} + \rho_n g &= -n_n m_i \nu_{nc}(v_n - v_c),\\
\rho_{0e}\frac{\partial v_e}{\partial t} + \frac{\partial p_e}{\partial z} + \rho_e g &= -n_e m_e \nu_{en}(v_e - v_n),\\
\rho_{0i}\frac{\partial v_i}{\partial t} + \frac{\partial p_i}{\partial z} + \rho_i g &= -n_i m_i \nu_{in}(v_i - v_n),
\end{aligned} \tag{4.15}$$

where we used the fact that in a hydrogen plasma $m_i \approx m_n$. Clearly, the evolution of charged particles will be driven by neutrals, which is natural in such weakly ionised and highly collisional plasmas. The above equations, together

with the mass and energy conservation equations (4.2, 4.4) will be used to determine the evolutionary equations of waves associated with various species and the property of these waves in the presence of gravitational stratification.

With the simplifications listed above, we can reduce the system of equations to

$$\frac{\partial^2 v_e}{\partial t^2} - c_S^2 \frac{\partial^2 v_e}{\partial z^2} + \gamma g \frac{\partial v_e}{\partial z} + \nu_{en} \left(\frac{\partial v_e}{\partial t} - \frac{\partial v_n}{\partial t} \right) = 0, \tag{4.16}$$

$$\frac{\partial^2 v_i}{\partial t^2} - c_S^2 \frac{\partial^2 v_i}{\partial z^2} + \gamma g \frac{\partial v_i}{\partial z} + \nu_{in} \left(\frac{\partial v_i}{\partial t} - \frac{\partial v_n}{\partial t} \right) = 0, \tag{4.17}$$

$$\frac{\partial^2 v_n}{\partial t^2} - c_S^2 \frac{\partial^2 v_n}{\partial z^2} + \gamma g \frac{\partial v_n}{\partial z} + \nu_{ni} \left(\frac{\partial v_n}{\partial t} - \frac{\partial v_i}{\partial t} \right) = 0. \tag{4.18}$$

Inspired from the results in Chapter 3, equations 4.16– 4.18 can be written in the standard form of telegrapher's equations for the three species, by introducing new functions of the form

$$v_\alpha(z,t) = (\gamma p_{0\alpha})^{-1/2} Q_\alpha(z,t).$$

After some straightforward calculations, the three momentum equations can be written as

$$\frac{\partial^2 Q_e}{\partial t^2} - c_S^2 \frac{\partial^2 Q_e}{\partial z^2} + \omega_e^2 Q_e = -\nu_{en} \left(\frac{\partial Q_e}{\partial t} - \chi^{1/2} \frac{\partial Q_n}{\partial t} \right), \tag{4.19}$$

$$\frac{\partial^2 Q_i}{\partial t^2} - c_S^2 \frac{\partial^2 Q_i}{\partial z^2} + \omega_i^2 Q_i = -\nu_{in} \left(\frac{\partial Q_i}{\partial t} - \chi^{1/2} \frac{\partial Q_n}{\partial t} \right), \tag{4.20}$$

$$\frac{\partial^2 Q_n}{\partial t^2} - c_S^2 \frac{\partial^2 Q_n}{\partial z^2} + \omega_n^2 Q_n = 0, \tag{4.21}$$

where,

$$\omega_\alpha^2 = -\frac{3}{4} \frac{\gamma^2 g^2}{c_S^2} - \gamma g \frac{d}{dz} (\ln \rho_{0\alpha}) - \frac{\gamma g}{2} \frac{d}{dz} \left(\ln c_S^2 \right),$$

are the acoustic cut-off frequencies for each species, and χ is the ionisation fraction defined as $\chi = \rho_{0i}/\rho_{0n} = \mu \rho_{0e}/\rho_{0n} \ll 1$.

It is straightforward to show that the above equations can be written as a form of Klein-Gordon equation by introducing a new function for each species of the form

$$Q_\alpha(z,t) = q_\alpha(z,t) \exp(\lambda_\alpha t),$$

where the values of the parameters λ_α are chosen such that the first-order

derivatives with respect to t vanish. Indeed, by choosing

$$\lambda_e = -\frac{\nu_{en}}{2}, \quad \lambda_i = -\frac{\nu_{in}}{2}, \quad \lambda_n = -\frac{\nu_{ni}}{2},$$

the system of equations describing the spatial and temporal evolution of waves for the three species becomes

$$\frac{\partial^2 q_e}{\partial t^2} - c_S^2 \frac{\partial^2 q_e}{\partial z^2} + \tilde{\Omega}_e^2 q_e = \nu_{en} \chi^{1/2} e^{(\nu_{en}-\nu_{ni})t/2} \left(\frac{\partial q_n}{\partial t} - \frac{\nu_{ni}}{2} q_n \right), \tag{4.22}$$

$$\frac{\partial^2 q_i}{\partial t^2} - c_S^2 \frac{\partial^2 q_i}{\partial z^2} + \tilde{\Omega}_i^2 q_i = \nu_{in} \chi^{1/2} e^{(\nu_{in}-\nu_{ni})t/2} \left(\frac{\partial q_n}{\partial t} - \frac{\nu_{ni}}{2} q_n \right), \tag{4.23}$$

$$\frac{\partial^2 q_n}{\partial t^2} - c_S^2 \frac{\partial^2 q_n}{\partial z^2} + \tilde{\Omega}_n^2 q_n = 0, \tag{4.24}$$

where

$$\tilde{\Omega}_e^2 = \omega_e^2 - \frac{\nu_{en}^2}{4}, \quad \tilde{\Omega}_i^2 = \omega_i^2 - \frac{\nu_{in}^2}{4}, \quad \tilde{\Omega}_n^2 = \omega_n^2 - \frac{\nu_{ni}^2}{4}, \tag{4.25}$$

are the squares of the collision-modified cut-off frequencies for electron, ion, and neutral sound waves, respectively.

In order to estimate the magnitude and importance of these modified cut-off frequencies, we plot their variation with height, where the values of various physical parameters (e.g. densities, temperatures, etc.) are taken from the VAL IIIC atmospheric model (see Figure 4.3), with the blue, yellow and red line corresponding to the variation for neutrals, ions and electrons, respectively. It is clear that in the region of the interest (but true for the whole weakly ionised solar atmosphere) these quantities are negative, meaning that collisional effects are more important than stratification effects and collisions between particles will prevent any growth of waves' amplitudes. This result implies that gravitational effects can be confidently neglected when discussing the propagation of waves in a multi-fluid framework, so the dynamics of waves can be described within the framework of a homogeneous (non-stratified)plasma. As a result, the $\tilde{\Omega}_\alpha^2$ coefficients of the last terms on the left-hand side of equations 4.22–4.24 will be negative, therefore, waves will propagate with no cut-off frequency.

We can carry out a normal mode analysis for the homogeneous part of equations 4.22-4.24, by assuming perturbations proportional to $e^{i(kz-\omega t)}$, where k is the wavenumber of waves and ω is the frequency. Now the governing

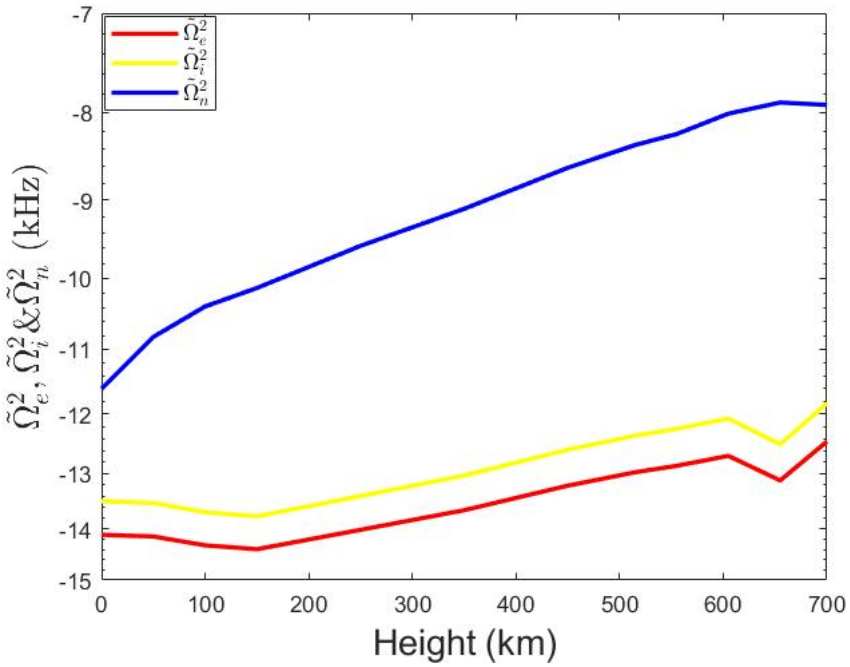

Figure 4.3: The variation with height of the square of the collision-modified cut-off frequencies for electron, ion, and neutral acoustic-gravity waves based on equations. 4.25 and assuming a VAL IIIC atmospheric model. The values are given on logarithmic scale.

equations for the three species reduce to the dispersion relations

$$\omega^2 = k^2 c_S^2 - \tilde{\Omega}_\alpha^2. \tag{4.26}$$

Clearly, waves will propagate (i.e. $\omega^2 > 0$) provided the wavenumbers attached to these waves satisfy the conditions

$$k_c^e > \frac{\tilde{\Omega}_e}{c_S} \approx \frac{\nu_{en}}{2c_S},\ k_c^i > \frac{\tilde{\Omega}_i}{c_S} \approx \frac{\nu_{in}}{2c_S},\ k_c^n > \frac{\tilde{\Omega}_n}{c_S} \approx \frac{\nu_{ni}}{2c_S}, \tag{4.27}$$

where the quantities k_c^α constitute the values of the wavenumber cut-off corresponding to the three species.

With the gravitational effects safely neglected we can treat the problem of dynamics in a homogeneous plasma, allowing us to discuss a more complex model. Without loss of generality, we can assume a two dimensional propagation in the xz plane. In this case the governing linearised equations 4.2–4.4 for the three species become

$$\frac{\partial \rho_\alpha}{\partial t} + \rho_{0\alpha}\left(\frac{\partial v_{x\alpha}}{\partial x} + \frac{\partial v_{z\alpha}}{\partial z}\right) = 0, \tag{4.28}$$

$$\rho_{0\alpha}\frac{\partial v_{x\alpha}}{\partial t}+\frac{\partial p_\alpha}{\partial x}=\sum_{\alpha'\neq\alpha}P_{\alpha\alpha'}, \tag{4.29}$$

$$\rho_{0\alpha}\frac{\partial v_{z\alpha}}{\partial t}+\frac{\partial p_\alpha}{\partial z}=\sum_{\alpha'\neq\alpha}P_{\alpha\alpha'}, \tag{4.30}$$

$$\frac{\partial p_\alpha}{\partial t}=c_S^2\frac{\partial \rho_\alpha}{\partial t}. \tag{4.31}$$

After long but straightforward calculations, the system of governing equations can be reduced to a system of partial differential equations for each species

$$\left(c_S^2\frac{\partial^2}{\partial x^2}-\frac{\partial^2}{\partial t^2}-\nu_{\alpha\alpha'}\frac{\partial}{\partial t}\right)v_{x\alpha}+c_S^2\frac{\partial^2 v_{z\alpha}}{\partial x\partial z}+\nu_{\alpha\alpha'}\frac{\partial v_{x\alpha'}}{\partial t}=0, \tag{4.32}$$

$$\left(c_S^2\frac{\partial^2}{\partial z^2}-\frac{\partial^2}{\partial t^2}-\nu_{\alpha\alpha'}\frac{\partial}{\partial t}\right)v_{z\alpha}+c_S^2\frac{\partial^2 v_{x\alpha}}{\partial x\partial z}+\nu_{\alpha\alpha'}\frac{\partial v_{z\alpha'}}{\partial t}=0. \tag{4.33}$$

Next, in the above two equations we apply a Fourier analysis, writing all velocity components proportional to $\exp(ik_x+ik_z-i\omega t)$. Using the compatibility condition of the system of equations written for the amplitude of velocities, we obtain the dispersion relation of the three acoustic modes in the form of a sixth order polynomial of the form

$$\left(-\omega^2+k^2c_S^2-i\omega\nu_{en}\right)\Big[\omega^4+i\omega^3(\nu_{in}+\nu_{ni})-\omega^2(\nu_{in}\nu_{ni}-\nu_{ni}^2+2k^2c_S^2)$$

$$-i\omega k^2c_S^2(\nu_{in}+\nu_{ni})+k^4c_S^4\Big]=0. \tag{4.34}$$

The variation of the real and imaginary parts of the dimensionless frequency (in units of the electron gyro-frequency) with respect to the dimensionless frequency kc_S/Ω_{Be} are shown in Figures 4.4 and 4.5 for the acoustic modes associated to the neutral, ion and electron species shown by blue, red and black solid lines, respectively. To produce these figures the characteristic values of physical parameters were chosen to be $c_S = 10$ km s^{-1}, $T = 4465$ K, $\nu_{in} = 1.8\times10^8$ Hz, $\nu_{ni} = 2\times10^4$ Hz, $\nu_{en} = 5.5\times10^8$ Hz and $\Omega_{Be} = 1.5\times10^8$ Hz. The cut-off values given by equation 4.27 are represented as vertical dotted lines. In practice these plots display the variation of the dimensionless frequencies with the wavenumber (or its inverse, the wavelength). It is clear that in this region the sound waves associated to neutrals propagate practically with no cut-off value and their frequency increases with decreasing the wavelength. Their dispersion curve follows the $\omega = kc_S$ line and these waves propagate

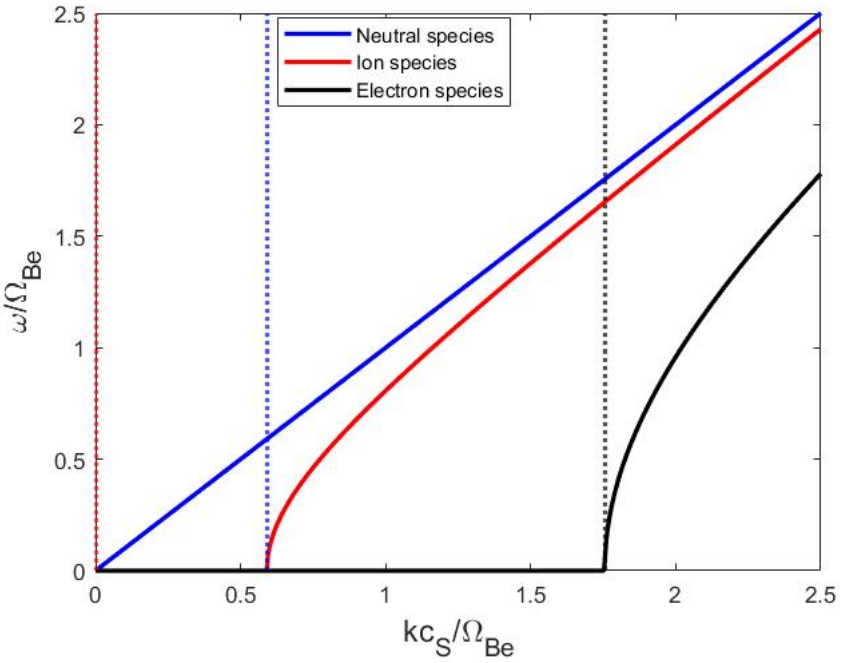

Figure 4.4: The real part of frequencies of modes (in units of the electron gyrofrequency, Ω_{Be}) given by equation 4.34 in terms of the dimensionless variable kc_S/Ω_{Be} for the sound waves associated to the three species. Here the variation of the frequency for neutral, ion and electron sound waves are given by blue, red and black solid lines, respectively).

practically with no damping (see Figure 4.5).

Given the high collisional frequency between ions and neutrals, the frequency of ion sound waves quickly becomes equal to the frequency of neutral sound waves. For large values of the wavelength (small values of kc_S/Ω_{Be} sound waves associated with ions propagate only if their wavenumber is larger than a critical value that can be defined as $k \geq \nu_{in}/2c_S \approx 9.2$ km^{-1}. Below the critical wavenumber ion sound waves are simple entropy modes (Goedbloed et al., 2004; Murawski et al., 2011; Soler et al., 2013*b*), i.e. non-propagating. The frequency of entropy modes is purely imaginary and involves perturbations in the plasma density (or internal energy), but not in pressure. The transition of these waves from entropy, non-propagating waves, to acoustic propagating waves occurs at the critical wavenumber. For propagating ion sound waves their frequency increases with decreasing wavelength and their damping rate is independent on the wavelength of waves. Finally, the sound waves associated with electrons have a much higher cut-off value and will propagate when $k \geq \nu_{en}/2c_S \approx 27.3$ km^{-1}. Although the electron-related sound waves show initially a distinct behaviour compared to the other two modes (due to the

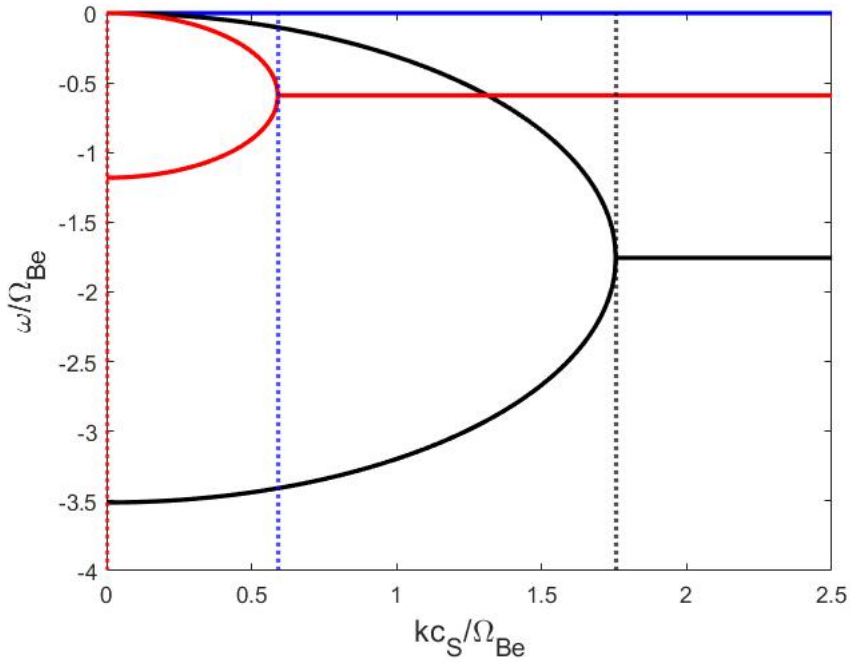

Figure 4.5: The same as in Figure 4.4, but here we plot the variation of the imaginary part of the frequencies, as given by equation 4.34.

increased mobility of electrons), for decreasing wavelengths, the frequency of these waves will tend to the frequency of neutral sound waves. The imaginary part of the electron sound waves is shown in Figure 4.5 (black lines). Similar to the ion sound waves, as long as the wavenumber is smaller than the critical value, these waves are non-propagating, entropy waves. For wavenumbers larger than the critical value, waves have a wavelength-independent strong damping. Comparing the magnitude of the real and imaginary parts of the frequency it is obvious that while initially these waves have a strong damping, for smaller wavelengths the waves become weakly damped.

The important result of these figures is that the collisional frequencies play an essential role in the propagation of waves. Waves will be damped with rate that depend only on collisional frequency. In addition, the critical wavenumbers of waves are determined by the strength of collisions between species.

4.4.2 Waves in Region II

The variation of the collisional and gyro-frequencies with height shown in Figure 4.1 reveals that at heights roughly corresponding to the base of the chromosphere, the collisional frequency of electrons falls below the electron gyro-frequency, therefore, electrons become magnetised. At the same time the

collisional frequency of ions is still above the ion gyro-frequency, meaning that ions are still not affected by the magnetic field and their dynamics of predominantly driven by the collisions with neutrals. As a result, the dynamics of electrons and ions becomes different, however they form a single fluid since the collisional frequency of electrons with ions is still very strong (see Figure 4.2). In frequency domain Region II corresponds to $\Omega_{Bi} < \omega < \Omega_{Be}$, where $\Omega_{Be,i}$ were defined earlier. The strong collisional coupling between neutrals and ions prevents ions to magnetise. Electrons moving along the magnetic field, drift due to $\mathbf{E} \times \mathbf{B}$ in the transversal direction, while ions will continue to move together with neutrals. Here $\mathbf{E}$ is the electric field generated as a result of the different motion of electrons and ions.

The disassociation of charged particles results in generation of an electric current $\mathbf{J} = en_e(\mathbf{v}_i - \mathbf{v}_e)$. This current will generate an electric force ($en_e\mathbf{E}$) aimed to oppose the movement of ions.

We assume a uni-directional homogeneous magnetic field of the form $\mathbf{B}_0 = B_0\hat{\mathbf{z}}$. Based on the results we obtained earlier, gravitational effects will be neglected.

Since we are dealing with a two-fluid plasma, the momentum equation for charged particles can be obtained by combining the linearised momentum equations of electrons and ions

$$\rho_{0e}\frac{\partial \mathbf{v}_e}{\partial t} + \nabla p_e = -en_e(\mathbf{E} + \mathbf{v}_e \times \mathbf{B}_0) - \rho_e\nu_{en}(\mathbf{v}_e - \mathbf{v}_n), \tag{4.35}$$

$$\rho_{0i}\frac{\partial \mathbf{v}_i}{\partial t} + \nabla p_i = +en_i\mathbf{E} - \rho_e\nu_{in}(\mathbf{v}_i - \mathbf{v}_n). \tag{4.36}$$

As a result, the momentum equation for charges becomes

$$\rho_{0c}\frac{\partial \mathbf{v}_c}{\partial t} + \nabla p_c = -en_e\mathbf{v}_e \times \mathbf{B}_0 - \rho_{0c}\nu_{cn}(\mathbf{v_c} - \mathbf{v_n}), \tag{4.37}$$

where

$$\rho_{0c} = \rho_{0e} + \rho_{0i}, \quad \mathbf{v}_c = \frac{\rho_{0i}\mathbf{v}_i + \rho_{0e}\mathbf{v}_e}{\rho_{0c}},$$

$$\nu_{cn} = \frac{\rho_{0i}\nu_{in} + \rho_{0e}\nu_{en}}{\rho_{0c}},$$

are the total density of charged species, the velocity of the center of the mass, and the collisional frequency of charged fluid weighed by the density of the two species. Finally, the momentum conservation of neutrals can be simply

written as

$$\rho_{0n}\frac{\partial \mathbf{v}_n}{\partial t} + \nabla p_n = -\rho_{0n}\nu_{nc}(\mathbf{v}_n - \mathbf{v}_c). \tag{4.38}$$

Despite the two-fluid approximation, only electrons are magnetised and, through collisions, electrons are perturbing the ion population. We should also keep in mind that neutrals and ions are still coupled, which results in a strong drag force resulting in the bulk of ion velocity, $\mathbf{v}_i$ closely matching the velocity of the neutral gas. With the charged particles having different motion (electrons gyrating around the equilibrium magnetic field and ions having a rectilinear motion advected by neutrals) the quasi-neutrality of the plasma is going to be perturbed, however the electric field generated will always aim to restore the quasi-neutrality of the system. Ions are still more strongly coupled to neutrals than to electrons since

$$\frac{\nu_{in}}{\nu_{ie}} \approx \frac{n_n}{n_i}\frac{\sigma_{in}}{\sigma_{ie}}\mu^{3/2} \gg 1.$$

Therefore, the current can be written as $\mathbf{J} \approx en_e(\mathbf{v}_n - \mathbf{v}_e)$ or

$$\mathbf{v}_e = \mathbf{v}_n - \frac{\mathbf{J}}{en_e}. \tag{4.39}$$

The role of the current generated in this layer of the solar atmosphere thanks to the disassociation of charged particles was discussed in details in an earlier study by Krasnoselskikh et al. (2010), who showed that these currents are formed around the layer where electron gyrofrequency and collisional frequency are comparable. Currents can also effectively dissipate via ohmic dissipation resulting in typical temperature increases with altitude as large as $0.1 - 0.3$ eV km^{-1}. The heat generated as a result of dissipation can create additional ionisation of particles, leading to the modification in the thermal equilibrium of the plasma. In addition, the currents can generate local magnetic fields (acting as dynamos) comparable with the background magnetic field. The idea of current dissipation in the partially ionised solar atmosphere is relatively new aspect of solar atmospheric research, and remains to be seen how much the dissipation of these currents contribute to the global process of chromospheric plasma heating.

Taking into account the Ampére's law, we can write the momentum equation for the charged species as

$$\rho_{0c}\frac{\partial \mathbf{v}_c}{\partial t} + \nabla p_c = -en_e\mathbf{v}_n \times \mathbf{B}_0 + \frac{1}{\mu_0}(\nabla \times \mathbf{b}) \times \mathbf{B}_0 - \rho_{0c}\nu_{cn}(\mathbf{v_c} - \mathbf{v_n}). \tag{4.40}$$

Since the magnetic field is present in the above equation, we will also need to derive the induction equation from the momentum equation for electrons, assuming that the electron inertia and electron pressure can be neglected. As a result we have

$$en_e(\mathbf{E}+\mathbf{v}_e\times\mathbf{B})=(\nu_{ei}+\nu_{en})\frac{m_e}{e}\mathbf{J}, \tag{4.41}$$

where we took into account equation 4.39. Using the same equation on the left hand side of the above relation, we obtain

$$\mathbf{E}+\mathbf{v}_n\times\mathbf{B}-\frac{1}{en_e}\mathbf{J}\times\mathbf{B}=\nu_e\frac{m_e}{e^2n_e}\mathbf{J}, \tag{4.42}$$

where $\nu_e = \nu_{en}+\nu_{ei}$ is the total collisional frequency of electrons. After taking the curl of the above equation and using Faraday's law of induction ($\nabla\times\mathbf{E}=-\partial\mathbf{B}/\partial t$), we obtain

$$\frac{\partial\mathbf{B}}{\partial t}=\nabla\times(\mathbf{v}_n\times\mathbf{B})-\frac{1}{en_e}\nabla\times(\mathbf{J}\times\mathbf{B})-\frac{m_e\nu_e}{e^2n_e}\nabla\times\mathbf{J}, \tag{4.43}$$

which means that when ions and neutrals are strongly coupled, the neutrals get magnetized. The last two terms of the above equation are the Hall term that renders waves to be dispersive on scales of the order of the ion inertial length and the resistive term that contains, as coefficient, the resistivity due to electrons moving along the magnetic field (and describes the dissipation of field-aligned currents). The currents in this model can dissipate through the collisions of electrons not only with ions, but also with neutrals.

The governing equations in Region II will be the mass conservation equations for charged particles and neutrals given by equation 4.2, the momentum equations for ions and neutrals (4.37 and 4.38), the induction equation 4.41 and the energy equations for the two species (similar to the linearised equation 4.4), considering, again, an adiabatic process. Similar to the waves studied in Region I, we assume a two-dimensional dynamics and write $\mathbf{k}=(k_x,0,k_z)$ or $\mathbf{k}=(k\sin\theta,0,k\cos\theta)$, where θ is the angle between the direction of propagation and the z axis. We also assume waves oscillating in time, so we consider all perturbations proportional to $e^{-i\omega t}$, where ω is the complex frequency.

The combination of all these equations results in the system of equations written for the components of velocity, as

$$(\omega^2-k_x^2c_S^2+i\chi\omega\nu_{cn})v_{nx}-k_xk_zc_S^2v_{nz}-i\chi\omega\nu_{cn}v_{cx}=0, \tag{4.44}$$

$$(\omega^2-k_z^2c_S^2+i\chi\omega\nu_{cn})v_{nz}-k_xk_zc_S^2v_{nx}-i\chi\omega\nu_{cn}v_{cz}=0, \tag{4.45}$$

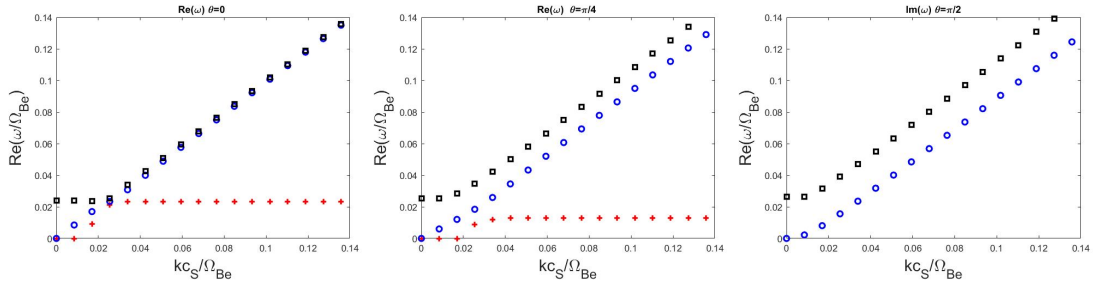

Figure 4.6: Real part of the frequency (in units of the electron gyro-frequency, Ω_{Be}) in terms of the dimensionless frequency kc_S/Ω_{Be}, as solution of the system of equations 4.44–4.47. The three panels correspond to a parallel propagation (left panel), waves propagating at a $\pi/4$ angle with respect to the magnetic field (central panel) and perpendicular to the field (right panel). The coloured curves correspond to charged slow waves (red), neutral slow wave (blue) and fast waves (black).

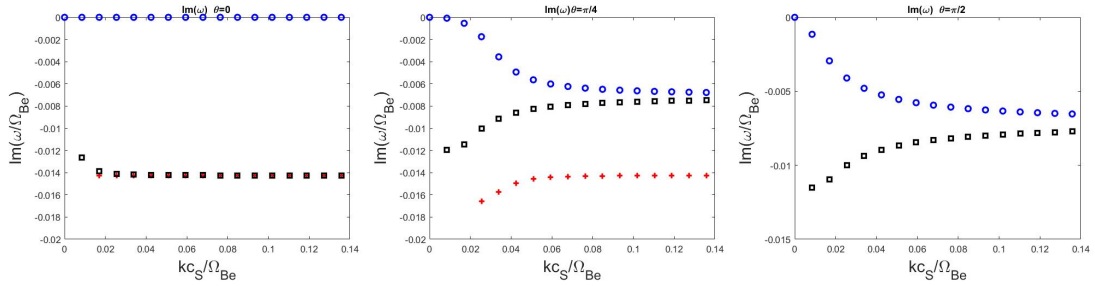

Figure 4.7: The same as Figure 4.6, but here we plot the imaginary parts of the frequency. The colours correspond to the type of waves defined in Figure 4.6.

$$(\omega^2 - k_x^2 c_S^2 + i\omega\nu_{cn})v_{cx} - k_x k_z c_S^2 v_{cz} - i\omega\left(\frac{k_z^2 c_A^2}{i\omega - \eta k^2} + \nu_{cn}\right) v_{nx} + \frac{i\omega k_x k_z c_A^2}{i\omega - \eta k^2} v_{nz} = 0, \tag{4.46}$$

$$(\omega^2 - k_z^2 c_S^2 + i\omega\nu_{cn})v_{cz} - k_x k_z c_c^2 v_{cx} - i\omega\left(\frac{k_x^2 c_A^2}{i\omega - \eta k^2} + \nu_{cn}\right) v_{nz} + \frac{i\omega k_x k_z v_A^2}{i\omega - \eta k^2} v_{nx} = 0, \tag{4.47}$$

where the constant η is the resistivity coefficient, valid in a partially ionised plasmas, and it is defined as

$$\eta = \frac{\nu_e m_e}{n_i \mu_0 e^2},$$

and $v_A = B_0/\sqrt{\mu_0 \rho_{0c}}$ is the Alfvén speed of the charged species.

The above homogeneous system of equations admits solutions only if the determinant of the matrix constructed by means of the coefficients multiplying the components of velocity for the two fluids is vanishing. The dispersion relation is solved numerically and the real and imaginary solutions are represented in Figures 4.6 and 4.7. The real and imaginary parts of the frequency are plotted in units of the electron gyro-frequency (Ω_{Be}) as a function of the dimensionless quantity kc_S/Ω_{Be} for the characteristic values in Region II: $T = 5650$ K, $B = 24.05$ G, $n_i = 1.06 \times 10^{17}$ m^{-3}, $v_A = 206.83$ km s^{-1}, $c_S = 11.42$ km s^{-1}, $\nu_{in} = 1.28 \times 10^6$ Hz and $\nu_e = 2.57 \times 10^7$ Hz. In these figures the possible modes are represented by symbols of different colours, so red crosses describe the solution of the dispersion relation corresponding to slow waves associated to charges, the slow wave associated to neutrals is shown by blue circles, and the fast mode is shown by black squares. The three panels correspond parallel propagation ($\theta = 0$), a $\pi/4$ inclined propagation with respect to the ambient magnetic field, and a perpendicular propagation, respectively.

The behaviour of the three waves shows a strong dependence with the propagation direction. In the case of parallel propagation for very small values of wavenumber, k, (very large wavelengths) the waves that propagate are the fast waves that have a phase speed determined mainly by the Alfvén speed and the neutral slow waves. Due to the strong coupling on neutrals and ions the frequency of these two waves is equal as the wavelength is decreasing. The slow waves associated to charged particles has a cut-off wavenumber and for decreasing wavelength the frequency of these waves becomes independent on their wavelength, i.e. they become non-dispersive.

The damping rate of waves propagating parallel to the magnetic field is

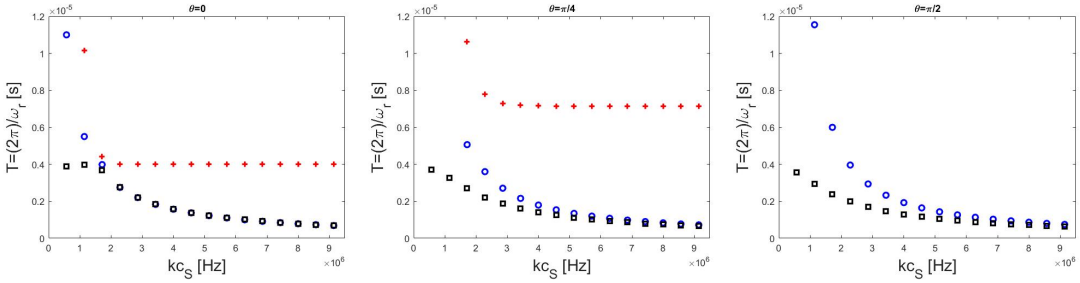

Figure 4.8: The same waves as in Figure 4.6, but here we display the period of waves in terms of the frequency of sound waves, kc_S.

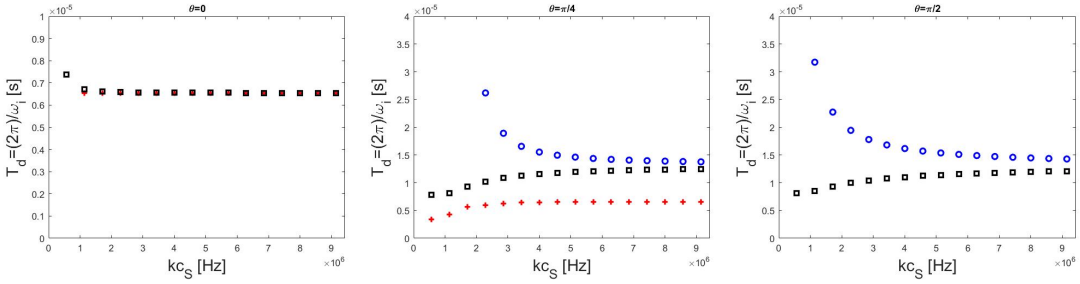

Figure 4.9: The same waves as in Figure 4.7, but here we show the damping times of waves in terms of the frequency of sound waves, kc_S.

shown in the left-hand panel of Figure 4.7. While the slow waves associated to the neutral particles propagate practically with no damping, the damping rates of slow waves of charged species and the fast waves are identical and show very little dependence on the wavelength of waves.

When the propagation direction is such that the wavevector makes an angle of $\pi/4$ with respect to the ambient magnetic field the slow waves due to the charged species has, again, a cut-off value and the propagation speed increases inversely proportional to the wavelength of waves. Similar to the parallel propagation, at a value of $kc_S/\Omega_{Be} \approx 0.05$, the speed saturates and becomes independent on the wavelength of the waves. Compared to the case of parallel propagation, these waves have a lower frequency.

Once the waves propagate in a non-parallel direction to the magnetic field, the fast and neutral-associated slow waves decouple. Their frequency is close to each other and they follow the same dependence on the wavelength. As before, frequency of the neutral slow waves increases monotonically along the direction

$\omega = kc_S$. The damping rates of these waves are shown in the middle panel of Figure 4.7. In the case of charged-related slow waves the damping rate becomes again independent on the wavelength of waves for $kc_S/\Omega_{Be} \approx 0.07$. These waves posses the largest damping rate. The damping rate of fast waves has a similar behaviour as in the case of parallel propagation and, again, it tends to saturate so that it becomes independent on the wavelength of waves. The damping rate of slow waves associated with neutrals has an interest behaviour since for large wavelengths, the damping rate of these waves is zero, i.e. these waves propagate with no damping. The damping rate of these waves increases, and saturates with decreasing the wavelength of waves. The damping rate of fast waves damp quickly for large wavelengths, and their damping rate decreases with the wavelength. For decreasing wavelengths the damping rate of fast waves also saturates and tends to be equal to the damping rates of slow waves associated to neutrals.

For propagation perpendicular to the background equilibrium magnetic field slow waves associated with charged particles ceases to exist, instead neutral slow waves and fast waves can propagate with frequencies that increase with decreasing wavelength. Similar to the previous cases, and the frequency separation between these two modes increases. The imaginary part of the frequency of these two waves show that with decreasing the wavelength the damping rate of neutral slow wave increases, while for fast waves, it decreases. For smaller wavelengths the damping rate of the two modes becomes almost independent on the wavelength of waves and they tend to converge towards the same value.

We have repeated these plots for higher heights in the solar chromosphere and the results show that the pattern of the real and imaginary parts of the frequencies shown in Figures 4.6 and 4.7 are preserved, the only change is a change of the values. Accordingly, with height, the real part of frequencies for neutral slow and fast waves are practically unaffected, however they tend to be closer to each other with the increase with height. In contrast the values of the frequencies for slow waves associated to charges decreases. The imaginary part of the frequencies corresponding to all three waves tends to decrease, meaning that with height these waves tend to have weaker damping.

The period and the damping times of waves corresponding to the field and plasma parameters mentioned earlier are shown in Figures 4.8 and 4.9. Here these quantities are plotted in terms of the frequency of sound waves, kc_S, or, since the sound speed is constant, in terms of the wavenumber, k. Apart

from the period of slow waves associated with the charged particles, where the period becomes constant for decreasing wavelength, the period of the other two ways decreases with the wavelength. In all cases the periods are of the order of 10^{-6}, i.e. the collisonal time between ions and neutrals.

When looking at the damping times shown in Figure 4.9, the curve corresponding to neutral slow waves propagating along the field is not shown because these waves propagate practically undamped. For any propagation angle the damping time of waves becomes gradually independent on the wavelength of waves, when their wavelength decreases.

A full picture of the propagation speed of the waves and their damping rate can be obtained by plotting these values in a Friedrich polar diagram (see Figure 4.10), where the equilibrium magnetic field points in the x-direction and the angle of propagation of waves covers a full 2π range. The diagrams shown in Figure 4.10 were obtained by assuming $kc_S/\Omega_{Be} = 0.035$ and a plasma-β parameter of 3×10^{-3}. In these plots the modes are represented by the same colours as in Figures 4.6 and 4.7. The dashed in the polar plots are used for reference values. For the real part of the frequency the blue and black dashed line correspond to 2 and 3.25 MHz, respectively. In the case of the imaginary part of the frequency the dashed blue and black lines correspond to 1.33 and 1.6 MHz.

From these diagrams it is obvious that fast waves propagate with the highest frequency in the perpendicular direction to the magnetic field, a similar characteristic as fast magnetoacoustic waves in fully ionised plasmas. In the solar atmospheric region we are investigating there are two slow waves associated to the two species, but the slow wave associated with the neutral species propagates always with a higher speed than the one that corresponds to charges. Due to the strong coupling between ions and neutrals, in the case of parallel propagation, the fast waves and slow waves due to neutrals propagate with the same frequency. For parallel propagation the frequency of neutral slow waves is always larger than the phase speed of slow waves associated with the charged particles.

In the right panel of Figure 4.10 we plot the absolute value of the damping rate of the three waves, when the propagation direction is, again, covering the full 2π range. It is clear that not only the propagation speed of waves depends on the propagation angle of waves, but also the damping rate.

First of all, the slow mode associated to the charged particles has the largest damping rate, and its value takes its minimum when these waves propagate

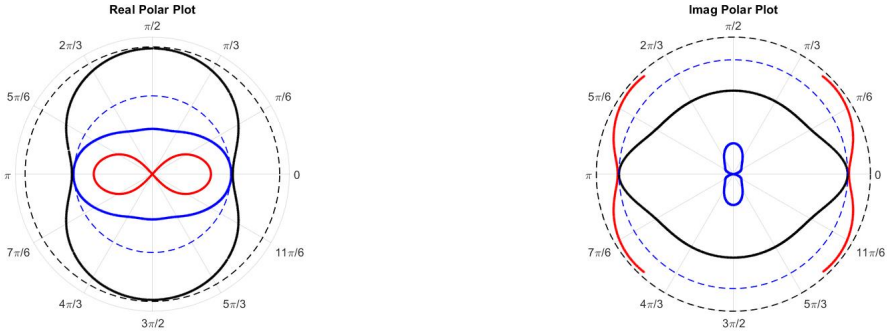

Figure 4.10: The polar (Friedrich) diagram of the real (left panel) and imaginary part (right panel) of the dispersion relation. Here the background magnetic field is along the x axis and the direction of waves' propagation is covering a whole 2π range. The colours are representing the same modes as defined in Figure 4.6. Note that in the right-hand side panel we plot the absolute value of the damping rate. The dashed lines correspond to the reference values of frequency and damping rate given in the text of the article. These figures were obtained for $kc_S/\Omega_{Be} = 0.035$

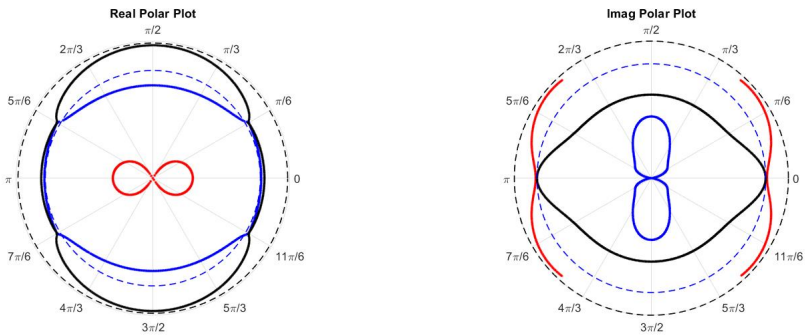

Figure 4.11: The same as in Figure 4.10, but here the polar plots have been obtained for the value $kc_S/\Omega_{Be} = 0.07$, i.e. shorter wavelengths.

along the direction of the magnetic field. The polar plot of imaginary part of the frequency (but also visible on the diagram corresponding to the real part) shows that these modes do not propagate when the angle of propagation is $\pm 2\pi/9 = 40^\circ$ with respect to the perpendicular direction.

The polar diagram of the damping rate of neutral slow waves (blue curve) also shows a very anisotropic behaviour. These waves propagate along the magnetic field lines with practically no damping, while their damping rate is maximum when they propagate perpendicular to the magnetic field. Among the three possible modes, the slow waves associated with the neutral species has the smallest damping rate.

Finally, fast waves have their largest damping rate when they propagate along the equilibrium magnetic field (where the damping rate is equal to the damping rate of slow waves), and their smallest damping rate is attained when they propagate across the magnetic field.

The same analysis was repeated for another value of kc_S/Ω_{Be} (here we considered the value of 0.07) to evidence the change in the properties of waves for shorter wavelengths (higher wavenumbers) and the results we obtained for the real and imaginary part of the frequency are shown in Figure 4.11. The differently coloured curves correspond to the same modes as in Figure 4.10, but here the reference levels (shown by the dashed lines) are at 5.5 and 6.9 MHz for the real part, and 1.33 and 1.6 MHz, respectively. The change in the size of the polar plot corresponding slow waves attached to the charged species is only apparent, instead the frequencies of slow modes associated to neutrals and the fast mode increase, however, we maintain the proportionality. Comparing the two polar plots we obtained for the real part of the frequencies, it is clear that with decreasing the wavelength, the domain where the frequencies of neutral slow waves and fast waves are approximately equal is increased, for the particular values chosen here the two waves have almost identical frequency for propagation angle corresponding to $\pm\pi/6 = 30^\circ$ with respect to the direction of the equilibrium magnetic field.

The polar plot corresponding to the damping rate of waves shows that, while the curves corresponding to slow waves connected to charges and fast waves do not show significant variation in terms of wavelength (with the reference curves showing the same values as before), the damping rate of slow waves associated to neutrals increases.

Finally, the polar plots shown here are qualitatively similar to the plots we would obtain for the propagation speed.

4.5 Conclusions

Our study deals with the properties of waves in weakly ionised plasmas, characteristic to the lower regions of the solar atmosphere, where the dynamics is determined mainly by the strong collisional coupling between particles.

First of all, our results showed that since we are dealing with very short wavelength waves, their dynamics is not affected by gravitational stratification. A comparative study of the collisional frequency associated with various species and the gyro-frequency of charged particles revealed the existence of two distinctive regions, where the first region covers the whole photosphere. In the first region the collisional frequency of charged particles are larger than the gyro-frequencies of charged particles, meaning that here the dynamics of particles is not affected by the presence of magnetic fields and the only waves that can propagate are acoustic in nature. Since the collisional frequency of electrons to ions and neutrals are very close to each other, the wave dynamics was described in a full three-fluid framework. These results show that in a multi-fluid description of plasma in the solar photosphere the effects of the magnetic field can be neglected.

Given the very low ionisation degree of the plasma, the neutral acoustic modes propagate undamped, and their amplitude is not affected by the collisions with other particles. In contrast, the acoustic modes associated with ions and electrons propagate only when their wavenumber is greater that a cut-off value, determined by the collisional frequency with neutrals. Their frequency tends to the frequency of neutral acoustic modes when their wavelength decreases. These waves are damped, but the damping rate does not depend on the wavelength of waves. For small wavelengths there is no distinction between various waves, all propagate with the frequency of the neutral species.

The second region corresponds to a frequency regime bounded by the two gyro-frequencies, so electrons become magnetised, while the dynamics of ions are still mainly driven by the collisions with neutrals. Thanks to the different dynamics of the charged particles, an electric current is generated, together with an electric field that opposes the disassociation of charges. In this region the charged particles become strongly coupled (their collisional frequency is much higher than the collisional frequency with neutrals), meaning that charged particles form a single fluid that interacts with neutrals through collisions.

In such plasmas waves become magnetoacoustic in nature, however the slow

waves associated with neutrals retains much of the characteristics of neutrals sounds waves in Region I, however, it propagates with no damping only when the wave propagates mainly along the magnetic field. In addition to the neutral slow waves, ion slow waves can also propagate, however these waves propagate with a cut-off and their frequency becomes fairly quickly independent on the wavelength of waves (non-dispersive). In contrast, the fast waves are non-dipersive only for very large wavelengths and become attached to neutral slow waves. The Friedrich polar diagram shows a strong dependence of frequency and damping rate with the propagation angle of waves.

Our analysis considered only the two-dimensional propagation of magneto-coustic waves. It is obvious that a full, three dimensional propagation, would recover an even richer spectrum of waves, however this (numerical) investigation would be subject to future studies.

CHAPTER 5
Conclusions and future research prospect

5.1 Thesis Summary

The study of waves in partially ionised plasma is a relatively new area of solar physics and has received considerable attention in the last decade. Results show that the spectrum and properties of waves in such plasmas is more complex than we could meet in fully ionised environments.

The aim of my research was the study of waves in partially ionised plasma in different regimes corresponding to to different layers in the solar atmosphere. In particular, our analysis was carried in two limiting cases: strongly ionised ($\rho_{0n}/\rho_{0i} \ll 1$) and weakly ionised ($\rho_{0n}/\rho_{0i} \gg 1$) plasma. These regimes are relevant for the upper and lower part of the solar atmosphere. The properties of waves was analysed using a multi-fluid approach, where the constituent species of the plasma were described by a different set of equations. The governing equations for each species were connected via the collisional terms, ensure an effective coupling and a momentum transfer between species.

A short introduction on the physical properties of the Sun, together with a brief historical overview of the solar studied is provided in Chapter 1. In addition, here we review the literature of partial ionised plasma in the solar atmosphere and other astrophysical areas, such as the Earth's ionosphere, molecular clouds, etc.

Chapter 2 covers the mathematical background of my research. Here I present the set of governing equations that will be used in later chapters, with their assumptions and limitations. The MHD-type equations are given for a three-fluid plasma, and a two-fluid approximation, both used extensively later. Since collisions between particles play a key role in our analysis, this chapter also contains a detailed description of the collisions between particles, the collisional cross-section and the collisional frequencies. Finally, we review the current state-of-the-art connected to magnetic and magnetoacoustic waves

in partially ionised plasmas, highlighting the major differences of these waves compared to their counterparts in fully ionised plasmas.

Waves in strongly ionised plasmas (the upper part of the solar chromosphere) plasma have been studied in Chapter 3, and here we investigate the spatial and temporal evolution of slow waves propagating in an expanding magnetic flux tube in a gravitationally stratified plasma environment. The properties of waves was studied using a two-fluid approach, where the interacting fluids are the charges and neutrals. The temporal and spatial evolution of waves was studied by solving the initial value problem using inverse Laplace transform for the charged and neutral species in section 3.4.1 and 3.4.2, respectively. Since we are interested in the asymptotic behaviour of waves over very large time scales, we choose to drive the system with a harmonic pulse in section 3.4.3 and a monochromatic source in section 3.4.4. Our results show that the neutral-acoustic mode has a larger amplitude and decays slower than the corresponding ion-acoustic modes. Given the strongly ionised limit only slow sausage waves associated with ions propagate with a cut-off frequency and waves will have a very rapid decay, even in the absence of the simplifications (see section 3.5).

Chapter 4 was devoted to the study of waves in weakly ionised plasma using the VAL IIIC atmospheric model (Vernazza et al., 1981). The variation of collisional and gyro-frequencies with height displayed in Figure 4.1 show that the weakly ionised solar atmosphere can be divided into two distinct regions, each with its own characteristics. The first region (up to a height of about to 600 km) corresponds to the regime where the collisional frequencies of electron and ions are larger than ion and electron gyro-frequencies, meaning that the effect of magnetic field can be neglected. Given the relative magnitude of collisional frequencies, the dynamics in this region is described by the three-fluid approximation. Our results presented in section 4.4.1 show that the acoustic modes connected to the neutral species propagate with no cut-off wavenumber and with a decreasing wavelength their frequency will increase. The acoustic wave associated to ions propagates only if the wavenumber satisfied the condition $k > 9.2$ km^{-1}. Finally, electron sound waves propagate if their wavenumber satisfies the condition $k > 27.3$ km^{-1}. In contrast to the fully ionised limit (where cut-off appear due to the plasma stratification), here all the above cut-off values are determined only by collisions. The damping rate of all species is represented in Figure 4.5. Clearly, the neutral sound wave propagates without damping, while the other two species have a strong damping, but the damping

rate is independent on the waves' wavelength.

On the other hand, in section 4.4.2, we discussed the properties of waves in the second region (up to 1,900 km), where the electron gyro-frequency is larger than the electron collisional frequency, meaning that electrons are magnetised, however the motions of ions is still driven by the collisions with neutrals. Due to the strong coupling between the charged species, they form a single fluid, therefore, the dynamics is described in the two-fluid approximation. Due to the different motion of charged particles, currents are developed. The dispersion relation was solved numerically, and the solutions were represented in Figures 4.6 and 4.7. The full picture of wave propagation for an arbitrary propagation angle is shown in the polar diagrams 4.10 and 4.11.

Finally, in the region above 1,900 km, where all collisional frequencies are below electron and ion gyro-frequencies, all charged particles will be magnetised and the properties of waves that can propagate in this region was discussed in Chapter 3.

5.2 Future work

The study of waves in solar partially ionised plasmas and their role in various mechanisms (e.g. stability, heating, plasma acceleration, etc.) is not fully developed. The results presented in this Thesis cover just a small area of this science, with plenty of directions along which our research can be continued in the future.

(i) Observations revealed that solar prominences contain approximately 90% hydrogen atoms, while the rest is made up of helium. Most studies of waves in partial ionised plasma assume the plasma has a single component (hydrogen), as this simplifies considerably the mathematical treatment.

Soler et al. (2010) and Zaqarashvili et al. (2011*a*) investigated the effect of helium on wave propagation in partially ionised plasma, discussing the propagation and damping of Alfvén waves in three fluid partially ionised plasma. They showed that damping rates have a peak near the ion-neutral collision frequency, but decrease for the higher part of the wave spectrum. In addition, they concluded that the collision of ions with neutral helium for the damping of Alfvén waves is important in some regions in chromosphere and corona. In this respect, it would be interesting to apply the approach presented in Chapter 3 to a partially ionised plasma taking into account the effect of neutral

and ionised helium on the damping of waves and the appearance of cut-off frequencies.

(ii) In the solar atmosphere, the study of the waves have been assumed the equilibrium ionisation, but this assumption is not always valid (in, e.g. high frequency waves and shock waves). Non-equilibrium ionisation has been considered as a inelastic collision between particles and appeared during heating or cooling of the plasma. Carlsson and Stein (2002) showed that dynamics occurring below the ionization/recombination relaxation times scales of 10^{-3} to 10^{-5} s will be affected by non-equilibrium effects in the chromosphere. Ballai (2019) investigated the wave properties in non-equilibrium partially ionised plasma, arriving at the problem of partial ionisation and non-equilibrium ionisation, introducing new aspects of plasma dynamics with implications for the evolution waves and their dissipation.

Inspired from results obtained in this thesis, we could use the developed techniques to study the behaviour of waves where the plasma is in ionisation non-equilibrium.

(iii) In Chapter 4 we have shown that due to the different motion of electrons and ions electric currents can be developed that could be subject to effective Ohmic dissipation, when electrons collide with ions and neutrals. Therefore, these currents can contribute to the chromospheric plasma heating.

Another way to expand the research of my Thesis is to investigate how effective this heating is and how well the heating rate produced by these currents can balance the energetic loss observed in the solar chromosphere. To evidence that, we could study the appearance and dissipation of currents assuming a simple VAL solar atmospheric model together with a realistic magnetic field.

APPENDIX A

Appendix

A.1 Evaluation of the integral in equation 3.51

The value of the integral that is given in equation 3.51 can be given in approximate form for large values of τ. The integral we have to estimate is

$$R(z,t) = \int_{t-P}^{t} \frac{e^{(\omega_n + i\omega)t}}{\tau^{3/2}}\, d\tau. \tag{A.1}$$

Using integration by parts we have

$$R(z,t) = \frac{1}{\omega_n + i\omega} \frac{e^{(\omega_n + i\omega)\tau}}{\tau^{3/2}}\Bigg|_{t-P}^{t} + \frac{3}{2(\omega_n + i\omega} \int_{t-P}^{t} \frac{e^{(\omega_n + i\omega)t}}{\tau^{5/2}}\, d\tau =$$

$$= \frac{1}{\omega_n + i\omega} \frac{e^{(\omega_n + i\omega)\tau}}{\tau^{3/2}} \left[1 + \frac{3}{2(\omega_n + i\omega)\tau}\right]_{t-P}^{t} +$$

$$\frac{15}{4(\omega_n + i\omega)^2} \int_{t-P}^{t} \frac{e^{(\omega_n + i\omega)t}}{\tau^{7/2}}\, d\tau.$$

The above relation can be re-arranged into

$$\int_{t-P}^{t} \frac{e^{(\omega_n + i\omega)t}}{\tau^{3/2}} \left(1 - \frac{15}{2\tau(\omega_n + i\omega)}\right) d\tau =$$

$$\frac{1}{\omega_n + i\omega} \frac{e^{(\omega_n + i\omega)\tau}}{\tau^{3/2}} \left[1 + \frac{3}{2(\omega_n + i\omega)\tau}\right]_{t-P}^{t}.$$

It is clear that for large values of τ the second terms in the two brackets are of the order of $\mathcal{O}(\tau^{-1})$ and therefore, they can be neglected. As a result, using the approximation 3.53 the integral $R(z,t)$ can be given as as

$$R(z,t) \approx \frac{e^{(\omega_n + i\omega)t}}{t^{3/2}(\omega_n + i\omega)} \left[1 - e^{-(\omega_n + i\omega)P}\right]. \tag{A.2}$$

A.2 Evaluation of the integral in equation 3.62

$$P(z,t) = \int_{z/c_{Sn}}^{t} \frac{e^{(\omega_n + i\omega)t}}{\tau^{3/2}}\, d\tau. \tag{A.3}$$

Using integration by parts we have

$$P(z,t) = \frac{1}{\omega_n + i\omega} \frac{e^{(\omega_n + i\omega)\tau}}{\tau^{3/2}}\Bigg|_{z/c_{Sn}}^{t} + \frac{3}{2(\omega_n + i\omega)} \int_{z/c_{Sn}}^{t} \frac{e^{(\omega_n + i\omega)t}}{\tau^{5/2}}\, d\tau =$$

$$= \frac{1}{\omega_n + i\omega} \frac{e^{(\omega_n + i\omega)\tau}}{\tau^{3/2}} \left[1 + \frac{3}{2(\omega_n + i\omega)\tau}\right]_{z/c_{Sn}}^{t} +$$

$$\frac{15}{4(\omega_n + i\omega)^2} \int_{z/c_{Sn}}^{t} \frac{e^{(\omega_n + i\omega)t}}{\tau^{7/2}}\, d\tau.$$

The above relation can be re-arranged into

$$\int_{z/c_{Sn}}^{t} \frac{e^{(\omega_n + i\omega)t}}{\tau^{3/2}} \left(1 - \frac{15}{2\tau(\omega_n + i\omega)}\right) d\tau =$$

$$\frac{1}{\omega_n + i\omega} \frac{e^{(\omega_n + i\omega)\tau}}{\tau^{3/2}} \left[1 + \frac{3}{2(\omega_n + i\omega)\tau}\right]_{z/c_{Sn}}^{t}.$$

It is clear that for large values of τ the second terms in the two brackets are of the order of $\mathcal{O}(\tau^{-1})$ and therefore, they can be neglected. As a result, the integral $P(z,t)$ can be given as

$$P(z,t) \approx \frac{1}{(\omega_n + i\omega)} \left[\frac{e^{(\omega_n + i\omega)t}}{t^{3/2}} - \frac{e^{(\omega_n + i\omega)z/c_{Sn}}}{(z/c_{Sn})^{3/2}}\right]. \tag{A.4}$$

A.3 The inverse Laplace transform of the inhomogeneous part of equation 3.45

Using the technique presented in the main body of the paper, the inverse Laplace transform of the inhomogeneous part of equation 3.45 that gives the particular solution of equation 3.38 is

$$q_n^{inh}(z,t) = \frac{iA_2V_0\left[\delta - \beta\gamma/4(1 + 2\Gamma_1^2)\right] e^{-i\omega z/c_T}}{P_1 + i\omega_i} \left[e^{(\nu_{ni}/2 + \Gamma_1)t} - e^{-i\omega t}\right] e^{\sqrt{\omega^2 - \omega_i^2}\, z/c_T}$$

$$- \frac{iA_2V_0\left[\delta - \beta\gamma/4(1 + 2\Gamma_2^2)\right] e^{-i\omega z/c_T}}{P_2 + i\omega_i} \left[e^{(\nu_{ni}/2 + \Gamma_2)t} - e^{-i\omega t}\right] e^{\sqrt{\omega^2 - \omega_i^2}\, z/c_T}$$

$$-\frac{iA_2V_0A_3\omega_i}{P_1^2+\omega_i^2}\left[\delta-\frac{\beta\gamma}{4}(1+2\Gamma_1^2)\right]\left\{\frac{1}{t^{3/2}}\left[P_1\sin\left(\omega_i t-\frac{3\pi}{4}\right)-\omega_i\cos\left(\omega_i t-\frac{3\pi}{4}\right)\right]\right.$$
$$\left.-\frac{e^{\Gamma_1 t}}{(z/c_T)^{3/2}}\left[P_1\sin\left(\omega_i\frac{z}{c_T}-\frac{3\pi}{4}\right)-\omega_i\cos\left(\omega_i\frac{z}{c_T}-\frac{3\pi}{4}\right)\right]\right\}$$
$$+\frac{A_2A_3V_0\omega}{P_2^2+\omega_i^2}\left[\delta-\frac{\beta\gamma}{4}(1+2\Gamma_2^2)\right]\left\{\frac{1}{t^{3/2}}\left[P_2\cos\left(\omega_i t-\frac{3\pi}{4}\right)-\omega_i\sin\left(\omega_i t-\frac{3\pi}{4}\right)\right]\right.$$
$$\left.-\frac{e^{\Gamma_2 t}}{(z/c_T)^{3/2}}\left[P_2\cos\left(\omega_i\frac{z}{c_T}-\frac{3\pi}{4}\right)-\omega_i\sin\left(\omega_i\frac{z}{c_T}-\frac{3\pi}{4}\right)\right]\right\}. \qquad \text{(A.5)}$$

where we used the notations

$$A_2=\frac{4\pi e^{-z/4\gamma H_n}}{\mathcal{G}(1-g/2\omega_i c_T)},$$

$$A_3=\sqrt{\frac{2\omega_i}{\pi}}\frac{1}{\omega^2-\omega_i^2}\frac{z}{c_T},$$

$$P_{1,2}=\frac{\nu_{ni}}{2}+\Gamma_{1,2}.$$

Bibliography

Aboudarham, J., Scholl, I., Fuller, N., Fouesneau, M., Galametz, M., Gonon, F., Maire, A. and Leroy, Y. (2008), Automatic detection and tracking of filaments for a solar feature database, *in* 'Annales geophysicae: atmospheres, hydrospheres and space sciences', Vol. 26, p. 243.

Alfvén, H. (1942), 'Existence of Electromagnetic-Hydrodynamic Waves', *Nature* **150**(3805), 405–406.

Alfvén, H. (1949), 'On the solar origin of cosmic radiation', *Physical Review* **75**(11), 1732.

Alharbi, A., Ballai, I., Fedun, V. and Verth, G. (2021), 'Slow magnetoacoustic waves in gravitationally stratified two-fluid plasmas in strongly ionized limit', *Monthly Notices of the Royal Astronomical Society* **501**(2), 1940–1950.

Alharbi, A., Ballai, I., Fedun, V. and Verth, G. (2022), 'Waves in weakly ionised solar plasmas', *Monthly Notices of the Royal Astronomical Society* **(submitted)**.

Almeida, J. S. (2003), 'Inter-network magnetic fields observed during the minimum of the solar cycle', *Astronomy & Astrophysics* **411**(3), 615–621.

Anzer, U. and Heinzel, P. (2005), 'On the nature of dark extreme ultraviolet structures seen by soho/eit and trace', *The Astrophysical Journal* **622**(1), 714.

Arons, J. and Max, C. E. (1975), 'Hydromagnetic waves in molecular clouds', *the Astrophysical Journal* **196**, L77.

Aschwanden, M. J. (2009), Hydrodynamic modeling of coronal loops with hinode and stereo, *in* 'The Second Hinode Science Meeting: Beyond Discovery-Toward Understanding', Vol. 415, p. 234.

Avrett, E. H. and Loeser, R. (2008), 'Models of the solar chromosphere and transition region from sumer and hrts observations: formation of the extreme-ultraviolet spectrum of hydrogen, carbon, and oxygen', *The Astrophysical Journal Supplement Series* **175**(1), 229.

Axford, W. and McKenzie, J. (1992), The origin of high speed solar wind streams, *in* 'Solar Wind Seven', Elsevier, pp. 1–5.

Ballai, I. (2019), 'Linear waves in a non-equilibrium ionisation partially ionised plasma', *Frontiers in Astronomy and Space Sciences* **6**, 39.

Ballai, I. (2020), 'Diagnostics of plasma ionisation using torsional alfén waves', *Astronomy & Astrophysics* **635**, L2.

Ballai, I. and Forgács-Dajka, E. (2010), The dynamical solar atmosphere, *in* 'Journal of Physics: Conference Series', Vol. 218, IOP Publishing, p. 012002.

Ballai, I., Oliver, R. and Alexandrou, M. (2015), 'Dissipative instability in partially ionised prominence plasmas', *Astronomy & Astrophysics* **577**, A82.

Ballester, J. L. et al. (2018*a*), 'Partially ionized plasmas in astrophysics', *Space Science Reviews* **214**(2), 58.

Ballester, J. et al. (2018*b*), 'The temporal behaviour of mhd waves in a partially ionized prominence-like plasma: Effect of heating and cooling', *Astronomy & Astrophysics* **609**, A6.

Balsara, D. S. (1996), 'Wave propagation in molecular clouds', *The Astrophysical Journal* **465**, 775.

Bateman, H. (1954), 'Tables of integral transforms'.

Berger, T. E., Shine, R. A., Slater, G. L., Tarbell, T. D., Okamoto, T. J., Ichimoto, K., Katsukawa, Y., Suematsu, Y., Tsuneta, S., Lites, B. W. et al. (2008), 'Hinode sot observations of solar quiescent prominence dynamics', *The Astrophysical Journal Letters* **676**(1), L89.

Berthold, W., Harris, A. and Hope, H. (1960), 'World-wide effects of hydromagnetic waves due to argus', *Journal of Geophysical Research* **65**(8), 2233–2239.

Braginskii, S. (1965), 'Transport processes in plasma, ed', *MA Leontovich (New York, USA: Consultants Bureau)* **201**.

Braileanu, B. P., Lukin, V., Khomenko, E. and De Vicente, A. (2019), 'Two-fluid simulations of waves in the solar chromosphere-ii. propagation and damping of fast magneto-acoustic waves and shocks', *Astronomy & Astrophysics* **630**, A79.

Carbonell, M., Forteza, P., Oliver, R. and Ballester, J. (2010), 'The spatial damping of magnetohydrodynamic waves in a flowing partially ionised prominence plasma', *Astronomy & Astrophysics* **515**, A80.

Carlsson, M. and Stein, R. F. (2002), 'Dynamic hydrogen ionization', *The Astrophysical Journal* **572**(1), 626.

Chmyrev, V., Bilichenko, S., Pokhotelov, O., Marchenko, V., Lazarev, V., Streltsov, A. and Stenflo, L. (1988), 'Alfvén vortices and related phenomena in the ionosphere and the magnetosphere', *Physica Scripta* **38**(6), 841.

Dapp, W. B. and Basu, S. (2010), 'Averting the magnetic braking catastrophe on small scales: disk formation due to ohmic dissipation', *Astronomy & Astrophysics* **521**, L56.

de la Cruz Rodriguez, J. and Socas-Navarro, H. (2011), 'Are solar chromospheric fibrils tracing the magnetic field?', *Astronomy & Astrophysics* **527**, L8.

De Moortel, I. (2005), 'An overview of coronal seismology', *Philosophical Transactions of the Royal Society A: Mathematical, Physical and Engineering Sciences* **363**(1837), 2743–2760.

De Pontieu, B., McIntosh, S., Martinez-Sykora, J., Peter, H. and Pereira, T. (2015), 'Why is non-thermal line broadening of spectral lines in the lower transition region of the sun independent of spatial resolution?', *The Astrophysical Journal Letters* **799**(1), L12.

Defouw, R. (1976), 'Wave propagation along a magnetic tube', *The Astrophysical Journal* **209**, 266–269.

Díaz, A., Soler, R. and Ballester, J. (2012), 'Rayleigh-taylor instability in partially ionized compressible plasmas', *The Astrophysical Journal* **754**(1), 41.

Dong, C. and Paty, C. S. (2011), 'Heating of ions by low-frequency alfvén waves in partially ionized plasmas', *Physics of Plasmas* **18**(3), 030702.

Fontenla, J., Avrett, E. and Loeser, R. (1990), 'Energy balance in the solar transition region. i-hydrostatic thermal models with ambipolar diffusion', *The Astrophysical Journal* **355**, 700–718.

Forteza, P., Oliver, R., Ballester, J. and Khodachenko, M. (2007), 'Damping of oscillations by ion-neutral collisions in a prominence plasma', *Astronomy & Astrophysics* **461**(2), 731–739.

Foukal, P. V. (2004), 'Solar astrophysics, 2nd', *Solar Astrophysics* p. 480.

Gilbert, H., Kilper, G. and Alexander, D. (2007), 'Observational evidence supporting cross-field diffusion of neutral material in solar filaments', *The Astrophysical Journal* **671**(1), 978.

Goedbloed, J. H., Goedbloed, J. and Poedts, S. (2004), *Principles of magnetohydrodynamics: with applications to laboratory and astrophysical plasmas*, Cambridge university press.

Golub, L. and Pasachoff, J. M. (2002), *Nearest star: the surprising science of our sun*, Harvard University Press.

Golub, L. and Pasachoff, J. M. (2010), *The solar corona*, Cambridge University Press.

Goodman, M. L. (2000), 'On the mechanism of chromospheric network heating and the condition for its onset in the sun and other solar-type stars', *The Astrophysical Journal* **533**(1), 501.

Gurnett, D. and Goertz, C. (1981), 'Multiple alfvén wave reflections excited by io: Origin of the jovian decametric arcs', *Journal of Geophysical Research: Space Physics* **86**(A2), 717–722.

Heinzel, P., Gunár, S. and Anzer, U. (2015), 'Fast approximate radiative transfer method for visualizing the fine structure of prominences in the hydrogen hα line', *Astronomy & Astrophysics* **579**, A16.

Herbold, G., Ulmschneider, P., Spruit, H. and Rosner, R. (1985), 'Propagation of nonlinear, radiatively damped longitudinal waves along magnetic flux tubes in the solar atmosphere', *Astronomy and Astrophysics* **145**, 157–169.

Hirzberger, J., Feller, A., Riethmüller, T. L., Schüssler, M., Borrero, J. M., Afram, N., Unruh, Y. C., Berdyugina, S. V., Gandorfer, A., Solanki, S. K. et al. (2010), 'Quiet-sun intensity contrasts in the near-ultraviolet as measured from sunrise', *The Astrophysical Journal Letters* **723**(2), L154.

Isenberg, P. A. and Hollweg, J. V. (1983), 'On the preferential acceleration and heating of solar wind heavy ions', *Journal of Geophysical Research: Space Physics* **88**(A5), 3923–3935.

Jephcott, D. (1959), 'Alfvén waves in a gas discharge', *Nature* **183**(4676), 1652–1654.

Jess, D. B., Mathioudakis, M., Erdélyi, R., Crockett, P. J., Keenan, F. P. and Christian, D. J. (2009), 'Alfvén waves in the lower solar atmosphere', *Science* **323**(5921), 1582–1585.

Kalkofen, W., Rossi, P., Bodo, G. and Massaglia, S. (1994), 'Propagation of acoustic waves in a stratified atmosphere, 1', *Astronomy and Astrophysics* **284**, 976–984.

Katsukawa, Y., Berger, T., Ichimoto, K., Lites, B., Nagata, S., Shimizu, T., Shine, R., Suematsu, Y., Tarbell, T., Tsuneta, S. et al. (2007), 'Small-scale jetlike features in penumbral chromospheres', *Science* **318**(5856), 1594–1597.

Khomenko, E. (2006), Diagnostics of quiet-sun magnetism, *in* 'Solar MHD Theory and Observations: A High Spatial Resolution Perspective', Vol. 354, p. 63.

Khomenko, E., Collados, M. and Díaz, A. J. (2016), 'Observational detection of drift velocity between ionized and neutral species in solar prominences', *The Astrophysical Journal* **823**(2), 132.

Khomenko, E., Collados, M., Shchukina, N. and Diaz, A. (2015), 'Evershed flow observed in neutral and singly ionized iron lines', *Astronomy & Astrophysics* **584**, A66.

Khomenko, E., Collados, M., Solanki, S., Lagg, A. and Bueno, J. T. (2003), 'Quiet-sun inter-network magnetic fields observed in the infrared', *Astronomy & Astrophysics* **408**(3), 1115–1135.

Khomenko, E., Vitas, N., Collados, M. and De Vicente, A. (2017), 'Numerical simulations of quiet sun magnetic fields seeded by the biermann battery', *Astronomy & Astrophysics* **604**, A66.

Khomenko, E. et al. (2014*a*), 'Fluid description of multi-component solar partially ionized plasma', *Physics of Plasmas* **21**(9), 092901.

Khomenko, E. et al. (2014*b*), 'Rayleigh-taylor instability in prominences from numerical simulations including partial ionization effects', *Astronomy & Astrophysics* **565**, A45.

Kohutova, P., Verwichte, E. and Froment, C. (2020), 'First direct observation of a torsional alfvén oscillation at coronal heights', *Astronomy & Astrophysics* **633**, L6.

Krasnoselskikh, V., Vekstein, G., Hudson, H., Bale, S. and Abbett, W. (2010), 'Generation of electric currents in the chromosphere via neutral-ion drag', *The Astrophysical Journal* **724**(2), 1542.

Krishan, V. (2016), *Physics of partially ionized plasmas*, Cambridge University Press.

Kuźma, B., Wójcik, D., Murawski, K., Yuan, D. and Poedts, S. (2020), 'Numerical simulations of the lower solar atmosphere heating by two-fluid nonlinear alfvén waves', *Astronomy & Astrophysics* **639**, A45.

Labrosse, N., Heinzel, P., Vial, J.-C., Kucera, T., Parenti, S., Gunßr, S., Schmieder, B. and Kilper, G. (2010), 'Physics of solar prominences: I—spectral diagnostics and non-lte modelling', *Space Science Reviews* **151**(4), 243–332.

Lagg, A., Solanki, S., Riethmüller, T., Pillet, V. M., Schüssler, M., Hirzberger, J., Feller, A., Borrero, J., Schmidt, W., del Toro Iniesta, J. et al. (2010), 'Fully resolved quiet-sun magnetic flux tube observed with the sunrise/imax instrument', *The Astrophysical Journal Letters* **723**(2), L164.

Laroussi, M. (2020), 'Cold Plasma in Medicine and Healthcare: The New Frontier in Low Temperature Plasma Applications', *Frontiers in Physics* **8**, 74.

Leake, J. E., Arber, T. and Khodachenko, M. (2005), 'Collisional dissipation of alfvén waves in a partially ionised solar chromosphere', *Astronomy & Astrophysics* **442**(3), 1091–1098.

Leake, J. E., Lukin, V. S., Linton, M. G. and Meier, E. T. (2012), 'Multi-fluid simulations of chromospheric magnetic reconnection in a weakly ionized reacting plasma', *The Astrophysical Journal* **760**(2), 109.

Li, Z.-Y., Krasnopolsky, R., Shang, H. and Zhao, B. (2014), 'On the role of pseudodisk warping and reconnection in protostellar disk formation in turbulent magnetized cores', *The Astrophysical Journal* **793**(2), 130.

Lithwick, Y. and Goldreich, P. (2001), 'Compressible magnetohydrodynamic turbulence in interstellar plasmas', *The Astrophysical Journal* **562**(1), 279.

Lundquist, S. (1949), 'Experimental investigations of magneto-hydrodynamic waves', *Physical Review* **76**(12), 1805.

Mackay, D., Karpen, J., Ballester, J., Schmieder, B. and Aulanier, G. (2010), 'Physics of solar prominences: Ii—magnetic structure and dynamics', *Space Science Reviews* **151**(4), 333–399.

Maneva, Y. G., Laguna, A. A., Lani, A. and Poedts, S. (2017), 'Multi-fluid modeling of magnetosonic wave propagation in the solar chromosphere: effects of impact ionization and radiative recombination', *The Astrophysical Journal* **836**(2), 197.

Martínez-Gómez, D., Soler, R. and Terradas, J. (2018), 'Multi-fluid approach to high-frequency waves in plasmas. iii. nonlinear regime and plasma heating', *The Astrophysical Journal* **856**(1), 16.

Martínez-Sykora, J., De Pontieu, B., Carlsson, M. and Hansteen, V. (2016), 'On the misalignment between chromospheric features and the magnetic field on the sun', *The Astrophysical Journal Letters* **831**(1), L1.

Mathers, C. (1980), 'Transverse mhd shock waves in a partly ionized plasma. part 1. structure equations and topology', *Journal of Plasma Physics* **24**(1), 103–120.

Mathioudakis, M., Jess, D. B. and Erdelyi, R. (2013), 'Alfvén waves in the solar atmosphere', *Space Science Reviews* **175**(1-4), 1–27.

McIntosh, P. S. (1990), 'The classification of sunspot groups', *Solar Physics* **125**(2), 251–267.

McIntosh, S. W., De Pontieu, B., Carlsson, M., Hansteen, V., Boerner, P. and Goossens, M. (2011), 'Alfvénic waves with sufficient energy to power the quiet solar corona and fast solar wind', *Nature* **475**(7357), 477–480.

Mitchner, M. and Kruger Jr, C. H. (1973), *Partially ionized gases*, John Wiley and Sons, Inc., New York.

Morfill, G., Kong, M. G. and Zimmermann, J. (2009), 'Focus on plasma medicine', *New Journal of Physics* **11**(11), 115011.

Mouschovias, T. C. (1991), 'Magnetic braking, ambipolar diffusion, cloud cores, and star formation-natural length scales and protostellar masses', *The Astrophysical Journal* **373**, 169–186.

Murawski, K. and Musielak, Z. (2010), 'Linear alfvén waves in the solar atmosphere', *Astronomy & Astrophysics* **518**, A37.

Murawski, K., Zaqarashvili, T. and Nakariakov, V. (2011), 'Entropy mode at a magnetic null point as a possible tool for indirect observation of nanoflares in the solar corona', *Astronomy & Astrophysics* **533**, A18.

Murphy, N. A. and Lukin, V. S. (2015), 'Asymmetric magnetic reconnection in weakly ionized chromospheric plasmas', *The Astrophysical Journal* **805**(2), 134.

Okamoto, T. J. and De Pontieu, B. (2011), 'Propagating waves along spicules', *The Astrophysical Journal Letters* **736**(2), L24.

Oliver, R., Soler, R., Terradas, J. and Zaqarashvili, T. (2016), 'Dynamics of coronal rain and descending plasma blobs in solar prominences. ii. partially ionized case', *The Astrophysical Journal* **818**(2), 128.

Pandey, B. and Wardle, M. (2006), 'Ion dynamics and the magnetorotational instability in weakly ionized discs', *Monthly Notices of the Royal Astronomical Society* **371**(2), 1014–1024.

Pardi, A., Ballai, I., Marcu, A. and Orza, B. (2014), 'Sausage mode propagation in a thick magnetic flux tube', *Solar Physics* **289**(4), 1203–1214.

Parenti, S. (2014), 'Solar prominences: observations', *Living Reviews in Solar Physics* **11**(1), 1.

Parker, E. (1979), 'Cosmical magnetic fields 274-297, 359–391'.

Pfaff, R. F. (2012), 'The near-earth plasma environment', *Space science reviews* **168**(1), 23–112.

Picone, J. et al. (2002), 'Nrlmsise-00 empirical model of the atmosphere: Statistical comparisons and scientific issues', *Journal of Geophysical Research: Space Physics* **107**(A12), SIA–15.

Pillet, V. M., Lites, B. and Skumanich, A. (1997), 'Active region magnetic fields. i. plage fields', *The Astrophysical Journal* **474**(2), 810.

Priest, E. (2014), *Magnetohydrodynamics of the Sun*, Cambridge University Press.

Priest, E. R. (2012), *Dynamics and structure of quiescent solar prominences*, Vol. 150, Springer Science & Business Media.

Rae, I. and Roberts, B. (1982), 'Pulse propagation in a magnetic flux tube', *The Astrophysical Journal* **256**, 761–767.

Raizer, Y. (1991), 'Gas discharge physics'.

Roberts, B. and Webb, A. (1978), 'Vertical motions in an intense magnetic flux tube', *Solar Physics* **56**(1), 5–35.

Romeuf, D., Meunier, N., Noëns, J.-C., Koutchmy, S., Jimenez, R., Wurmser, O. and Rochain, S. (2007), 'Analysis of broad-band hα coronagraphic observations', *Astronomy & Astrophysics* **462**(2), 731–741.

Sakai, J. and Smith, P. (2008), 'Modeling penumbral microjets by two-fluid simulations', *The Astrophysical Journal Letters* **687**(2), L127.

Shanmugasundaram, V. and Murty, S. (1978), 'Structure of shock waves in partially ionized argon', *Journal of Plasma Physics* **20**(3), 419–451.

Shu, F. H. (1992), 'Books-Received - the Physics of Astrophysics - V.2 - Gas Dynamics', *Journal of the British Astronomical Association* **102**, 230.

Shu, F. H., Adams, F. C. and Lizano, S. (1987), 'Star formation in molecular clouds: observation and theory', *Annual review of astronomy and astrophysics* **25**(1), 23–81.

Solanki, S. (2009), Photospheric magnetic field: Quiet sun, *in* 'Solar Polarization 5: In Honor of Jan Stenflo', Vol. 405, p. 135.

Solanki, S., Lagg, A., Aznar Cuadrado, R., Orozco Suárez, D., Collados, M., Wiegelmann, T., Woch, J., Sasso, C. and Krupp, N. (2006), Measuring the magnetic vector with the he i 10830 å line: A rich new world, *in* 'Solar Polarization 4', Vol. 358, p. 431.

Soler, R., Díaz, A., Ballester, J. and Goossens, M. (2012), 'Kelvin–helmholtz instability in partially ionized compressible plasmas', *The Astrophysical Journal* **749**(2), 163.

Soler, R., Oliver, R. and Ballester, J. (2010), 'Time damping of non-adiabatic magnetohydrodynamic waves in a partially ionized prominence plasma: effect of helium', *Astronomy & Astrophysics* **512**, A28.

Soler, R., Terradas, J., Oliver, R. and Ballester, J. L. (2019), 'Energy transport and heating by torsional alfvén waves propagating from the photosphere to the corona in the quiet sun', *The Astrophysical Journal* **871**(1), 3.

Soler, R., Terradas, J., Oliver, R. and Ballester, J. L. (2021), 'Resonances in a coronal loop driven by torsional alfvén waves propagating from the photosphere', *The Astrophysical Journal* **909**(2), 190.

Soler, R. et al. (2013*a*), 'Alfvén waves in a partially ionized two-fluid plasma', *The Astrophysical Journal* **767**(2), 171.

Soler, R. et al. (2013*b*), 'Magnetoacoustic waves in a partially ionized two-fluid plasma', *The Astrophysical Journal Supplement Series* **209**(1), 16.

Spitzer, L. (1962), 'Jr., physics of fully ionized gases'.

Srivastava, A. K., Shetye, J., Murawski, K., Doyle, J. G., Stangalini, M., Scullion, E., Ray, T., Wójcik, D. P. and Dwivedi, B. N. (2017), 'High-frequency torsional alfvén waves as an energy source for coronal heating', *Scientific Reports* **7**(1), 1–7.

Stancil, P., Havener, C., Krstić, P., Schultz, D., Kimura, M., Gu, J.-P., Hirsch, G., Buenker, R. and Zygelman, B. (1998), 'Charge transfer in collisions of c+ with h and h+ with c', *The Astrophysical Journal* **502**(2), 1006.

Stangalini, M., Erdélyi, R., Boocock, C., Tsiklauri, D., Nelson, C. J., Del Moro, D., Berrilli, F. and Korsós, M. B. (2021), 'Torsional oscillations within a magnetic pore in the solar photosphere', *Nature Astronomy* pp. 1–6.

Sutmann, G., Musielak, Z. and Ulmschneider, P. (1998), 'Acoustic wave propagation in the solar atmosphere. iii. analytic solutions for adiabatic wave excitations', *Astronomy and Astrophysics* **340**, 556–568.

Tandberg-Hanssen, E. (1974), *Solar Prominences*, Vol. 12.

Tandberg-Hanssen, E. (2013), *The nature of solar prominences*, Vol. 199, Springer Science & Business Media.

Terradas, J., Soler, R., Oliver, R. and Ballester, J. (2015), 'On the support of neutrals against gravity in solar prominences', *The Astrophysical Journal Letters* **802**(2), L28.

Thomas, J. H., Weiss, N. O., Tobias, S. M. and Brummell, N. H. (2002), 'Downward pumping of magnetic flux as the cause of filamentary structures in sunspot penumbrae', *Nature* **420**(6914), 390–393.

Title, A. M. (2007), The Quiet Sun Magnetic Fields, *in* K. Shibata, S. Nagata and T. Sakurai, eds, 'New Solar Physics with Solar-B Mission', Vol. 369 of *Astronomical Society of the Pacific Conference Series*, p. 125.

Trujillo Bueno, J., Asensio Ramos, A. and Shchukina, N. (2006), 'Solar polarization 4 (asp conf. ser. 358), ed', *R. Casini & BW Lites (San Francisco, CA: ASP)* **269**.

Tu, C.-Y. (1987), 'A solar wind model with the power spectrum of alfvénic fluctuations', *Solar physics* **109**(1), 149–186.

Tu, C.-Y. and Marsch, E. (1997), 'Two-fluid model for heating of the solar corona and acceleration of the solar wind by high-frequency alfvén waves', *Solar Physics* **171**(2), 363–391.

Tu, J. and Song, P. (2013), 'A study of alfvén wave propagation and heating the chromosphere', *The Astrophysical Journal* **777**(1), 53.

Vernazza, J. E., Avrett, E. H. and Loeser, R. (1981), 'Structure of the solar chromosphere. iii-models of the euv brightness components of the quiet-sun', *The Astrophysical Journal Supplement Series* **45**, 635–725.

Von Woedtke, T., Reuter, S., Masur, K. and Weltmann, K.-D. (2013), 'Plasmas for medicine', *Physics Reports* **530**(4), 291–320.

Vranjes, J. and Krstic, P. (2013), 'Collisions, magnetization, and transport coefficients in the lower solar atmosphere', *Astronomy & Astrophysics* **554**, A22.

Wang, Y.-M. and Stenborg, G. (2010), 'Spinning motions in coronal cavities', *The Astrophysical Journal Letters* **719**(2), L181.

Wójcik, D., Murawski, K. and Musielak, Z. (2019), 'Partially ionized solar atmosphere: Two-fluid waves and their cutoffs', *The Astrophysical Journal* **882**(1), 32.

Zaqarashvili, T., Carbonell, M., Ballester, J. and Khodachenko, M. (2012), 'Cut-off wavenumber of alfvén waves in partially ionized plasmas of the solar atmosphere', *Astronomy & Astrophysics* **544**, A143.

Zaqarashvili, T., Khodachenko, M. and Rucker, H. (2011*a*), 'Damping of alfvén waves in solar partially ionized plasmas: effect of neutral helium in multi-fluid approach', *Astronomy & Astrophysics* **534**, A93.

Zaqarashvili, T., Khodachenko, M. and Rucker, H. (2011*b*), 'Magnetohydrodynamic waves in solar partially ionized plasmas: two-fluid approach', *Astronomy & Astrophysics* **529**, A82.

Zaqarashvili, T., Khodachenko, M. and Soler, R. (2013), 'Torsional alfvén waves in partially ionized solar plasma: effects of neutral helium and stratification', *Astronomy & Astrophysics* **549**, A113.

Zhang, F., Poedts, S., Lani, A., Kuźma, B. and Murawski, K. (2021), 'Two-fluid modeling of acoustic wave propagation in gravitationally stratified isothermal media', *The Astrophysical Journal* **911**(2), 119.

Zhdanov, V. (1962), 'Transport phenomena in a partly ionized gas', *Journal of Applied Mathematics and Mechanics* **26**(2), 401–413.